1989

Cyclic tests of components of one-story reinforced concrete framewall-diaphragm assemblage, December 1989

Kai Yu

Ti Huang

Le-Wu Lu

514.3

CYCLIC TESTS OF COMPONENTS OF ONE-STORY REINFORCED CONCRETE FRAME-WALL-DIAPHRAGM ASSEMBLAGE

by

Kai Yu, Ti Huang and Le Wu Lu

Department of Civil Engineering

Fritz Engineering Laboratory

Lehigh University

Bethlehem, Pennsyvania

December, 1989

Acknowledgement

The work presented in this report was a part of a research project, "Seismic Response of Building Structure with Flexible Floor Diaphragms", conducted jointly at Lehigh University and the State University of New York at Buffalo (SUNY/Buffalo). The project is funded by the National Center for Earthquake Engineering Research headquartered at SUNY/Buffalo. The center is supported by the National Science Foundation and the State of New York.

The authors wishes to express their deep appreciation to the late Dr. Roger G. Slutter for his valuable consultation in model material processing and Dr. Harry G. Harris for allowing to use his machine to process reinforcing wires at Draxul University. Appreciation is also extended to the many associates at Fritz Laboratory for their day and night assistance during the experiments. Messrs. Russel Longenbach and Suk-Bong Kang helped in instrumenting the specimens and tests. Mr. Charles F. Hittinger and the technicians prepared the experiments.

Professor Andrei M. Reinhorn and Dr. Nader Panahshahi, the investigators at SUNY/Buffalo, are gratefully acknowledged for their valuable cooperation through the tests.

Table of Contents

Abstract 1
1. Introduction 3
2. Construction Procedure 6
Table2 9
Figure2 11
3. Description of the Cyclic Loading Tests 16
3.1 General 16
3.2 Data Aquisition systems 16
3.3 Test of Shear Wall 17
3.4 Test of Middle Frame 20
3.5 Slab Tests 23
Figure3 27
4. Experimental Results and Discussion 42
4.1 General 42
4.2 Shear Wall 43
4.3 frame 46
4.4 Slab 49
Table4 52
Figure4 58
5. Conclusions 90
References 92

List of Figures

Figure 2-1: Reinforcement of Beam-Edge Column Joint Region in Shear Wall 12
Figure 2-2: Reinforcement in Beam-Wall Joint Region in Shear Wall 12
Figure 2-3: Formwork and Reinforcement of Slab in Shear Wall 13
Figure 2-4: Wall and Footing Reinforcement of Shear Wall 13
Figure 2-5: Reinforcement in Beam-Column Joint Region of Frame 14
Figure 2-6: Construction of Frame 14
Figure 2-7: Reinforcement for Slab 15
Figure 3-1: Test Setup of Shear Wall 28
Figure 3-2: Typical Failure Mode at Bottoms of Shear Wall 29
Figure 3-3: Failure Mode of Shear Wall 29
Figure 3-4: Concrete Cracks on the N. Sides of Shear Wall 30
Figure 3-5: The Test Loading Program of Shear Wall 31
Figure 3-6: Test Setup of Frame 32
Figure 3-7: Deformation at Base Region of the E. Column 33
Figure 3-8: Deformation in Beam-Column Joint Region of Frame 34
Figure 3-9: Ultimate Stage of Frame 34
Figure 3-10: The Failure Mode of Frame 35
Figure 3-11: The Test Loading Program of Frame 36
Figure 3-12: Test Setup of Slab 37
Figure 3-13: Concrete Cracking Pattern of Slab 38
Figure 3-14: Slab Cracking Along the Support on the N. side 39
Figure 3-15: The Failure Mode of the S. Logitudinale Beam 39
Figure 3-16: The Failure Mode of Slab 40
Figure 3-17: The Test Loading Program of Slab 41
Figure 4-1: Load (P) vs. Dispalcement (D_t) of Shear Wall 59
Figure 4-2: Load (P) vs. Dispalcement (D_t) of Shear Wall (First 13 Cycles) 60
Figure 4-3: Load (P) vs. Displacement (D_t) of Shear Wall (Last 10 Cycles) 61
Figure 4-4: Moment (M) vs. Curvature (q_w) at Bottom of Shear Wall 62
Figure 4-5: Load (P) vs. Beam Curvature (q_b) of Shear Wall 63
Figure 4-6: Sideway Displacement of Shear Wall 64
Figure 4-7: Skeleton Curves of Shear Wall 65
Figure 4-8: Stiffness Deterioration in Each Cycle of Shear Wall 66
Figure 4-9: Energy Absorbed in Each Cycle of Shear Wall 67
Figure 4-10: Energy Dissipated in Each Cycle of Shear Wall 68
Figure 4-11: Accumulated Energy Absorbed in Shear Wall 69
Figure 4-12: Accumulated Energy Dissipated in Shear Wall 70
Figure 4-13: Load (P) vs. Displacement (D_t) of Frame 71
Figure 4-14: Load (P) vs. Column Curvature (q_c) of Frame 72
Figure 4-15: Load (P) vs. Beam Curvature (q_b) of Frame 73
Figure 4-16: Load (P) vs. Angle Change (g_{bc}) Between Beam and Column of Frame 74
Figure 4-17: Skeleton Curve of Frame 75

Figure 4-18: Stiffness Deterioration in Each Cycle of Frame 76
Figure 4-19: Energy Absorbed in Each Cycle of Frame 77
Figure 4-20: Energy Dissipated in Each Cycle of Frame 78
Figure 4-21: Accumulated Energy Absorbed in Frame 79
Figure 4-22: Accumulated Energy Dissipated in Frame 80
Figure 4-23: Load (P) vs. Displacement (D_t) of Slab 81
Figure 4-24: Moment (M) vs. Curvature (q_s) of Slab 82
Figure 4-25: Sideway Displacement of Slab 83
Figure 4-26: Skeleton Curve of Slab 84
Figure 4-27: Stiffness Deterioration in Each Cycle of Slab 85
Figure 4-28: Energy Absorbed in Each Cycle of Slab 86
Figure 4-29: Energy Dissipated in Each Cycle of Slab 87
Figure 4-30: Accumulated Energy Absorbed in Slab 88
Figure 4-31: Accumulated Energy Dissipated in Slab 89

List of Tables

Table 2-1: Summary of Concrate Strength 10
Table 4-1: Experimental Data of Shear Wall 53
Table 4-2: Experimental Data of Middle Frame 54
Table 4-3: Experimental Data of Slab 56

Abstract

A cooperative research project studying effect of floor diaphragm flexibility on seismic responses of building structure has been carried out at Lehigh University and the State University of New York at Buffalo (SUNY/Buffalo). As the first stage of the project, an one-story one-sixth scale reinforced concrete structural model consisting of shear walls, frames and floor diaphragms has been developed to be the test structure for this study (8). For the second stage, the quasi-static cyclic tests of the three components of the one-story reinforced concrete frame-wall-diaphragm assemblage at Lehigh University and the simulate earthquake tests on the assemblage structure have been completed (7). The test results of the three components (shear wall, middle frame, and slab), which were tested in Fritz Laboratory at Lehigh University, are presented in this report.

The three small scale concrete component structures were constructed based on the design of the one-story reinforced concrete frame-wall-diaphragm assemblage in the first stage of the project. The design details of the three components are identical to the corresponding portions in the assemblage structure. The shear wall and frame specimens were subjected primarily to quasi-static cyclic lateral loading and the slab specimen was subjected primarily to quasi-static cyclic in-plane loading.

The tests revealed that the small scale concrete component structures possessed large ductilities under cyclic loading if they were designed to satisfy the requirements of ACI 318-83 and its Appendix A. The good energy dissipating properties were observed during the three component tests. Severe stiffness degradation occurred during cyclic loading in the inelastic range of each specimen. The large additional weight on the shear wall and

frame specimens reduced the opennings of concrete in the vertical supporting members. The loading programs for the three components were designed to reveal the postelastic behavior of the concrete structure, the effect of small cyclic loading on structual behavior, and also to assistant in the decision of the loading strategy of the earthquake simulating tests on the complete assemblage structure at SUNY/Buffalo.

Chapter 1
Introduction

Floor slabs are used in multi-story buildings to serve many important structural functions. They not only transmit the gravity loads to the vertical structural systems, such as frames and shear walls, but also act integrally with the vertical systems in resisting lateral as well as gravity loads. The primary action of the slabs for these two functions is out-of-plane bending, a problem which has been studied extensively. The analytical tools necessary to predict out-of-plane slab behavior are readily available.

Distribution of lateral loads to parallel vertical structural systems is another important function of the floor slabs. When a building is subjected to a severe earthquake, the inertial forces generated in the floor slabs must be transferred to the vertical structural systems through the diaphragm action of the slabs. The performance of the diaphragm action of the floor slab is controlled primarily by its in-plane stiffness. In many structures, a reasonable estimate of the inertial force distribution can be achieved by assuming that the slabs act as rigid diaphragms. However, for structures in which the stiffness of the vertical system and the stiffness of the slab system do not differ greatly, diaphragm deformation of the floors must be explicitly considered in analysis.

There is currently insufficient knowledge to determine whether the rigid-diaphragm assumption will lead to adequate design for a given structure, whether the diaphragm flexibility requires special consideration, and how to define the rigidity of a horizontal diaphragm relative to the stiffness of the vertical lateral load resisting systems. Although the need for such information has been recognized by structural engineers, only a small amount of

analytical and experimental research has been conducted, especially on reinforced concrete diaphragms.

In recent years, research has been carried out to study the in-plane characteristics of reinforced concrete floor diaphragms (3, 4, 5), and approximate analytical models have been proposed for investigating the effect of diaphragm flexibility on seismic building responses (1, 2, 6). The distribution of seismic forces to the vertical structural elements has been found to be very complex, especially after the floor diaphragms have experienced significant cracking and yielding. All available methods of analysis for structures with flexible diaphragms use very simple models to represent the behavior of the various structural elements. Furthermore, the results of those analyses have not been sufficiently verified by tests performed on three-dimensional structures.

An analytical and experimental research program is being conducted on a cooperative basis between Lehigh University and SUNY/Buffalo. The primary objective of the program is to understand the effect of the diaphragm flexibility on the redistribution of lateral forces to the vertical structural system after the floor slab system has experienced inelastic deformation. This is to be achieved by conducting a series of tests on a one story 3D reinforced concrete structure under lateral loads up to collapse load level. The test results will be used to correlate with analytical predictions and to develop specific procedures for the analysis of inelastic building systems including the effect of in-plane slab flexibility.

As the experimental study of the project, the three small scale reinforced concrete component structures were tested upto ultimate strength stage under quasi-static cyclic loading in the Fritz Laboratory at Lehigh University and the one-story reinforced concrete wall-frame-

diaphragm assemblage structure was tested under simulate earthquake loading on the shaking table at SUNY/Buffalo. This report will only cover the experimental study on the three component structures which was completed at Lehigh University.

The objective of the three small scale component structures was to clearly understand the hysteretic behavior of the components of the assemblage structure under seismic loading. Consequently, with the help of understanding its component behavior, the tests of the assemblage structure under quasi-static cyclic loading at Lehigh University and under simulate earthquake loading on the shaking table at SUNY/Buffalo will be correctly orientated and the expected test results can be achieved.

The corelation of the test results of the components with theoretical predictions and the test results of the assemblage will be presented in separate reports.

Chapter 2
Construction Procedure

The construction of small scaled model structures usually requires more time and sophisticated skill than the corresponding full size structures. In the construction of the three small scaled component specimens (shear wall, frame, and slab), the difficulties were encountered in forming reinforcement cages, making the formworks, and placing concrete. The construction was completed at Fritz Laboratory by a local construction company.

The stirrups for the specimens were formed by the technicians of the laboratory in order to achieve more accurate dimension. For such small scaled structures, the stirrups were very critical for holding the main reinforcing bars in the right positions. The slight change in diemnsion of the cages would cause a large percentage change in the section strength of members. The smooth G14 used for the stirrups was straightened first from the coils and then bended into required shape by using molds. The total number of the stirrups is 300 for the shear wall, 332 for the frame and 292 for the slab.

For the three component specimens, all main reinforcing steels (longitudinal steel in the beams and columns of specimens) comprised of single length of wire. The column steel and wall steel were anchored into a 4.0 in. high stud

column and stud wall at the tops of column and shear wall to simulate the confining effect from the suppier structures. At the base of each column and wall, the longitudinal steel were anchored by a 7.0 in. developing length with 3.0 in. bending in 90 degrees. The bending were tied to the bottom main steels in the footings. A kind of small chair bended from a thin wire was

used to support beam and slab reinforcing bars to obtain an accurate concrete cover.

It is desirable to place construction joints in such positions that they have minimal effect on the behavior of the structure, which is always considered in real structural constructions. However, since the shear wall and frame component specimens have only one story, there were no onstruction joints for these two specimens.

The method of construction used was to construct one piece of formwork for each specimen. The forms were pasted with form wax before the steel cages were put in position. For ensuring good concrete compaction at the footings of the frame columns and shear walls and safe anchorage of main steels into the footings, the tops of the footing forms of shear wall and frame were open for the convenient to place the footing concrete. In order to achieve solid walls, the concrete was placed in two stages due to the small cross sections of the walls. At the middle height of the wall, the form plate was cut on one side and leave the upper part open. After the lower part was solided with concrete, the upper wall was covered by a form plate and concrete was cased from the top of the wall. Because of the limit of the capacity of the concrete mixing machine avaliable in the laboratory, total three batch of concrete were made for the three small scaled component specimens, one batch for the footing of the shear wall, one for the upper structure of the shear wall and the slab, and one for the frame. The concrete was solided by inserting a small vibrator inside the form and at the meantime, the formwork was vibrated by attaching a large vibrator on the surface of the formworks.

The specimens were covered by plastic sheets immediately after the construction was compleshed and cured under a normal laboratory

condition withspraying water on the specimens once a week for four weeks. For each batch of concrete mixture, 12 cylinders of 3 in by 6 in were made to monitor the concrete strength for the different ages and they were cured under the same condition as the specimens. The formwork was stripped when the specimen was scheduled to be tested.

Figs. 2-1 to 2-7 give some details about reinforcing and construction of the three specimens.

The concrete cylinders were tested for each specimen on following concrete ages: 7 days, 28 days, and the testing dates. The summary of the concrete strength on these cylinder tests for the three specimens is given in Table 2-1. The strength values in the table are the average values on all tested cylinders for each test date.

Table2

Table 2-1: Summary of Concrate Strength

	Shear Wall	Frame	Slab
7 day	2697	2943	2697
28 day	3190	3780	3190
Test day	4550 (100 days)	4650 (179 days)	4400 (230 days)

Figure2

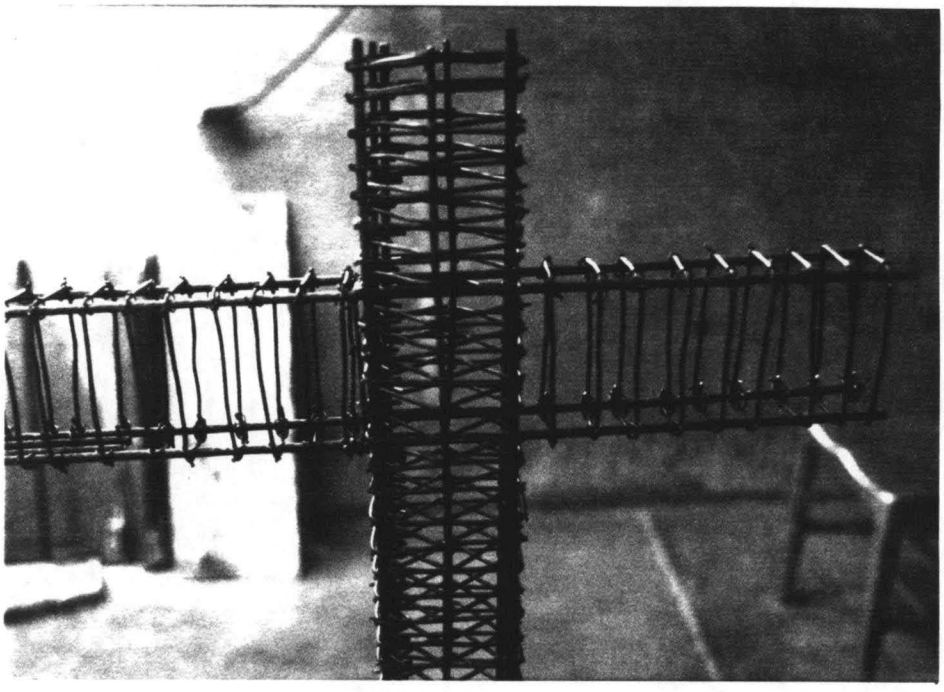

Figure 2-1: Reinforcement of Beam-Edge Column Joint Region in Shear Wall

picture to be developed from a slide

Figure 2-2: Reinforcement in Beam-Wall Joint Region in Shear Wall

Figure 2-3: Formwork and Reinforcement of Slab in Shear Wall

Figure 2-4: Wall and Footing Reinforcement of Shear Wall

Figure 2-5: Reinforcement in Beam-Column Joint Region of Frame

Figure 2-6: Construction of Frame

Figure 2-7: Reinforcement for Slab

Chapter 3
Description of the Cyclic Loading Tests

3.1 General

The seismic responses of the three component specimens (shear wall, frame and slab), were investigated by conducting the quasi-static cyclic loading tests on them under the proposed loading programs (8). To obtain the full range of the hysteretic behaviors of the component structures, the specimens were tested upto ultimate strength.

The loading procedures for all the three component tests were initially controlled by loads first which gradually increased upto the yielding loads. After the displacements of the specimens reached the defined yielding values Δ_y, corresponding to the yield strength. Then the loading procedures were shifted to the displacement contolling with displacement increment of approximate 0.5 Δ_y for each consequent peak cycle. When the lateral loads were remained less than 75% of the maximum load or the ductilities were over 5, the failure stages for the specimens were defined and the tests were accomplished.

The testing procedures for the three component specimens are described in following sections.

3.2 Data Aquisition systems

A data acquisition system, B & F, was used for the shear wall and frame specimens to collect data from electrical instruments. The data were then transferred to a microcomputer which recorded the data on floppy disks and meantime the data were also printed out in a hard copy. For the slab specimen, a data acquisition system called R.D.P. was used to collect data

which were recorded on floppy disks by a portable computer. For the convenient in processing data, each load step recorded as one file. The detail illustration of the instrumentation for each specimen was shown in Reference (Yu).

3.3 Test of Shear Wall

The lateral cyclic loads generated by a mechanical jack through a 20k load cell at the end of the shear wall were applied in quasi-static manner (8). The acting line of the loads is located at 1 in below the top surface of the slab. The initial zero displacement stage of the test specimen was taken as the point of initial lateral deflection due to self-weight and the additional hanging weight. The testing setup of the specimen and the pattern of the hanging weight is shown in Fig. 3-1. The test specimen was transversely supported by two steel angles to prevented of out of loading plane deflection happening. The initial lateral displacement at the loading point due to self-weight and the additional weight was 0.0005 in. which is neglected in later data processing.

The test specimen was set in West-East direction. The East direction loading was referred as the positive load and the West direction loading as the negative load. The total 23 test cycles were conducted on the shear wall tests. The first 8 cycles were controlled by load in considering of indentifying the yielding stage of the test specimen. The first cycle was started with its peak load of 3.0 kips in both directions and a increment of 3.0 kips was used for the second cycle. For the next 6 load controlling cycles, the lateral load was increased in a step of 1. kip and the peak load for cycle 8 was 11.0 kips for the two loading directions. Several initial cracks due to bending were first observed along the tension sides near the bottoms of the walls under a

positive peak load of 6. kips in the second cycle. At the same time, there were also some initial cracks on the beam near the beam-wall conjunction area. When the negative peak load of the second cycle was reached, the similar initial tension cracks were observed on the other sides of the walls. As the lateral load increased, several major tension cracks developed near the bases of the walls from the initial cracks and many small new cracks were developed. At the meantime, shear cracks developed in both directions on the walls.

After the test specimen was subjected to the first 8 cycle loadings, the structure suffered severe damage at the bases of the walls and its response appeared inelastically. Subsequently, the loading was shifted to the displacement controlling for the rest cycles. In cycle 9, the defined yield displacement, Δ_y (0.005H, H = height of the shear wall specimen), was reached with a positive peak load of 12.53 kips. The negative peak load of this cycle was 12.78 kips under the same displacement value, Δ_y. In the following every new peak cycles (not repeated cycles), the displacement was increased in a step of approximate 0.5 Δ_y except the last cycle which was increased by Δ_y. At the displacement of $1.5\Delta_y$ (0.0075H), the lateral load approached its maximum values in both directions, 13.67 kips for the positive direction and 13.52 kips for the negative direction. At these maximum lateral loads, the cracks penetrated through the full wall width at the bases of the walls. The opening of the major cracks measured was 0.016 in. in the walls and 0.013 in. in the beam. The residual lateral displacement at zero load was 0.004H and accumulated rapidly as the displacement increased. This phenomenon was found due to shear deformation at the bases of the walls, the inelastic deformation of reinforcement and the opening of concrete cracks.

After the specimen passed through its maximum strength, the lateral displacement was mainly contributed by the reinforcement yielding and the concrete crack opening and closing. The peak load was keeping dropping in each new peak cycle. The first buckle of the reinforcing bars was observed on the east side of the west wall near the bottom with the positive peak load of cycle 13 and the concrete was crushed out. At the end of cycle 15, the four clip gages at the bases of the shear walls were out of range and taken away. Due to the severe deformation of the reinforcement, the main crack openings were significant large, 0.4 in. in the walls and 0.2 in. in the beam. The first fracture of reinforcing bars in the walls was happened on the east side of the west wall at the negative peak load of cycle 19. There were more bars fractured in last three cycles. However, there were no bar fractures in the beam were observed.

In cycle 23, the peak load had dropped about 38% of the maximum load in the positive direction and 55% in another. So the ultimate stage was defined and the tests was determinated. The maximum displacement was 1.08 in. in both loading directions.

The observations made during the test(see Fig. 3-5) are summarized as follows:

W1 Initial cracks for the positive loading.
W2 Initial cracks for the negative loading.
W3 A crack developed through the whole width at west end of slab.
W4 The yield strength reached for the positive loading.
W5 The yield strength reached for the negative loading. The cracks at the bases of the walls penetrated the full width of the walls.
W6 The maximum strength reached for the positive loading.
W7 The maximum strength reached for the negative loading.
W8 Concrete crushed out on the compression side of the east wall.
W9 Concrete pieces fell down on both tension and compression sides on each wall.
W10 Concrete pieces fell down again on the compression side on each wall.
W11 One reinforcing wire buckled on the east side of the west wall.
W12 Two reinforcing wires fractured on the east side of the west wall and load dropped 0.2 kips with displacement increasing 0.03 in..
W13 One wire fractured on the east side of the west wall.
W14 Two more wires were broken on the east side of the west wall.
W15 One more wire fractured on the same wall.
W16 Some wires fractures inside W. and E. walls.

Some failure modes of the structure and its elements and the concrete cracking pattern on the walls are shown in Figs. 3-2 to 3-4.

3.4 Test of Middle Frame

The middle frame specimen was tested on the same site as the shear wall specimen and the same loading mechanism was used as well as the nature of the applied lateral loading and the transverse support. The testing setup and the way of hanging the additional weights of the specimen are shown in Fig. 3-6. The initial lateral displacement due to the additional and self-weights was very small and negligible. So the zero lateral displacement was used for the initial zero load condition.

Total 28 test loading cycles were carried out on the middle frame specimen. For the frame specimen, the west-direction loading was referred

as the positive load and the east-direction loading as the negative load. This is opposite to the loading direction for the shear wall speciemns. The load controlling method was used for the first 12 cycles. The first cycle was started with a peak value of 0.1 kips and in the following 10 cycles increment of the peak load was 0.1 kips. The first initial concrete crack were observed at the bottoms of the both columns with a negative peak loading of 0.4 kips in cycle 4. At the top range of the columns, the initial concrete cracks did not appear until cycle 8 with a peak load of 0.8 kips. The beam had its first concrete crack when the load reached 0.9 kips in cycle 9. At this moment, the slab still remained uncracking. Some new cracks developed as the load increased in each new peak cycle in the columns and beam and the displacement likely more concentrated on several major cracks near the column bottoms. In cycle 10, the peak lateral displacement approached 0.1H (0.41 in.) with a peak load of 1.0 kips for the both loading directions, where H = the height of the middle frame. This peak displacement was defined as Δ_y. After this cycle, the loading procedure was shifted to the displacement controlling method. In order to simulate the nature of the earthquake loads, a few small cycles were repeated once several new peak cycles were conducted. For these new peak cycles, a loading step of approximate Δ_y was used for the increment of the lateral displacement.

After the specimen observed its yielding displacement, Δ_y, the cracks near the bottoms of the columns opened severely and new cracks developed toward the center range of the columns. As the lateral displacement increased more deformation concentrated on the major cracks which located at the bottom and top of the columns. At the peak values of the both loading directions in cycle 16, the maximum opening of these cracks was 0.04 in.. In cycle 20, the structure reached its ultimate

strength, the maximum lateral peak load was 1.2 kips for the positive direction loading. The ultimate strength, 1.16 kips, for the negative direction loading was reached in cycle 21. After the structure observed its ultimate strength, the peak load dropped about 6% of the maximum load in every consequent cycle. The dropped load observed during the crack checking when the displacement was hold unchanged could be caused by creeping in tension steel and compressed concrete. The response of the structure was just like a mechanism with four plastic hinges each one of them located at one end of the columns at the ultimate loading stage.

Through the whole procedure of the tests, there were only two cracks on the slab, one at near each beam-column joint area. The two cracks along the full width of the slab were both developed in cycle 23. The reason for their later appearing was due to the large ratio of the T-section beam stiffness to column stiffness. This large ratio forced the most deformation at the beam-column joint concentrated into the ranges at the tops of column. At the peak displacement of cycle 24, the LVDT at the top of the specimen were out of range for measuring the lateral displacement and replaced by two 6 in. mechanical dial gages. In the last few cycles, there were no new cracks developed. But the major cracks at the bottoms of the columns opened as wide as 0.2 in.. There were no shear cracks observed in column through the tests.

At the peak loading in cycle 28 in the negtive direction, one reinforcing bar fractured in the west column and the peak load dropped about 24% of the maximum load for the both loading directions. So the ultimate stage was reached and the tests were determinated. The lateral displacement was 3.24 inches for the both loading directions.b at the final stage.

The observations made during the test(see Fig. 3-11 are summarized as follows:

F1 The initial cracks in columns for the negative loading.
F2 The initial cracks in columns for the positive loading.
F3 The first crack on the beam at the west end.
F4 The first crack on the beam at the east end.
F5 The yield strength reached for the positive loading.
F6 The yield strength reached for the negative loading.
F7 The ultimate strength reached for the negative loading.
F8 The ultimate strength reached for the positive loading.
F9 A crack developed through the whole width of the slab at the west end of the beam.
F10 A crack developed through the whole width of the slab at the east end of the beam.
F11 Concrete crushed out at the bottoms of columns.
F12 One wire fractured at the bottom of the west column.
F13 One wire fractured at the bottom of the east column.
F14 One more wire fractured at the bottom of the west column.

Figs. 3-7 to 3-10 give the details of the failure modes and deformation of the structure and its elements.

3.5 Slab Tests

The slab specimen was set-up with a fixed support at one end and a roller support at another (see Fig. 3-12). The fixed end support was used to simulate the symmetric effect of the inertial force about the middle frame in the assemblage model structure. The in-plane cyclic loads were generated by a mechanical jack through a 20 kips load cell which was connected to the loading frame. The in-plane quasi-static loads were applied to the specimen through a triangle loading frame which was attached to the roller supported end of the slab. The acting line of the in-plane loads was located at a level of the center of the slab. The in-plane load was applied in North-South direction. The north loading was referred as the positive direction and the south loading as the negative direction. The steel blocks for the additional weight were hanged one by one underneath the slab to avoid

the effects of sudden loading. After all the steel blocks were put in position, the slab suffered of one crack along the fixed support at the top surface of the slab, which extended through the full width of the slab. This crack was due to the negative bending moment of the self-weight and additional hanging block weight. There were also eight cracks on each longitudinal beam in their center range due to the positive bending moment. (the beams along the supports were referred as transverse beams). These prior test cracks caused no initial in-plane displacement. So the initial in-plane displacement for zero load was zero.

Total 29 test cycles had been applied to the specimen to complete the tests. The load controlled procedure was used for the first 4 loading cycles by considering the same reason in the shear wall and frame specimens. The first cycle was started with a peak in-plane load of 0.3 kips and the peak load was increased by a step of 0.3 kips in next three cycles. During these four cycles, there were no new cracks appearing. However, the crack along the fixed support (main crack) due to the weights kept opening as the in-plane load increased. The opening of the main crack was 0.02 in. at the peak in-plane displacement in cycle 4. From cycle 5, the test procedure was shifted to the displacement controlling in regarding the severe damage in the slab. In considering of the nature of the shaking table tests, many small loading cycles were conducted before the structure reached its yielding strength. Except the repeated cycles, the in-plane displacement in a step of 0.02 to 0.03 in. for each new cycles. In these cycles, the first new crack appeared near the roller supported beam in cycle 5. This crack was caused by the combination of the negative bending of weight and the in-plane bending of the applied load. In cycle 6, some new cracks under the slab developed along each side of the slab in the

longitudinal direction for both loading directions. But the top surface of the slab still remained uncrack. The reason was that the positive bending moment of weights forced most slab concrete in compression condition. Up to cycle 9, for the first time, some tension cracks formed at the top of the slab and at the meantime, some shear cracks also developed near the fixed support. For the negative load in this cycle, a crack along the top of the north longitudinal beam shown up, which was perpendicular to the loading direction. In cycle 15, the opening of the main crack was 0.2 in. (10 times as in cycle 4) with a 0.205 in. of peak in-plane displacement. At this time the second major crack formed along the critical section in the slab (15 in. from the fixed supported end). A crack along the top of the south longitudinal beam was also formed.

The in-plane displacement reached its yielding displacement, Δ_y, (0.005H), with a peak load of 2.68 kips in the positive loading direction and a peak load of 2.56 kips in the negative loading direction in cycle 9. After this point, the slab went into its plastic range of response. For the rest peak loading cycles, the in-plane displacement was increased in a step of $0.5\Delta_y$ until the failure stage reached. As the in-plane displacement approached its ultimate value, more deformation concentrated on the second main major crack along the critical section where the negative slab reinforcemnt was determinated. In cycle 23, the legs of the loading steel triangle were buckled out of the loading plane. In order to continue the tests, some small steel channels were clamped to the triangle legs to make them more stiffer. In the plastic range of the deformation, the in-plane load continuously increased for each new peak cycle until some slab reinforcing bars fractured in cycle 28 for both loading directions. At this time the opening of the main crack was 0.75 in. and the second major crack was .25 in.. The

settlement at the center of the longitudinal beams was upto 2.375 in.. The peak load reached its maximum strength load of 2.66 in cycle 26 for the negative loading and of 2.92 kips in cycle 27 for the positive loading. In considering the damage of the slab and due to the limit of the jack stroke, the failure stage was defined in cycle 29 although the in-plane load dropped only about 5% of the maximum strength.

The observations made during the test (see Fig. 3-17) are summarized as follows:

S1 The initial crack (the first major crack) along the fixed supporting end due to the selfweight and the additional hanging weight.
S2 The initial crack on the slab due to the in-plane loading for the positive direction.
S3 The initial crack on the slab due to the in-plane loading for the negative direction.
S4 The second major crack developed along the critical section.
S5 A new crack formed along the longitudinal beam on the north side of the slab.
S6 A new crack formed along the longitudinal beam on the south side of the slab.
S7 The yield strength reached for the positive loading.
S8 The yield strength reached for the negative loading.
S9 The maximum strength reached for the negative loading.
S10 Three or four slab reinforcing wires fractured on the north side of the slab near the fixed supporting end. Some concrete pieces fell down at the center range of the north longitudinal beam.
S11 The maximum strength reached for the positive loading.
S12 More wires fractured in the slab.
S13 Some concrete pieces fell down at the center range of the south longitudinal beam.

Figs. 3-13 to 3-16 illustrate the details of the cracks and the failure mode of the slab.

Figure3

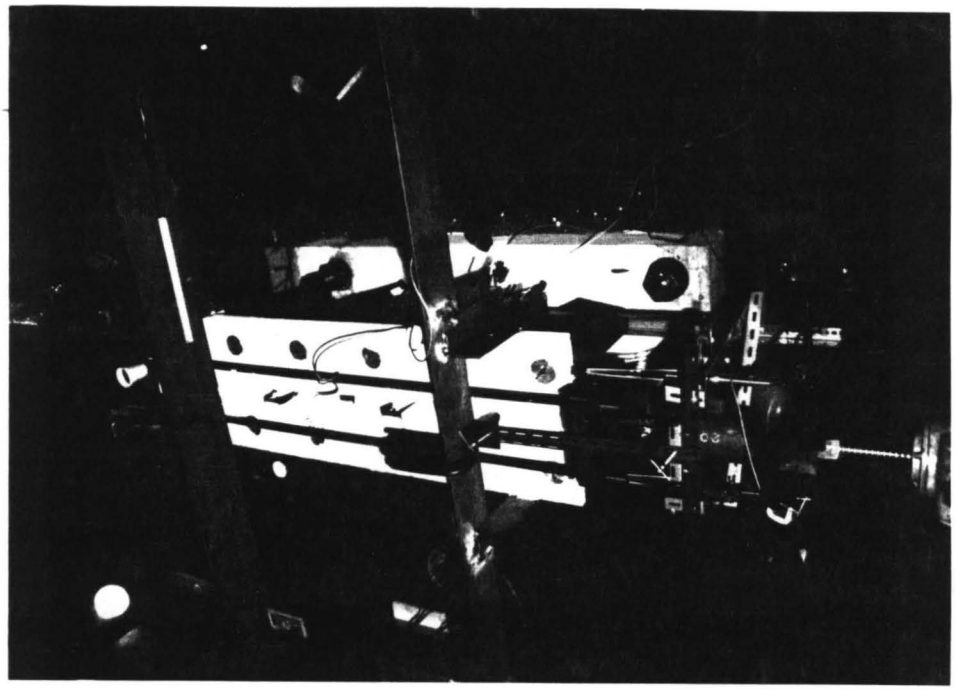

Top View

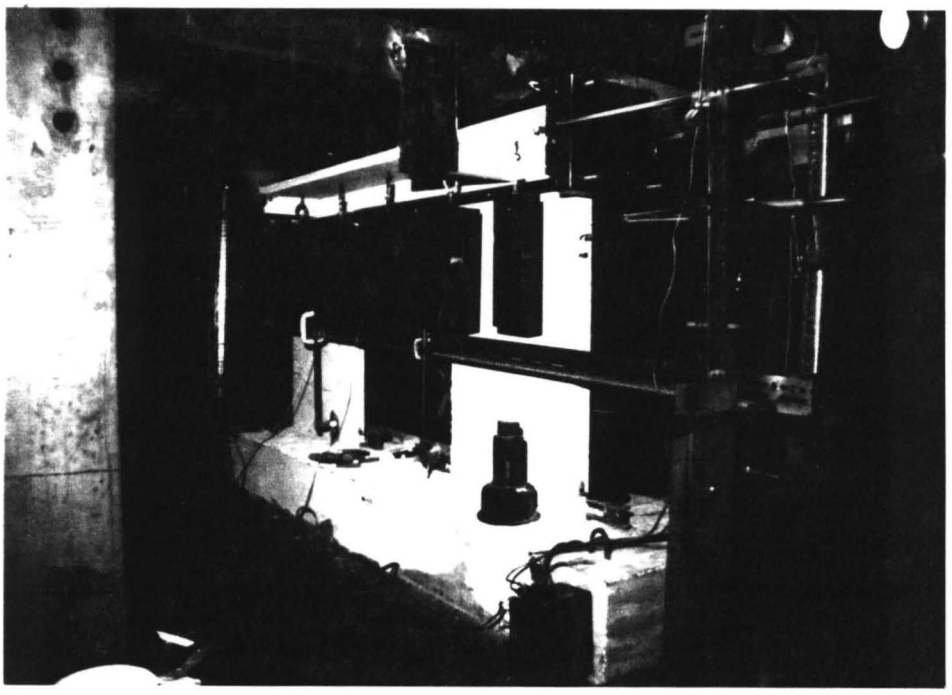

Side View

Figure 3-1: Test Setup of Shear Wall

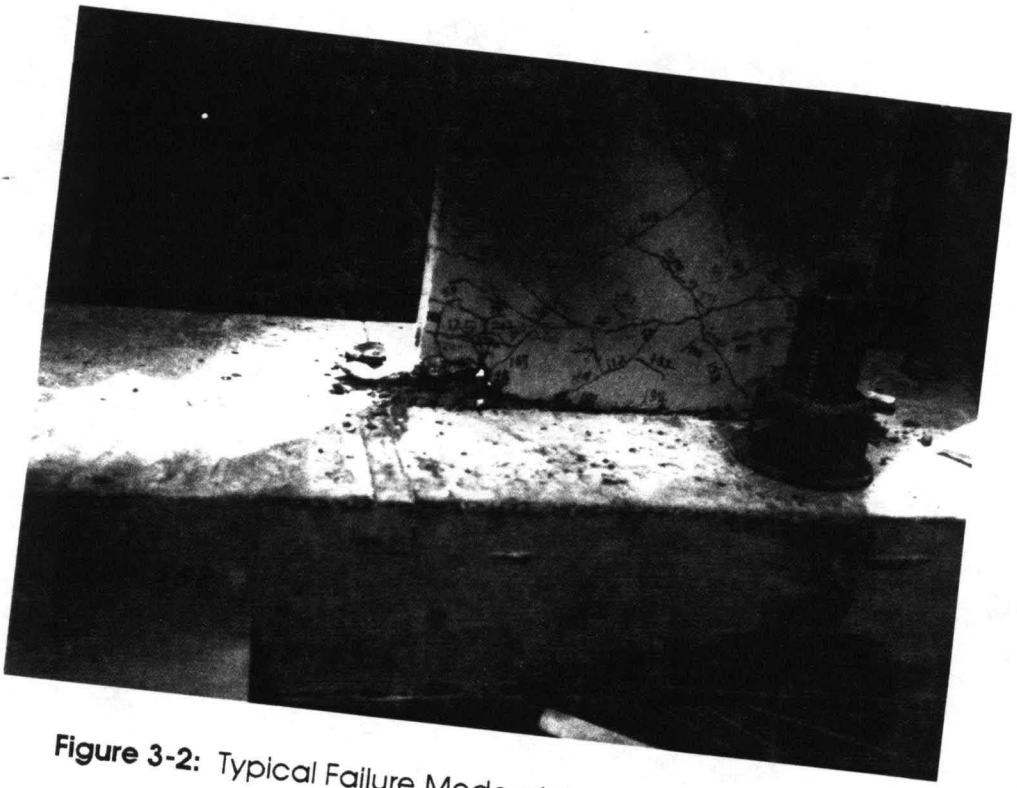

Figure 3-2: Typical Failure Mode at Bottoms of Shear Wall

Figure 3-3: Failure Mode of Shear Wall

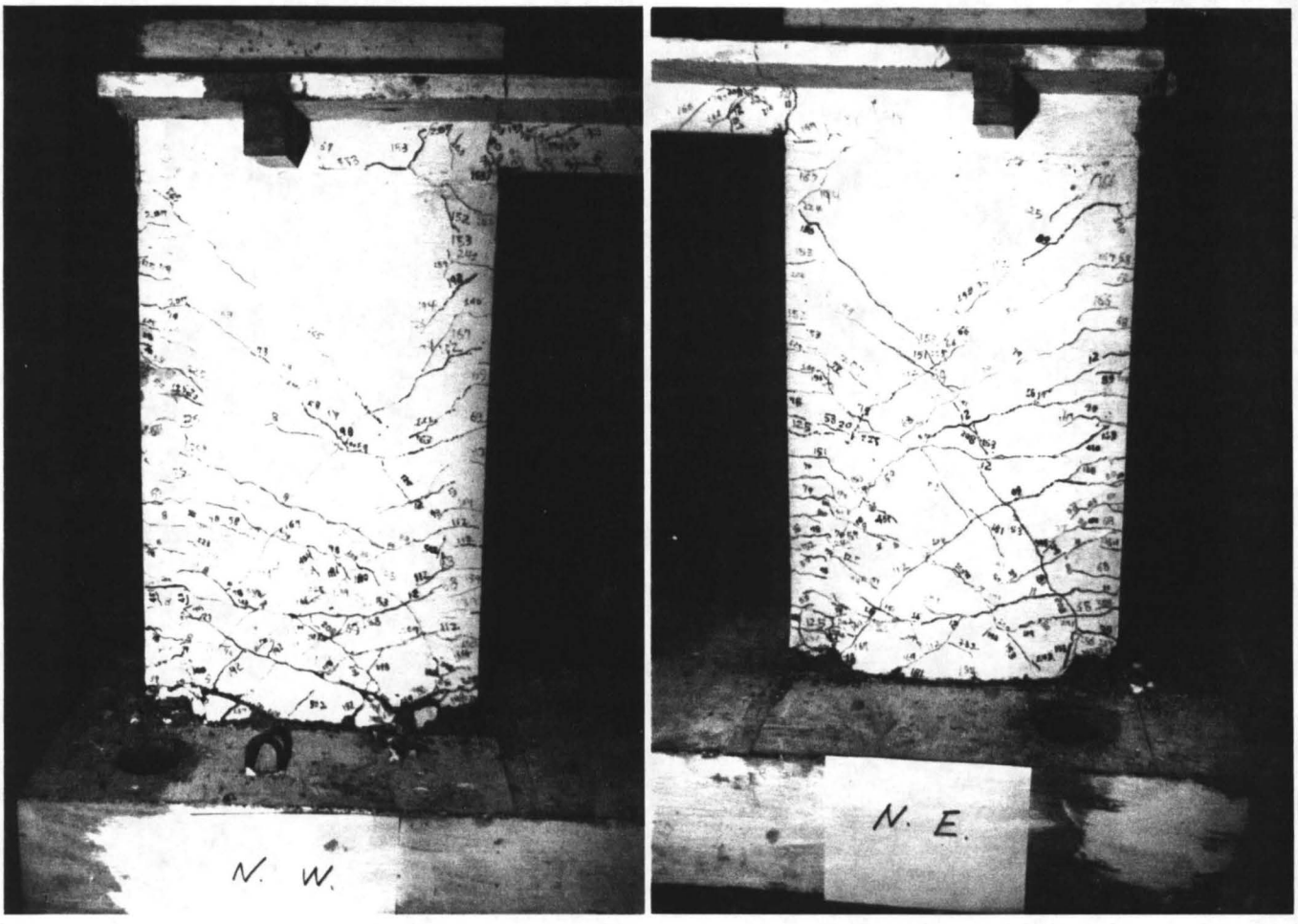

Figure 3-4: Concrete Cracks on the N. Sides of Shear Wall

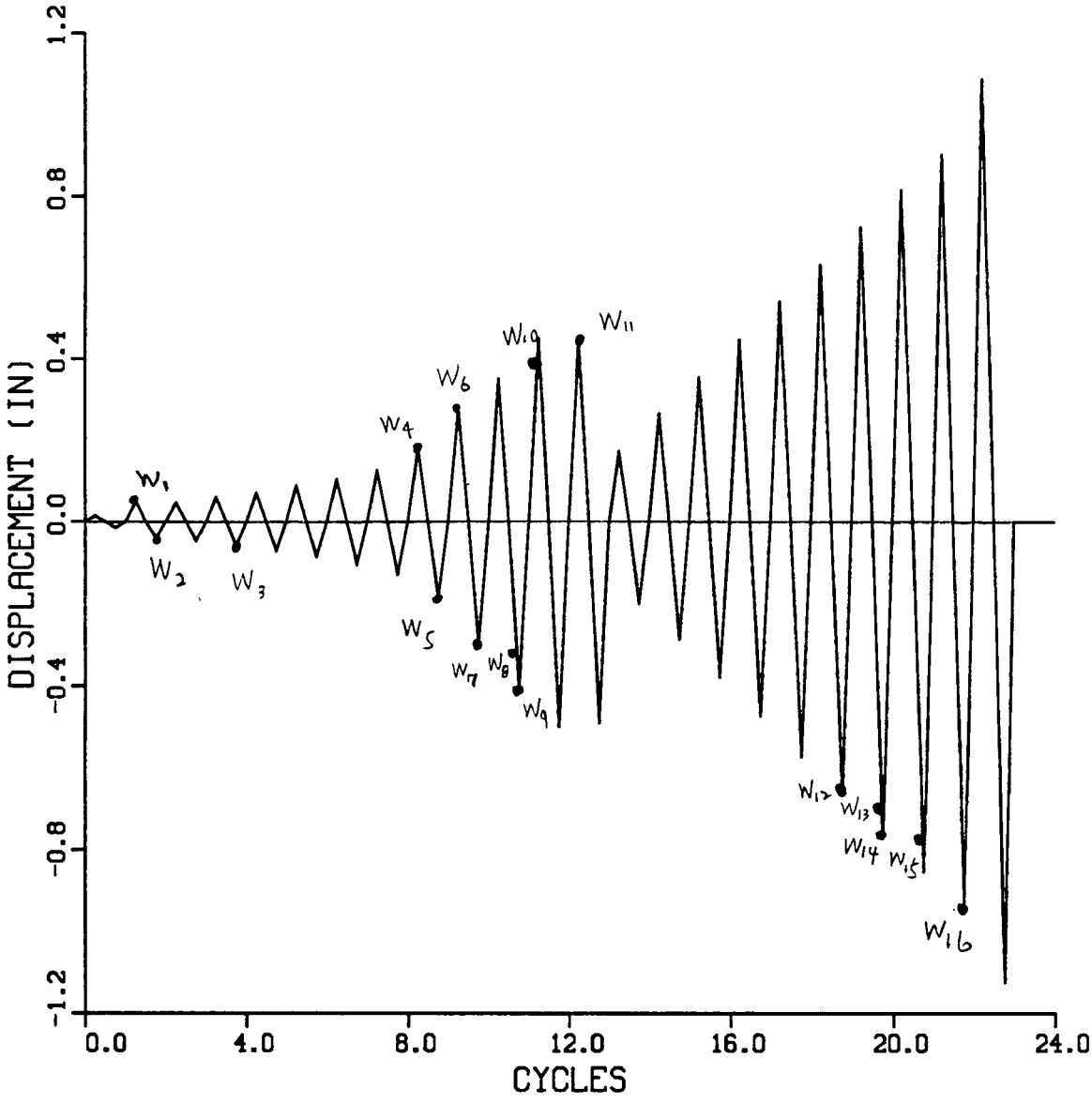

Figure 3-5: The Test Loading Program of Shear Wall

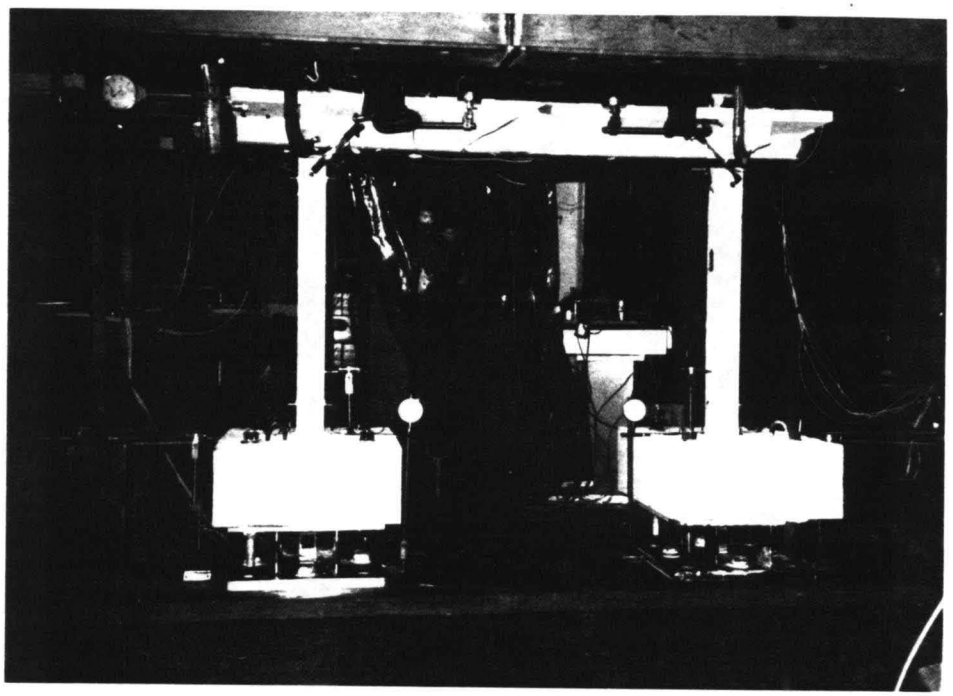

Specimen without Additional Weight

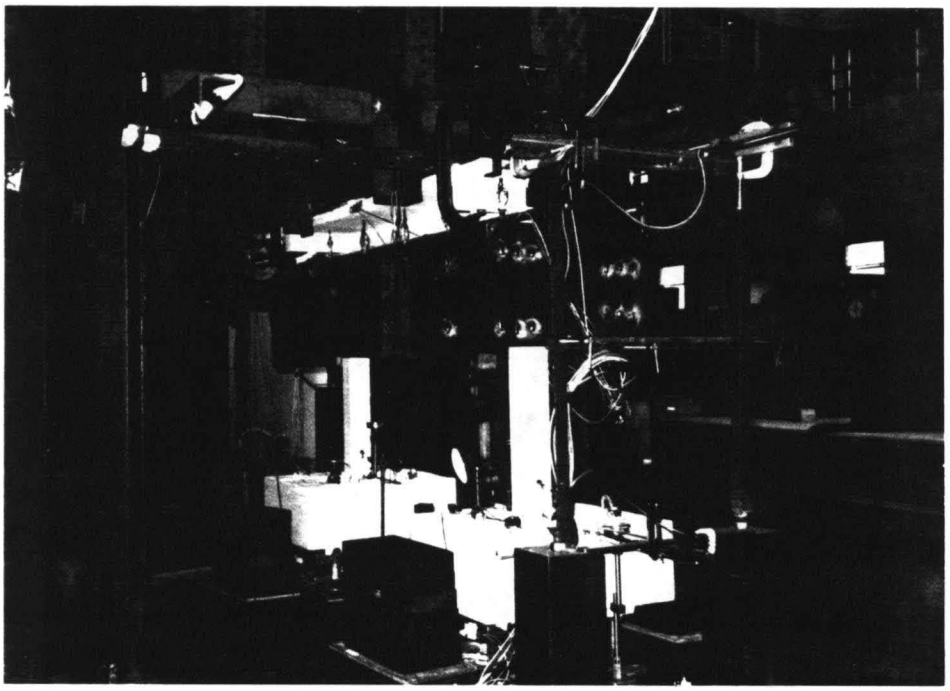

Specimen with Additional Weight

Figure 3-6: Test Setup of Frame

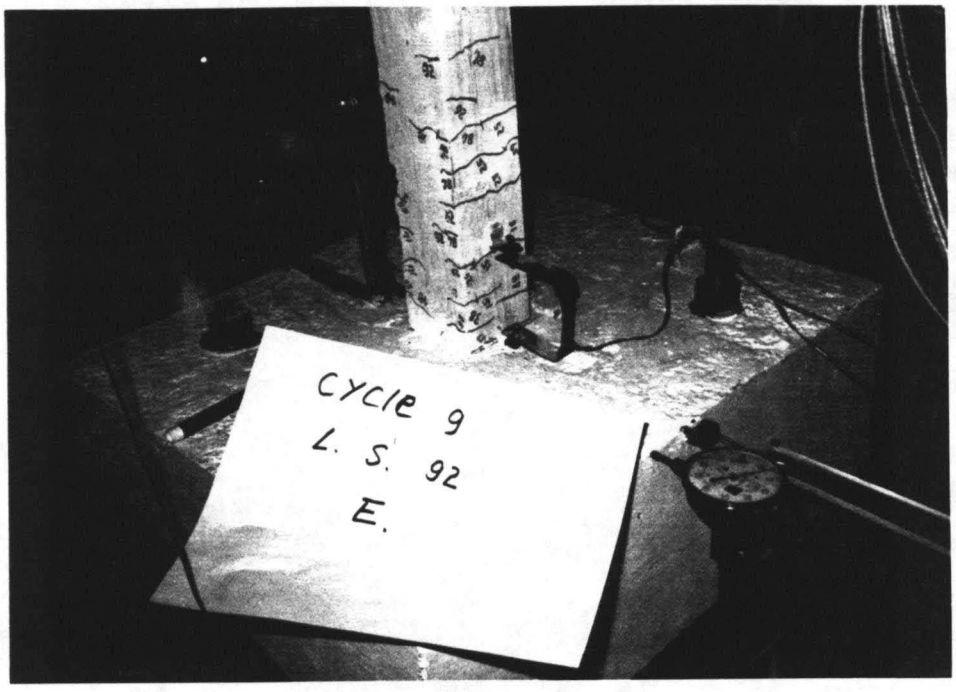

Initial Stage

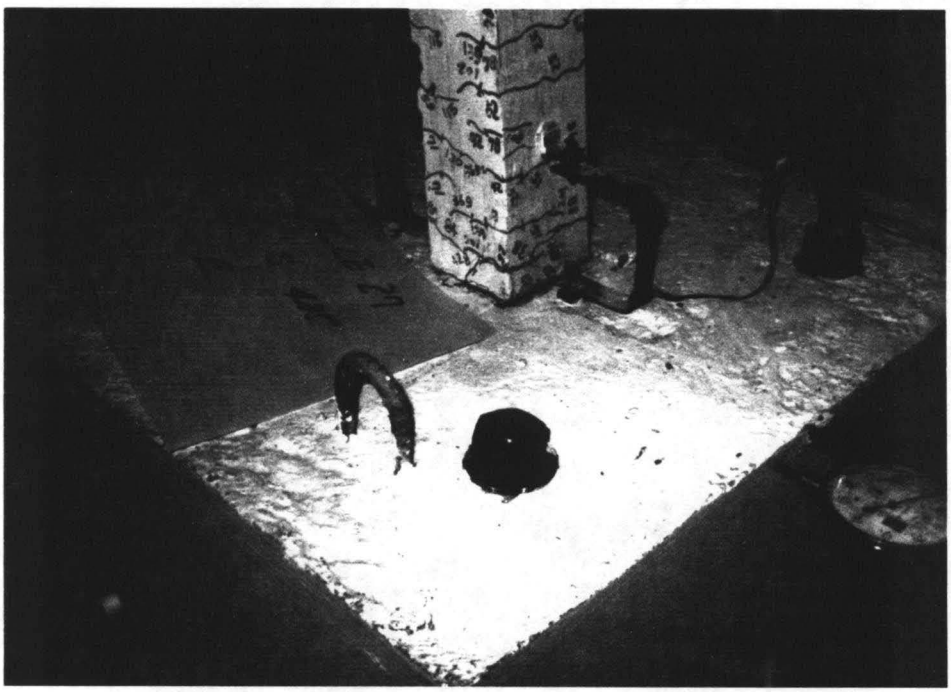

Ultimate Stage

Figure 3-7: Deformation at Base Region of the E. Column

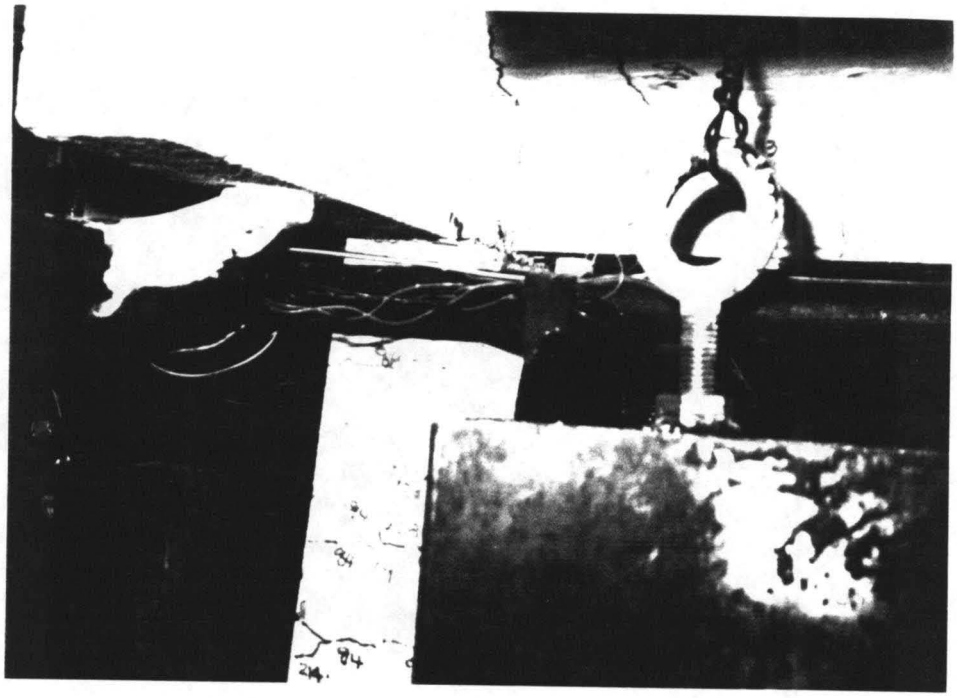

Figure 3-8: Deformation in Beam-Column Joint Region of Frame

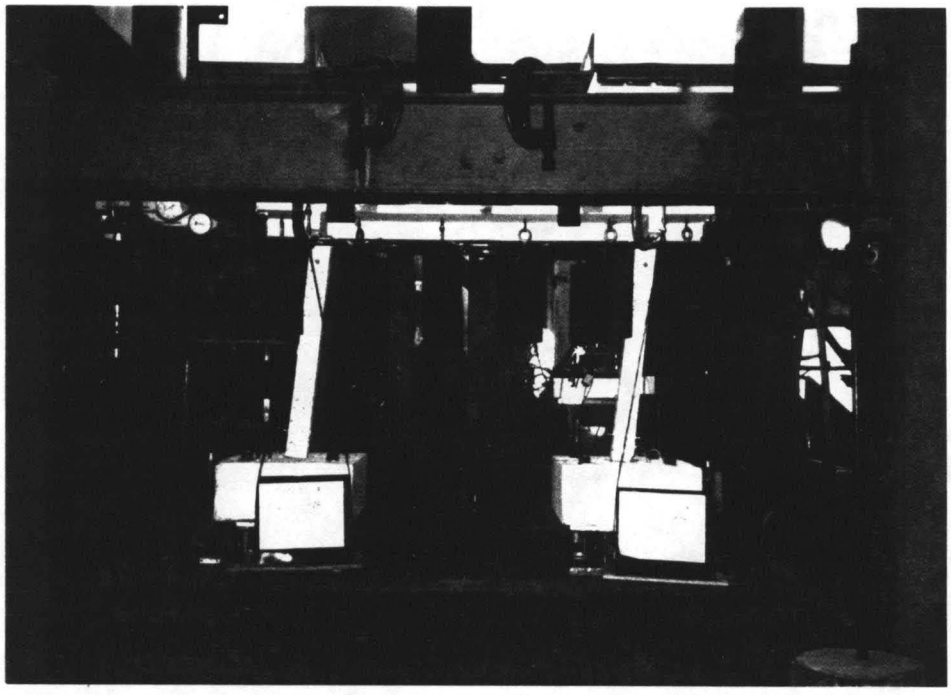

Figure 3-9: Ultimate Stage of Frame

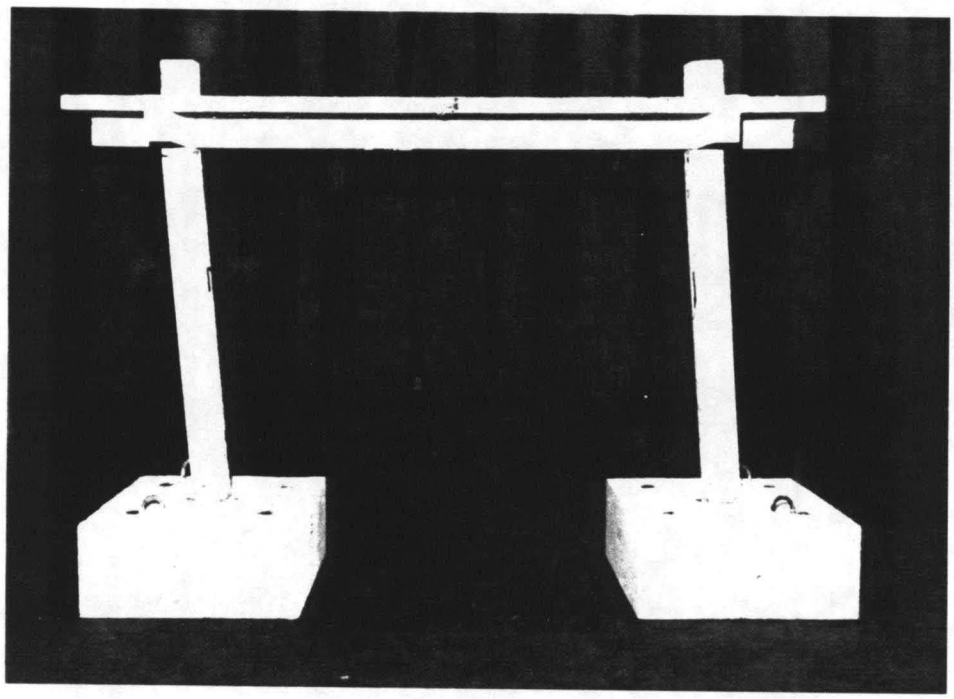

Figure 3-10: The Failure Mode of Frame

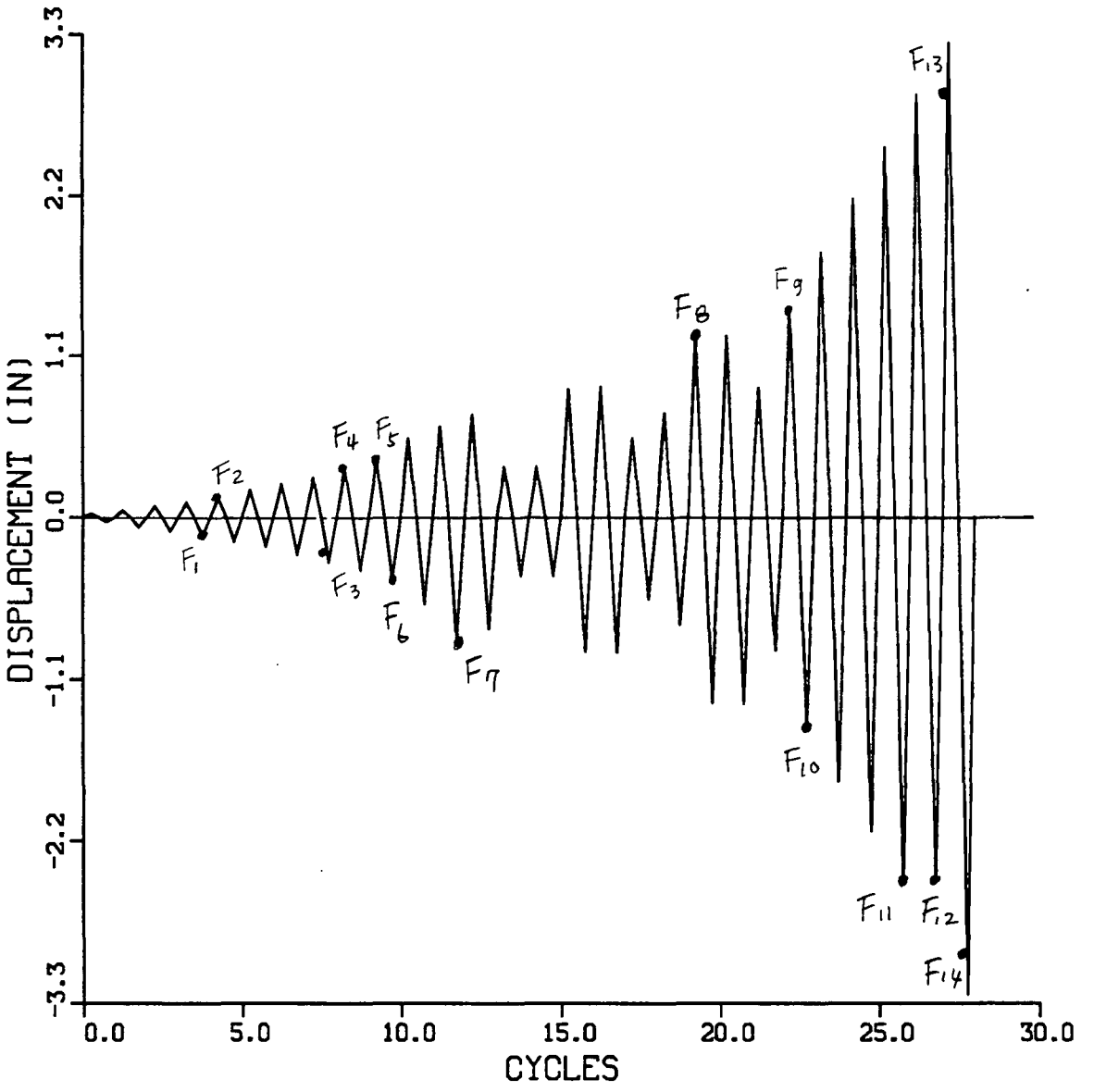

Figure 3-11: The Test Loading Program of Frame

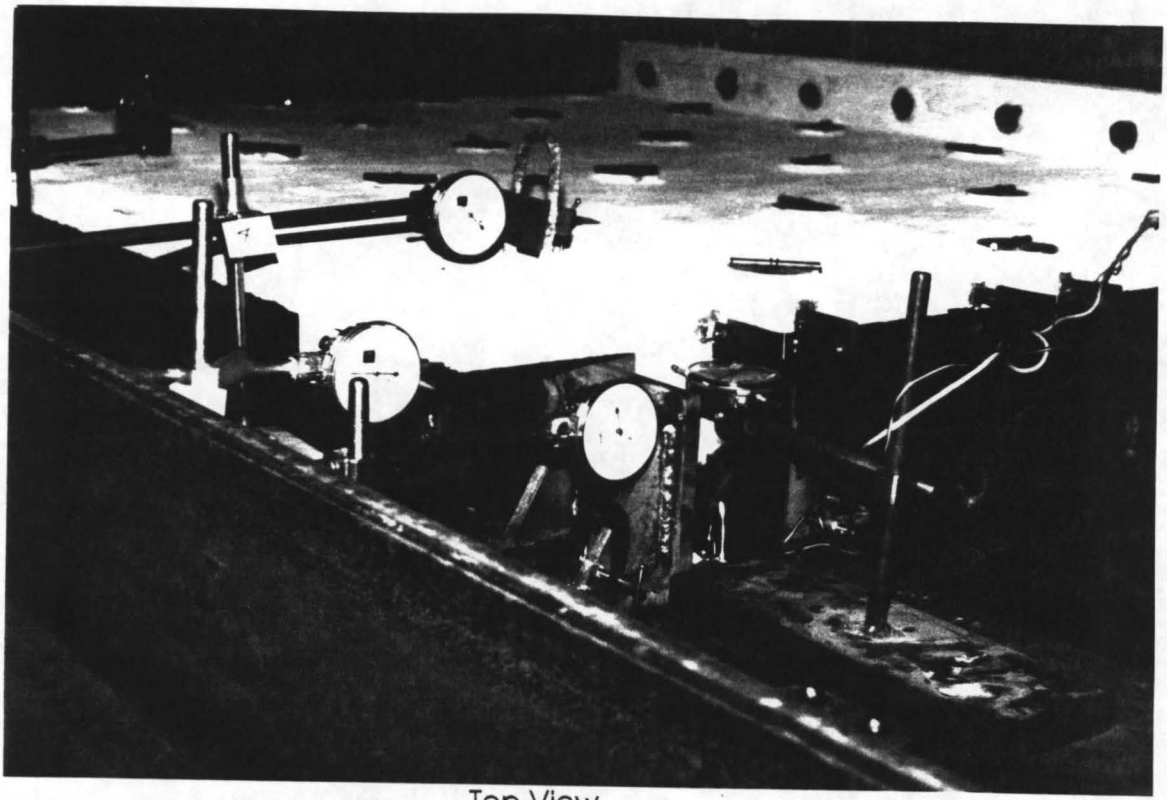

Top View

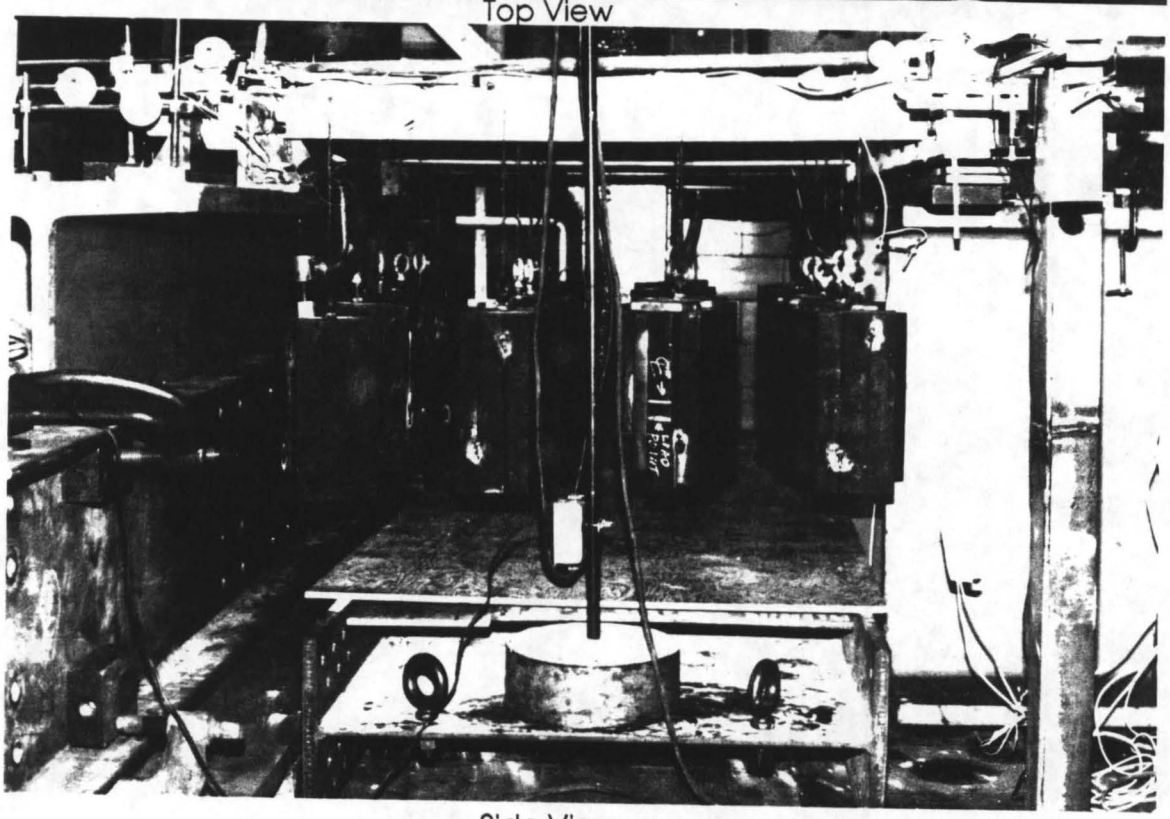

Side View

Figure 3-12: Test Setup of Slab

Initial Stage

Ultimate Stage

Figure 3-13: Concrete Cracking Pattern of Slab

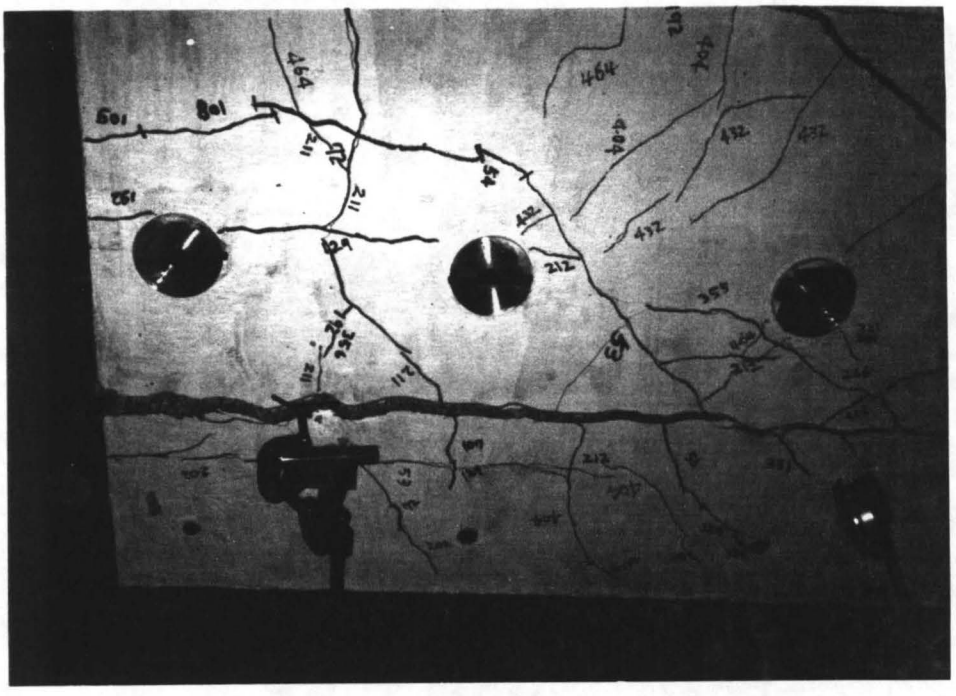

Figure 3-14: Slab Cracking Along the Support on the N. side

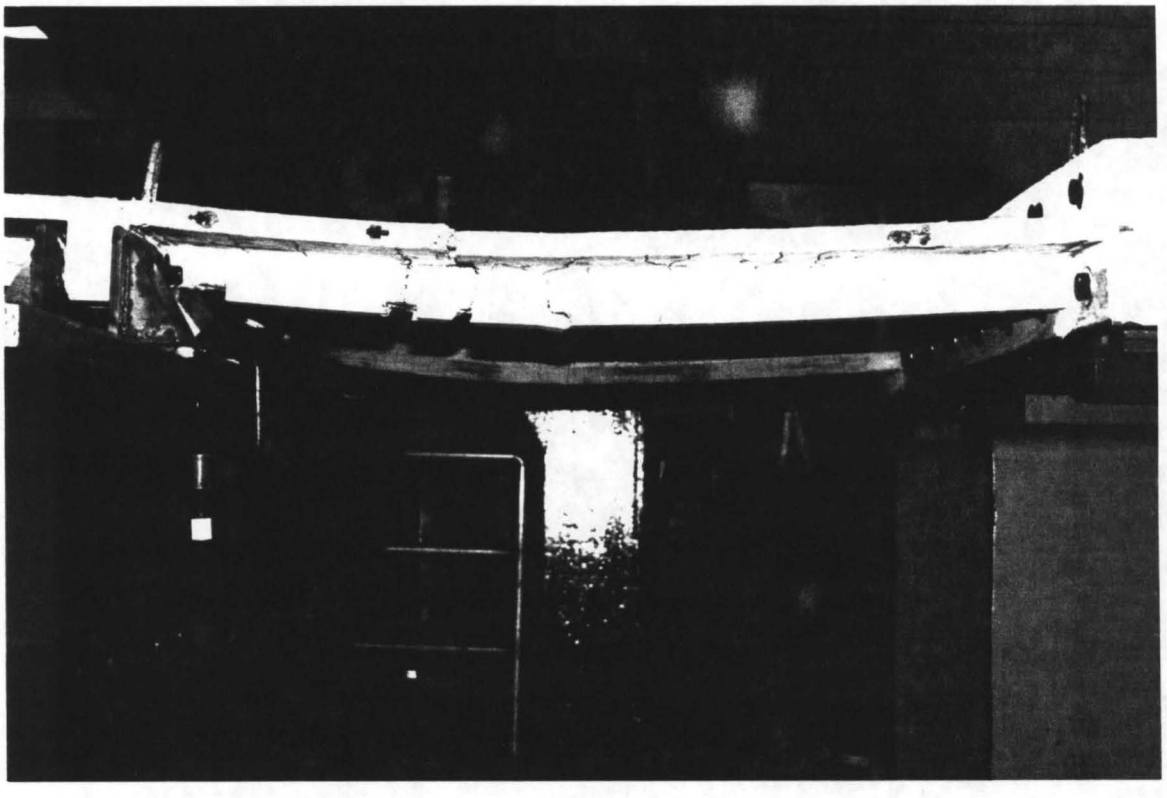

Figure 3-15: The Failure Mode of the S. Logitudinale Beam

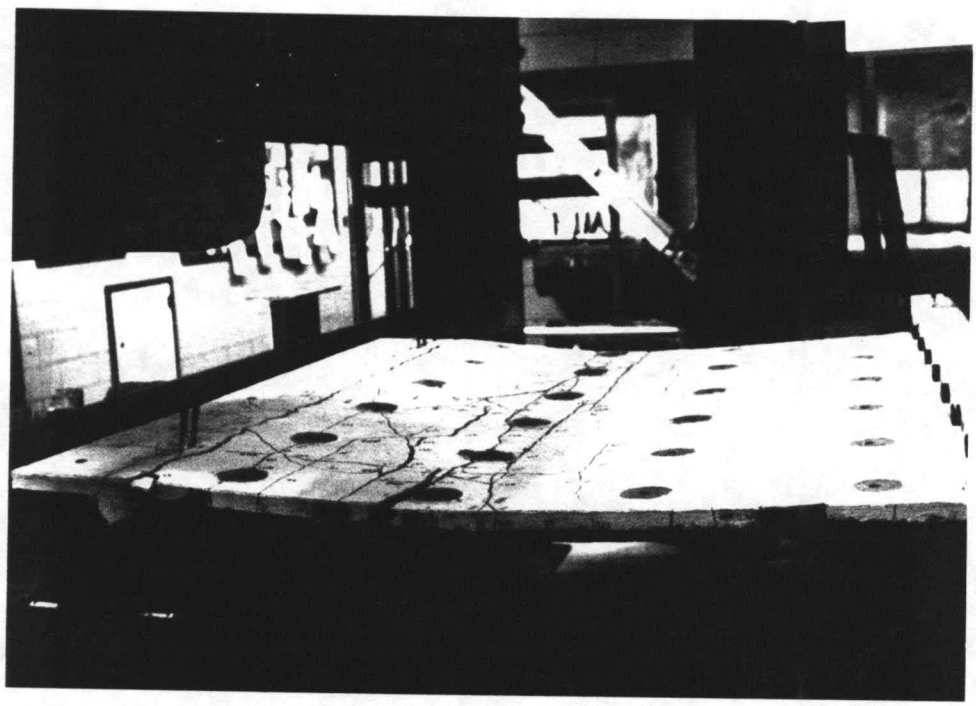

Figure 3-16: The Failure Mode of the Slab

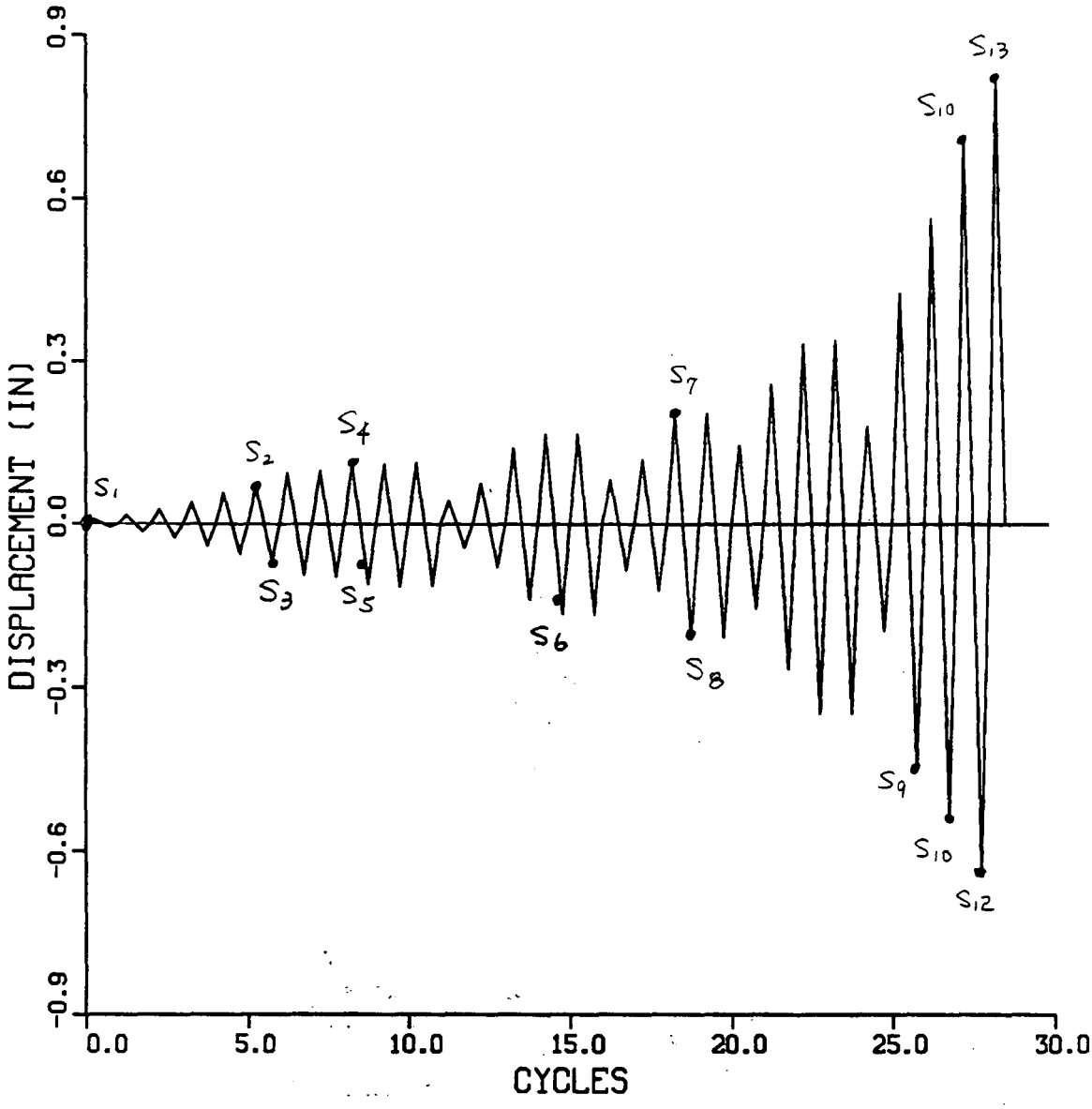

Figure 3-17: The Test Loading Program of Slab

Chapter 4
Experimental Results and Discussion

4.1 General

The experimental data of the three component structures had been processed in detail with more attention on the overall behaviors of the specimens. In this chapter, the processed experimental results of the three component specimens are presented in tables and figures. The overall behaviors of the component structures and their some elemental behaviors are described in form of load-deformation plots. The hysteresis diagrams, characterizing the overall behavior of specimen and the behavior of its components, are as follows:

P-Δ_t : hysteresis diagram of the overall behavior of specimen.

P-θ_b : hysteresis diagram of linking beam rotation.

M-θ_w : hysteresis diagram of shear wall rotation.

P-θ_c : hysteresis diagram of column rotation.

P-γ_{bc} : Hysteresis diagram of angle change between beam and column.

M-θ_s : Hysteresis diagram of slab rotation.

where P = the lateral load applied on the shear wall and frame specimens and the in-plane load applied on the slab specimen, M = the bending moment at the rotating section of specimens, Δ_t = the total displacement of the specimen (measured at the top for the shear wall and frame specimens and at the end for the slab specimen); θ_b = the rotation of the critical sections in the linking beams, θ_w = the rotation at the base of the shear wall, θ_c = the rotation of the critical sections in the columns, γ_{bc} = the angle change between the center lines of beam and column, and θ_s = the

rotation of the critical section of the slab.

4.2 Shear Wall

The test results of the shear wall specimen are shown as the lateral load-deformation relationships in Figs. 4-1 to 4-12. The peak loads for each cycle and the corresponding deformation at the peak points for the specimen are listed in Table 4-1.

The numbers at the some peak points indicate the cycle numbers as shown in Figs. 4-1 and 4-2. As described in the previous chapter, a total of 23 displacement cycles were applied on the shear wall specimen. The lateral load (P) vs. the top displacement (Δ_t) relationship of the shear wall specimen is plotted in Fig. 4-1. From the diagram, it is clear to see that the specimen remained essentially elastic through the first eight cycles The loading procedure of these eight cycles was controlled by load. However, due to the effect of small cracks in concrete, the stiffness of the shear wall deteriorated significantly in these cycles (see Fig. 4-8).

The ductility of the shear wall is 5.97 for the positive direction and 6.05 for the negative direction. In the calculation of the ductility, the deflection corresponding to the yielding strength is 0.1825 in. for the positive direction and 0.1862 in for the negative direction and the deflection corresponding to the ultimate strength is 1.0892 in. for the positive direction and 1.1256 in. for the negative direction. This large ductility is satisfied for the requirement in the seismic load resisting design for such type of structures.

The diagram of Fig. 4-1 was replotted in two diagrams separately, Figs. 4-2 and 4-3. The first 13 loading cycles were plotted in Fig. 4-2 and the last 10 cycles were plotted in Fig. 4-3. In these two separated load-deflection hysteresis diagrams, the seismic behavior of the specimen primaryly

changed from its bending-dominative behavior into its shearing-dominative behavior. In Fig. 4-2, the hysteresis loops are spindle-shaped in which the deflection was mainly contributed by bending deformation of the specimen. However, in Fig. 4-3, the hysteresis loops are pinched severely and the displacement of the structure was mainly contributed by the shearing deformation. For the same amplitude of the top displacement, the energy dissipated in a pinched loop was much smaller than that in a spindle-shaped loop. The hysteresis diagram of the last 10 cycles illustrates the significant strength degradation and severe stiffness deterioration of the structure.

By comparing the hysteresis loops in the two diagrams, it is obviously noted that the strength and stiffness of the structure were reduced significantly after a few small loading cycles were conducted when the structure observed its maximum strength point. The reason for this change is that the aggregate and steel got loose from concrete when some small loading cycles were applied on the structure. This phenomenon is reflecting the nature of seismic and also shaking table load. In a real problem, an acceleration of earthquake usually possesses many small cycles.

The maximum strength of the specimen was reached when the structure was still dominated by bending deformation. However, its ductility obtained 60% from the shearing deformation and the failure appeared the shearing failure mode. This may not be true in case of a tall shear wall in which the ratio of the height of the wall to its width is much larger and the failure mode will be in the bending failure.

The moment (M) vs. curvature (θ_w) hysteresis relationship at one base of the shear wall is represented in Fig. 4-4. This hysteresis diagram only consisted of the first 15 loading cycles because the clip gages measuring the base curvature were out of range at the end of cycle 15 due to the severe

damage of concrete and the large opening at the bases of the walls. The diagram shows that the curvature is not symmetric for cycles 12 and 13. The moment was acquired by multiplying the total load (P) by the height of the wall and divided by 2, in which the moment in each wall was assumed to be the same.

Fig. 4-5 gives the lateral load (P) vs. beam curvature (θ_b) hysteresis relationship of the linking beam for 22 cycles. The elemental behavior of the beam is symmetric and similar to the global hysteresis behavior of the shear wall specimen.

The sideway displacement was measured by three LVDT's at one end of the specimen (8). The three measuring points were respectively at levels of 14, 28 and 36 in. respectively. The data from these three points were plotted in Fig. 4-6 for the major peak cycles. The overall behavior of the specimen is displayed by two skeleton curves of the lateral load (P) vs. the top deflection (Δ_t) in Fig. 4-7. The curve 1 is obtained by connecting the peak displacement points of the first 10 cycles and the curve 2 by connecting the peak displacement points of the last 13 cycles.

The initial stiffness deterioration for each loading cycle in the shear wall tests was plotted in Fig. 4-8. The maximum stiffness is 224.72 kips/in and the minimum stiffness is 2.13 kips/in. The stiffness was calculated from the first load step for the two loading directions in each cycle. At the ultimate stage, only 0.95% of the initial stiffness was left. The hysteresis of absorbed and dissipated energy in the tests were represented by the diagrams in Figs. 4-9 to 4-12. The diagrams in Figs. 4-9 to 4-10 were respectively the energy absorbed and dissipated in each cycle during the tests. According to these figures, the maximum dissipated energy happened in cycle 12 in which the behavior of the specimen was dominated by bending deformation. In later

cycles with larger displacements, the dissipated energy was reduced contineously due to the effect of the pinched loops. In accumulated energy curves in Figs. 4-11 and 4-12, the plateau of the curves indicate that there were several small loading cycles applied on the structure.

4.3 frame

The results of the frame specimen are shown in Figs. 4-13 to 4-22. The hysteresis diagrams, characterizing the overall behavior of the specimen and its elemental behaviors are displayed in Figs. 4-13 to 4-17. The peak loads for each cycle and the corresponding deformation at the peak points for the specimen are listed in Table 4-2.

The lateral load (P) vs. the top displacement (Δ_t) relationship of the specimen is represented in Fig. 4-13. The numbers at the peak points in the diagram indicate the cycle number during the tests. This load-deformation hysteresis diagram clearly shows that the structure has a good symmetrical seismic behaviors for the two loading directions. The behavior of the structure could be considered to be elastic for the first 9 cycles. But, the structural stiffness was reduced in every cycle due to concrete cracks excepted two cycles for the negative loading in which the stiffness gained some value. The reason for the increases may be due to the incorrect measurement in the load or displacement (see Fig. 4-18).

The ductility of the frame specimen is 8.50 for the positive direction and 7.68 for the negative direction. In the calculation, the deflection corresponding to the yielding strength is 0.381 in. for the positive direction and 0.422 in. for the negative direction and the deflection corresponding to the ultimate strength is 3.237 in. for the positive direction and 3.239 in. for the negative direction. The property of the large ductility of the frame is

favorited in resisting seismic loads. And this large ductility was also desired for the tests on the assemblage structure because the adequate ductility of the middle frame without collapse would allowed the slab got into plastic range which in consequence triggered the redistribution of inertial force.

The hysteresis behavior of the frame is stable up to cycle 20 with a corresponding ductility of 3.11 and then the strength began to degradate for each additional cycle. The cyclic behavior of the specimen was dominated by bending deformation throughout the whole test procedure.

The elemental hysteresis behaviors of the structures are displayed in Figs. 4-14 to 4-15. The diagrams in these three figures contained the test results for the first 24 cycles. Fig. 4-14 gives the lateral load (P) vs. the column curvature (θ_c) hysteresis of the specimen. The curvature was measured at the base of the right column of the frame. Fig. 4-15 gives the lateral load (P) vs. the beam curvature (θ_b) hysteresis which was measured at the end of the beam where a plastic hinge was formed. The hysteresis loops of the column curvature are spindle-shaped and indicate that the behavior of column was controlled by bending deformation. The hysteresis loops of the beam curvature are pinched to some extent and indicate that the behavior of the beam was contributed by both bending and shearing deformation. The shearing deformation of the beam curvature was induced by the additional weights on the specimen. For the first 24 cycles, the curvature ductilities 6.41 for the column deformation and 3.61 for the beam deformation. They are the average values for the two loading direction. The fact of the column observing a larger curvature ductility than beam means that the deflection of the frame gained more contribution from column deformation than from the beam deformation. Fig. 4-16 gives the lateral load (P) vs. the angle change (γ_{bc}) between the center lines of beam

and column.

The envelope of hysteresis behavior of the frame is shown in Fig. 4-17. The diagram is plotted by connecting the peak displacement points of major peak loading cycles. The overall behavior of the structure is distinctly classified into three stages in this diagram: the elastic behavior, plastic deformation and the load dropping. In the first stage, the displacement of the frame was combinated by the elastic deformation of steel and concrete and concrete cracking. In the second stage, the opening and closing of concrete cracks and inelastic deformation of steel were the major contribution of the displacement of the frame. For the third stage, the load dropping was caused by the concrete crushing and the buckling of the steel bars.

The stiffness deterioration for the whole test history of the frame is shown in Fig. 4-18. The diagram displays a consistent decreasing of the stiffness as the applied displacement increasing except only a few cycles. The maximum initial stiffness for the structure is 4.00 kips/in and the minimum ultimate stiffness is 0.55 kips/in.. 13.8% of the initial stiffness was left at the ultimate stage.

The hystories of the absorbed and dissipated energy for the frame tests are represented in Figs. 4-19 to 4-22. The energy absorbed and dissipated in each cycle is given respectively in Figs. 4-19 and 4-20. The maximum absorbed and dissipated energy happened in the last cycle. This indicated again that the hysteresis behavior of the frame was controlled by the bending deformation and the structure was stable for the future larger displacement. From these figures, it is also clearly to see that the structure dissipated the same amount of energy in the two loading directions. It is very important for structure possessing a symmetrical behavior in dissipating

the earthquake energy. Otherwise, the structure will be unstable if it accumulates too much deflection in one direction. Figs. 4-21 to 4-22 give the accumulated energy curves for the specimen. On these two curves, there are some kick points which are reflecting the small repeated loading cycles in the tests.

4.4 Slab

The test results of the slab specimen are shown in Figs. 4-23 to 4-31. The hysteresis diagrams, characterizing the overall behaviors of the specimen and its critical section behavior are displayed in Fig. 4-23 to 4-26. The peak load for each cycle and the corresponding deformation at the peak points for the specimen are listed in Table 4-3.

The in-plane load (P) vs. the in-plane displacement (Δ_t) relationship of the specimen is represented in Fig. 4-23. The numbers at the peak points in the diagram indicate the cycle number during the tests. The last cycle (29) was only applied in the positive direction because the loading frame was out of range. Similar to the shear wall and frame specimens, the load-deflection hysteresis relationship also shows that the slab has a good symmetrical seismic behaviors for the two loading directions. Due to the severe crack along the fixed supporting end caused by the additional hanging weights, the slab lost its essential stiffness before the in-plane load applied. During the test, the structure appeared in elastic behavior for the first 16 cycles. However, the structural stiffness during this stage was maintained by the elastic deformation of those reinforcing bars which were not yielded yet.

The ductility of the slab specimen is 3.51 for the positive direction and 3.14 for the negative direction based on the first 28 cycles. In the

calculation, the deflection corresponding to the yielding strength is 0.2006 in. for the positive direction and 0.2044 in. for the negative direction and the deflection corresponding to the ultimate strength is 0.7036 in. for the positive direction and 0.6428 in. for the negative direction.

The hysteresis behavior of the slab was stable up to cycle 28 for the positive direction and to cycle 27 for the negative direction. The hysteresis loops of the slab are spindle-shaped with slightly pinched. It means that the cyclic behavior of the specimen was dominated by bending deformation throughout the whole test procedure with some effect of the shearing deformation.

The in-plane bending moment (M) vs. the curvature (θ_s) hysteresis relationship is given in Fig. 4-24. The curvature hysteresis was measured at the critical section which was located about 15 in. from the fixed support end. The bending moment was obtained by multiplying the in-plane load by the arm which was measured from the loading jack to the critical section. The diagram shows a unsymmetrical hysteretic behavior of the section with most curvature accumulating in the positive direction for the large cycles. From the crack and yielding partan of the slab, it is clear to see that the deformation of the slab concentrated on the critical section for the positive direction, but the deformation was more uniformly distributed along the slab in the negative direction.

The sideway in-plane displacement history of the slab is plotted in Fig. 4-25 for the two loading directions for 17 peak cycles. The displacement was measured at four points along the edge of the slab (8). The four points were located respectively at 12, 24, 36 and 48 in. from the fixed supporting end. The global behavior of the slab is given by the skeleton curve in Fig. 4-26.

The initial stiffness deterioration for each loading cycle in the slab tests

was plotted in Fig. 4-27. The maximum stiffness is 48.39 kips/in. in the positive direction and the minimum stiffness is 1.88 kips/in. in the negative direction. The stiffness was calculated from the first load step for each loading direction in each cycle. At the ultimate stage, only 4% of the initial stiffness was left. The histories of absorbed and dissipated energy in the tests were represented in Figs. 4-28 to 4-31. The diagrams in Figs. 4-28 to 4-29 were respectively the energy absorbed and dissipated in each cycle during the tests. According to these figures, the maximum energy dissipated happened in cycle 28 (cycle 29 is not plotted). It implies that the slab would dissipated more energy if larger cycles were applied. In the accumulated energy curves in Figs. 4-30 and 4-31, the small curves in the plottings indicate that there were several small loading cycles applied on the structure.

Table4

Table 4-1: Experimental Data of Shear Wall

Load Point	Lateral Load (kips)	Top Displacement (in.)	Beam Curvature (rad.)	Shear Wall Curvaure (rad.)
1^{+}_{-}	3.00	.0147	.0001089	.0001289
1^{+}_{-}	-3.00	-.0152	-.0000930	-.0000836
2^{+}_{-}	6.00	.0507	.0003304	.0004723
2^{+}_{-}	-6.00	-.0412	-.0002527	-.0002417
3+	6.00	.0473	.0003458	.0005553
3-	-6.00	-.0480	-.0003946	-.0003652
4+	7.00	.0606	.0003643	.0004150
4-	-7.00	-.0602	-.0004663	-.0000415
5+	8.00	.0719	.0004509	.0006372
5-	-8.00	-.0727	-.0005064	.0003064
6+	9.00	.0894	.0005583	.0015417
6-	-9.00	-.0861	-.0006013	-.0001710
7+	10.00	.1051	.0007212	.0017676
7-	-10.00	-.1058	-.0006646	.0002963
8+	11.00	.1273	.0007664	.0010622
8-	-11.00	-.1290	-.0007815	-.0007205
9+	12.53	.1825	.0008716	.0013355
9-	-12.78	-.1862	-.0012871	-.0018743
10+	13.67	.2787	.0012655	.0041432
10-	-13.52	-.3002	-.0020560	-.0035880
11+	13.53	.3532	.0019937	.0060310
11-	-13.52	-.4038	-.0025531	-.0046168
12+	13.40	.4527	.0024606	.0168264
12-	-13.35	-.4992	-.0029658	-.0042783
13+	11.61	.4441	.0018901	.0129364
13-	-12.03	-.4905	-.0027135	-.0051961
14+	5.72	.1743	.0002909	-.0000189
14-	-2.57	-.1993	-.0008490	-.0011985
15+	6.94	.2668	.0007599	.0022527
15-	-4.70	-.2857	-.0010608	-.0018759
16+	8.87	.3564	.0012680	
16-	-8.03	-.3797	-.0014864	
17+	10.60	.4495	.0017888	
17-	-10.36	-.4734	-.0019534	
18+	10.65	.5431	.0022150	
18-	-11.36	-.5726	-.0024226	
19+	11.10	.6328	.0025740	
19-	-10.90	-.6655	-.0028324	
20+	10.94	.7264	.0030105	
20-	-10.03	-.7657	-.0032852	
21+	9.66	.8173	.0033843	
21-	-8.46	-.8539	-.0034871	
22+	8.45	.9040	.0036430	
22-	-7.46	-.9471	-.0036481	
23+	8.64	1.0892		
23-	-6.14	-1.1256		

Table 4-2: Experimental Data of Middle Frame

Load Point	Lateral Load (kips)	Top Displacement (in.)	Beam Curvature (rad.)	Column Curvature (rad.)	Angle Change Between B. & C. (rad.)
1+	.100	.025	-.00006	-.00025	.00042
1-	-.100	-.031	-.00008	-.00031	.00021
2+	.200	.047	.00001	.00013	.00078
2-	-.200	-.063	-.00026	-.00077	-.00112
3+	.300	.077	.00011	.00036	.00152
3-	-.300	-.092	-.00035	-.00100	-.00137
4+	.400	.103	.00024	.00058	.00192
4-	-.400	-.125	-.00033	-.00122	-.00210
5+	.500	.138	.00026	.00088	.00241
5-	-.500	-.161	-.00043	-.00145	-.00212
6+	.600	.186	.00040	.00120	.00313
6-	-.600	-.197	-.00057	-.00176	-.00270
7+	.700	.224	.00045	.00145	.00383
7-	-.700	-.248	-.00079	-.00206	-.00313
8+	.800	.267	.00053	.00175	.00454
8-	-.800	-.299	-.00098	-.00241	-.00414
9+	.900	.333	.00064	.00231	.00555
9-	-.900	-.354	-.00122	-.00277	-.00458
10+	1.000	.381	.00076	.00263	.00630
10-	-1.000	-.422	-.00141	-.00343	-.00556
11+	1.100	.531	.00111	.00427	.00797
11-	-1.100	-.587	-.00186	-.00535	-.00712
12+	1.150	.615	.00129	.00532	.00935
12-	-1.150	-.854	-.00234	-.00843	-.01109
13+	1.130	.695	.00135	.00607	.01114
13-	-1.020	-.756	-.00221	-.00730	-.00993
14+	.620	.337	.00092	.00236	.00776
14-	-.430	-.392	-.00127	-.00349	-.00471
15+	.620	.337	.00090	.00239	.00781
15-	-.430	-.395	-.00127	-.00346	-.00481
16+	1.170	.869	.00181	.00817	.01321
16-	-1.100	-.911	-.00251	-.00890	-.01277
17+	1.150	.886	.00186	.00833	.01354
17-	-1.060	-.915	-.00252	-.00890	-.01297
18+	.730	.532	.00145	.00453	.00967
18-	-.650	-.551	-.00166	-.00484	-.00701
19+	.956	.707	.00175	.00642	.01146
19-	-.885	-.731	-.00209	-.00677	-.00843
20+	1.200	1.228	.00239	.01266	.01767
20-	-1.120	-1.264	-.00298	-.01293	-.01797
21+	1.160	1.230	.00251	.01260	.01918
21-	-1.115	-1.269	-.00325	-.01276	-.01780
22+	.890	.877	.00207	.00849	.01523
22-	-.875	-.904	-.00249	-.00870	-.01368

Table 4-2, continued

23+	1.190	1.409	.00275	.01487	.02256
23-	-1.100	-1.432	-.00340	-.01485	-.02259
24+	1.190	1.805	.00335	.01907	.02856
24-	-1.095	-1.802	-.00395	-.01908	-.02972
25+	1.160	2.171			
25-	-1.070	-2.136			
26+	1.100	2.529			
26-	-1.060	-2.493			
27+	1.040	2.884			
27-	-1.000	-2.474			
28+	.912	3.237			
28-	-.900	-3.239			

Table 4-3: Experimental Data of Slab

Load Point	In-Plane Load (kips)	In-Plane Displacement (in.)	Slab Curvature (rad.)
1+	.300	.0069	.000000
1-	-.300	-.0056	-.000002
2+	.600	.0155	.000001
2-	-.600	-.0147	-.000003
3+	.900	.0250	.000002
3-	-.900	-.0256	-.000009
4+	1.200	.0386	.000002
4-	-1.200	-.0414	-.000010
5+	1.500	.0560	.000003
5-	-1.420	-.0547	-.000013
6+	1.700	.0686	-.000002
6-	-1.645	-.0703	-.000016
7+	1.990	.0930	.000009
7-	-1.950	-.0936	-.000016
8+	1.960	.0958	.000010
8-	-1.990	-.0969	-.000023
9+	2.090	.1095	.000016
9-	-2.130	-.1110	-.000028
10+	2.090	.1087	.000022
10-	-2.122	-.1152	-.000023
11+	2.130	.1103	.000016
11-	-2.090	-.1130	-.000028
12+	.960	.0410	-.000000
12-	-.690	-.0441	-.000017
13+	1.485	.0733	.000009
13-	-1.280	-.0797	-.000023
14+	2.408	.1372	.000021
14-	-2.250	-.1388	-.000041
15+	2.555	.1636	.000028
15-	-2.430	-.1653	-.000059
16+	2.535	.1646	.000033
16-	-2.375	-.1662	-.000062
17+	1.335	.0789	-.000001
17-	-1.030	-.0854	-.000034
18+	1.900	.1166	.000010
18-	-1.670	-.1230	-.000048
19+	2.683	.2006	.000066
19-	-2.560	-.2044	-.000086
20+	2.650	.2010	.000069
20-	-2.468	-.2080	-.000074
21+	2.050	.1436	.000025
21-	-1.622	-.1560	-.000043
22+	2.840	.2553	.000116
22-	-2.600	-.2654	-.000136

Table 4-3, continued

23+	2.865	.3313	.000269
23-	-2.600	-.3472	-.000305
24+	2.740	.3371	.000316
24-	-2.535	-.3471	-.000295
25+	1.755	.1776	.000032
25-	-1.090	-.1961	-.000092
26+	2.880	.4247	.000853
26-	-2.658	-.4504	-.000351
27+	2.920	.5618	.001568
27-	-2.618	-.5459	-.000039
28+	2.980	.7036	.002239
28-	-2.400	-.6428	.000197
29+	2.780	.8162	

Figure4

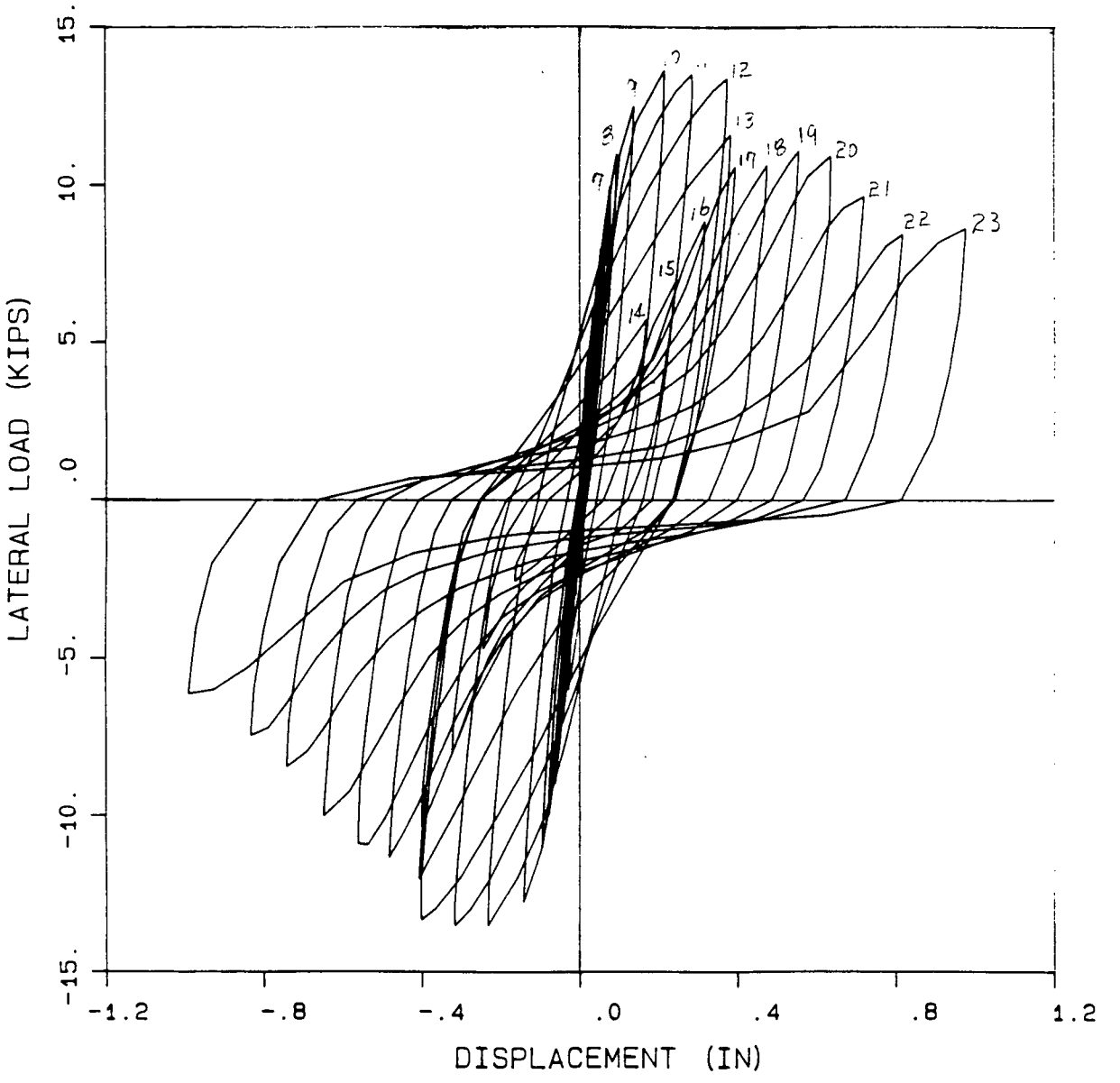

Figure 4-1: Load (P) vs. Dispalcement (Δ_t) of Shear Wall

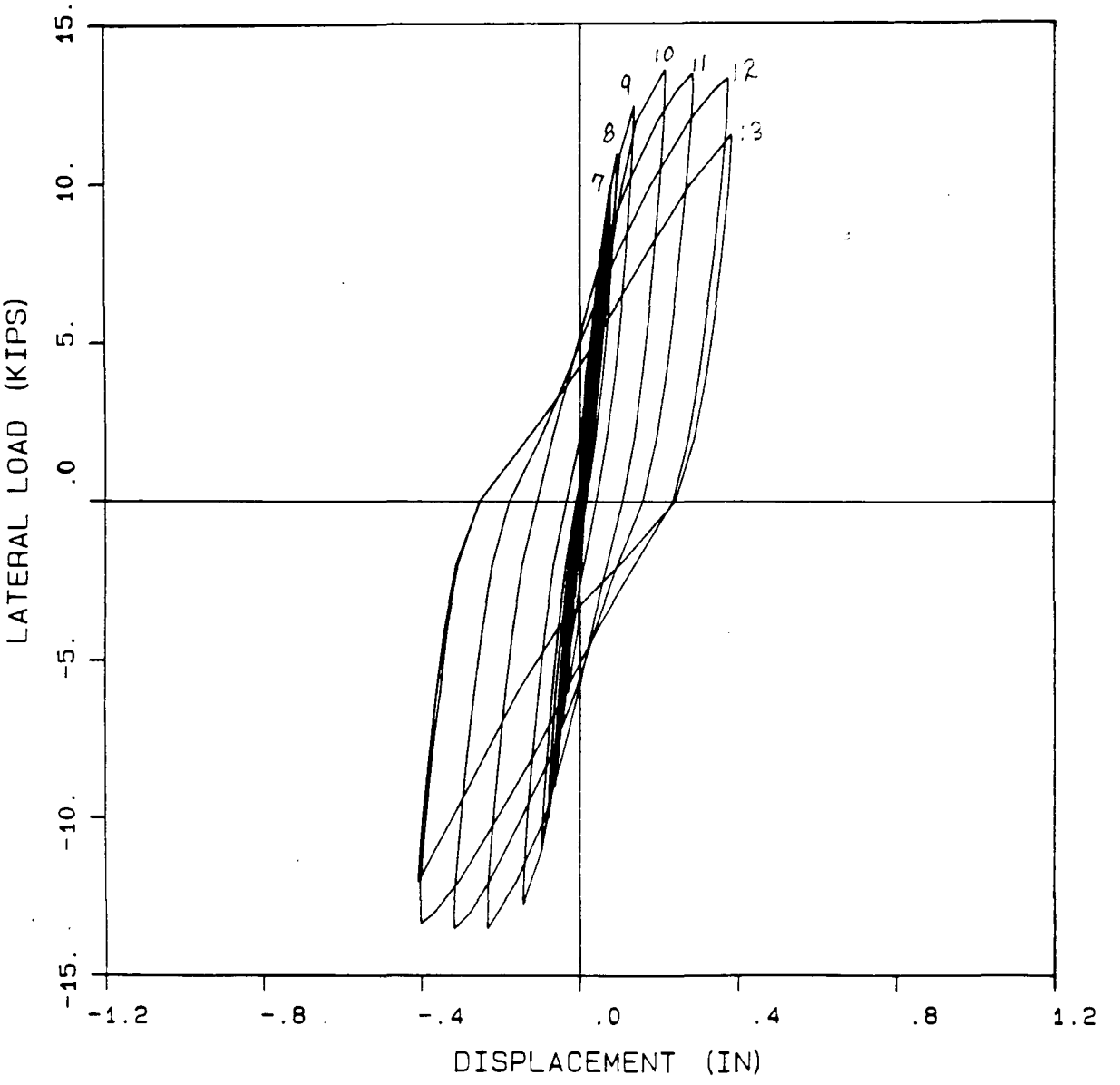

Figure 4-2: Load (P) vs. Dispalcement (Δ_t) of Shear Wall
(First 13 Cycles)

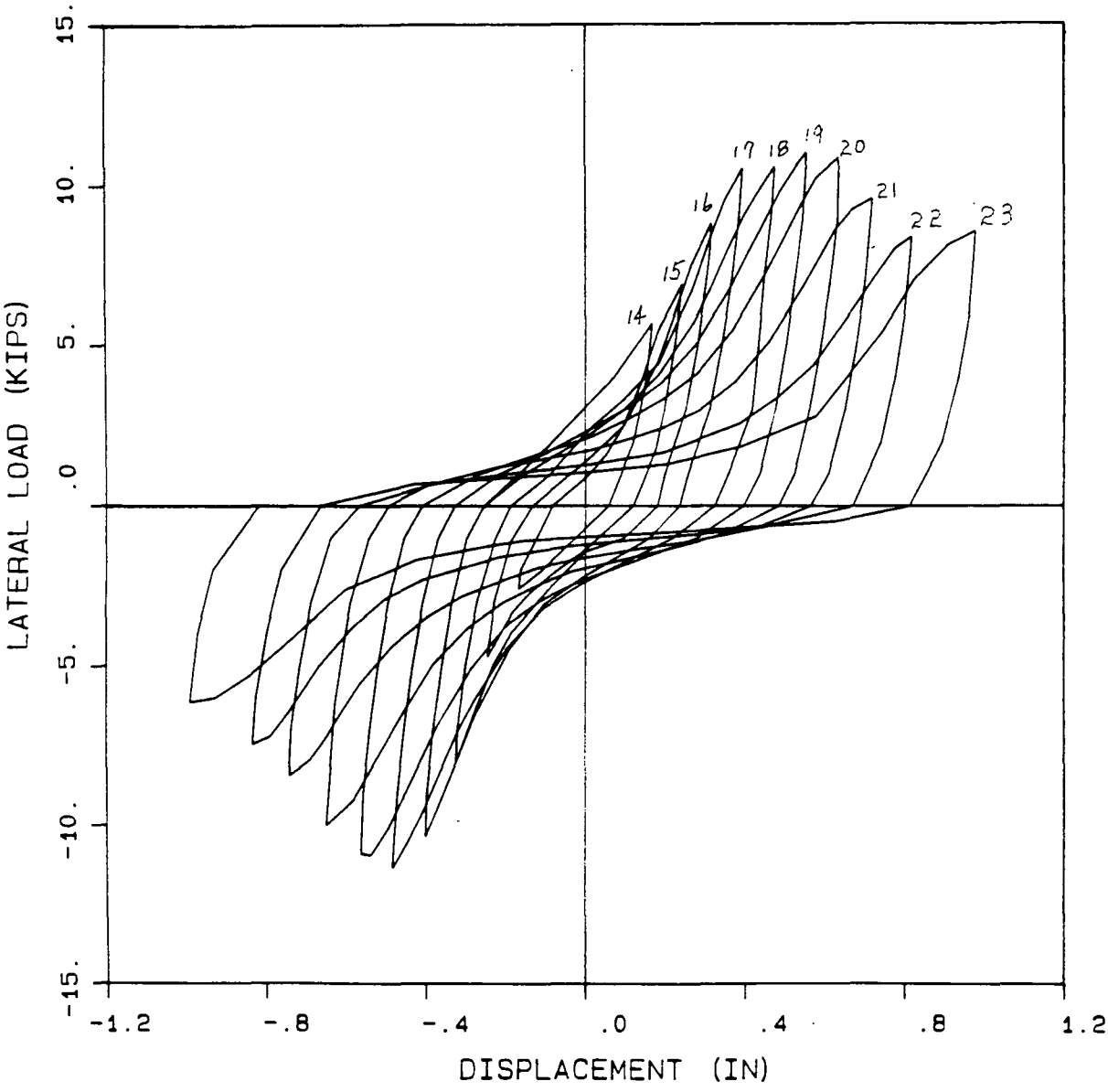

Figure 4-3: Load (P) vs. Displacement (Δ_t) of Shear Wall
(Last 10 Cycles)

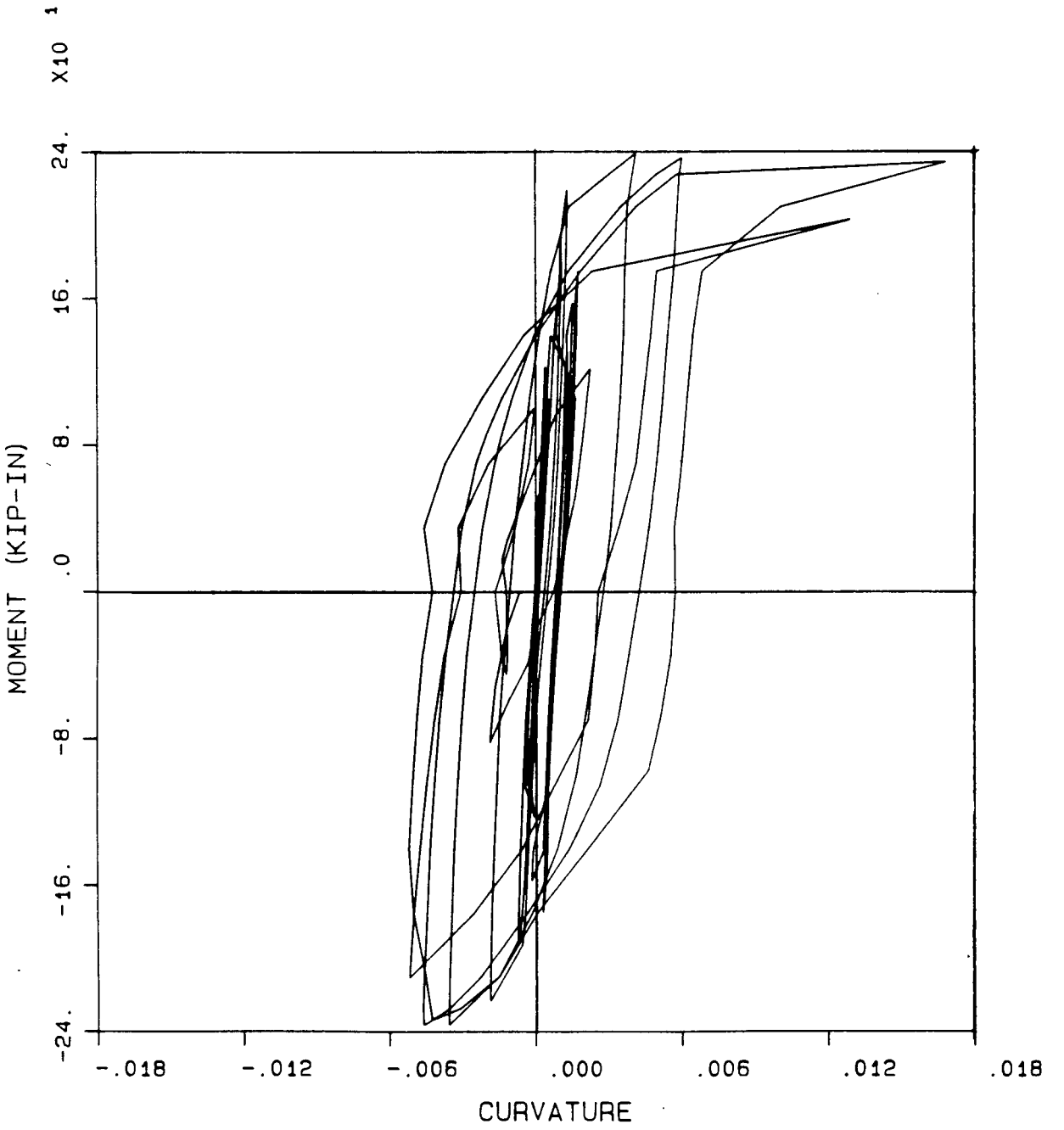

Figure 4-4: Moment (M) vs. Curvature (θ_w) at Bottom of Shear Wall

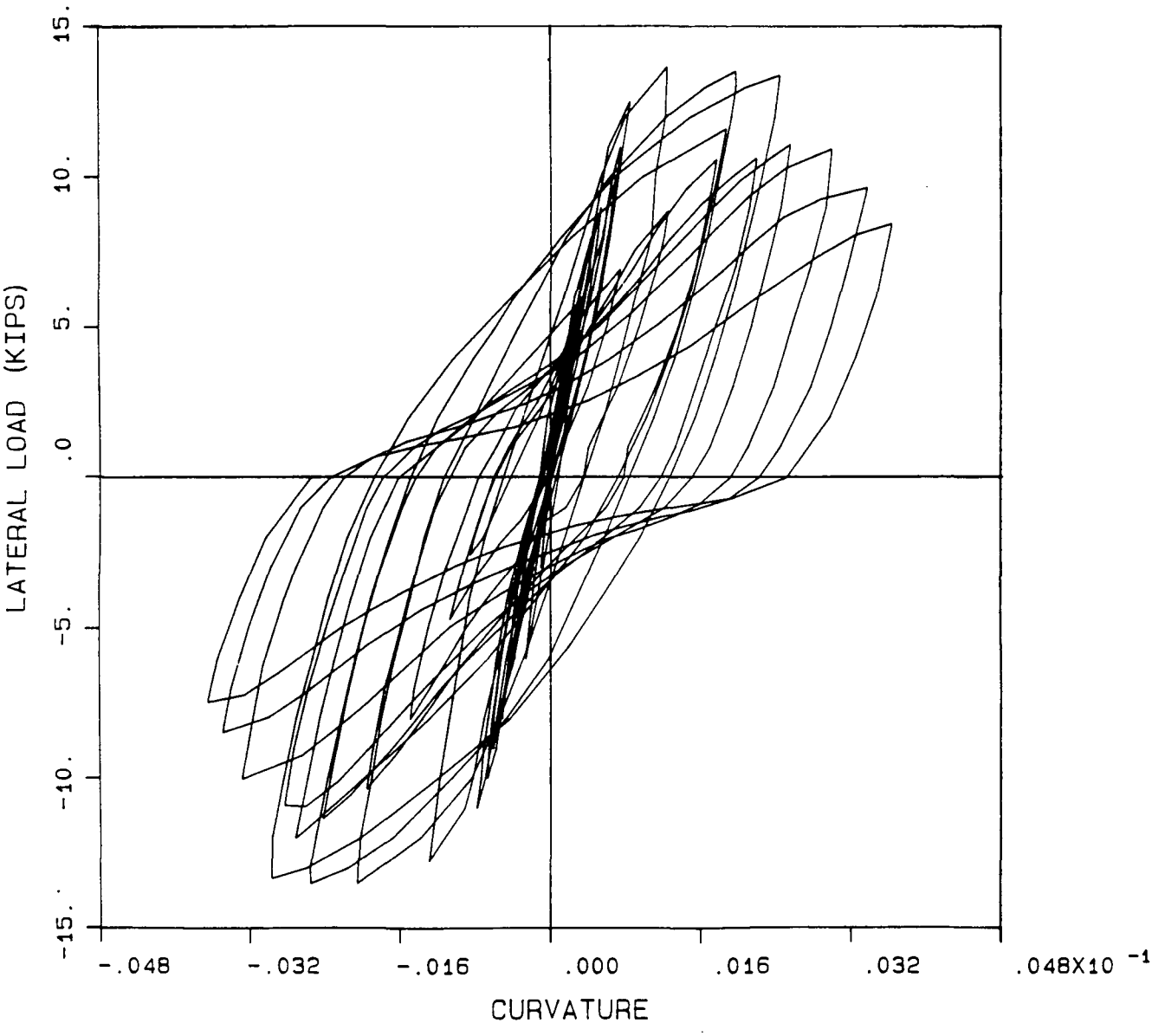

Figure 4-5: Load (P) vs. Beam Curvature (θ_b) of Shear Wall

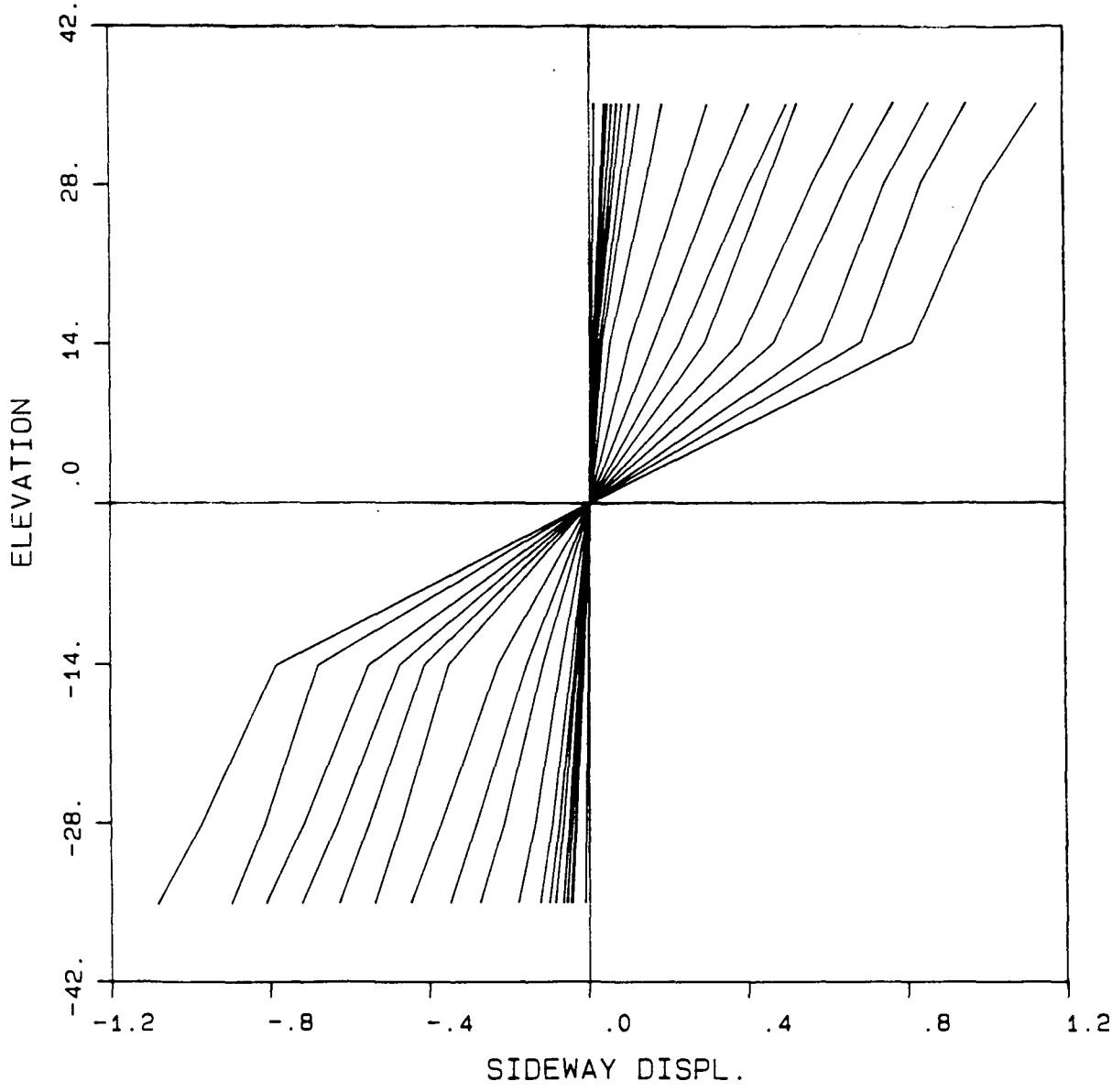

Figure 4-6: Sideway Displacement of Shear Wall

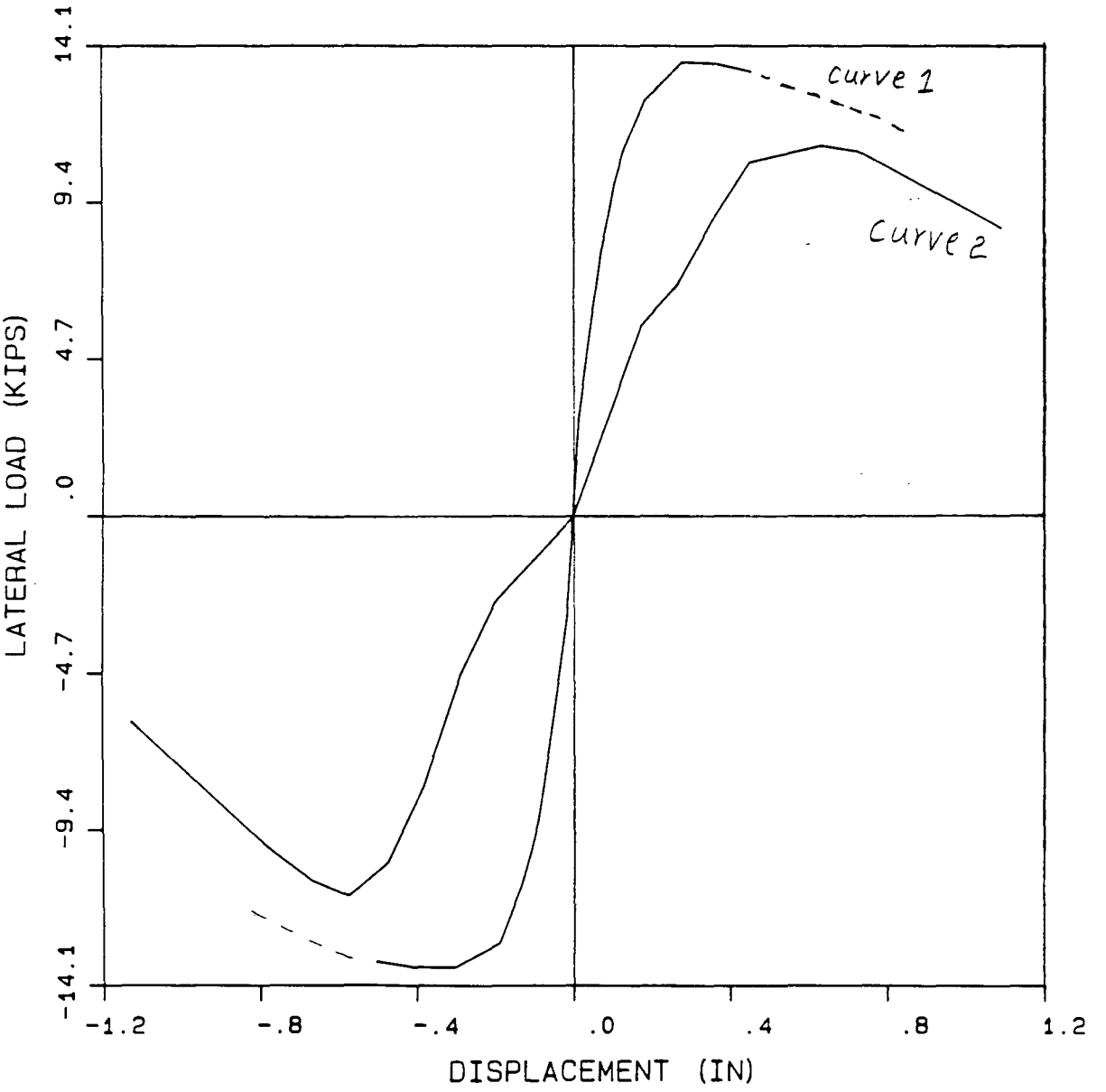

Figure 4-7: Skeleton Curves of Shear Wall

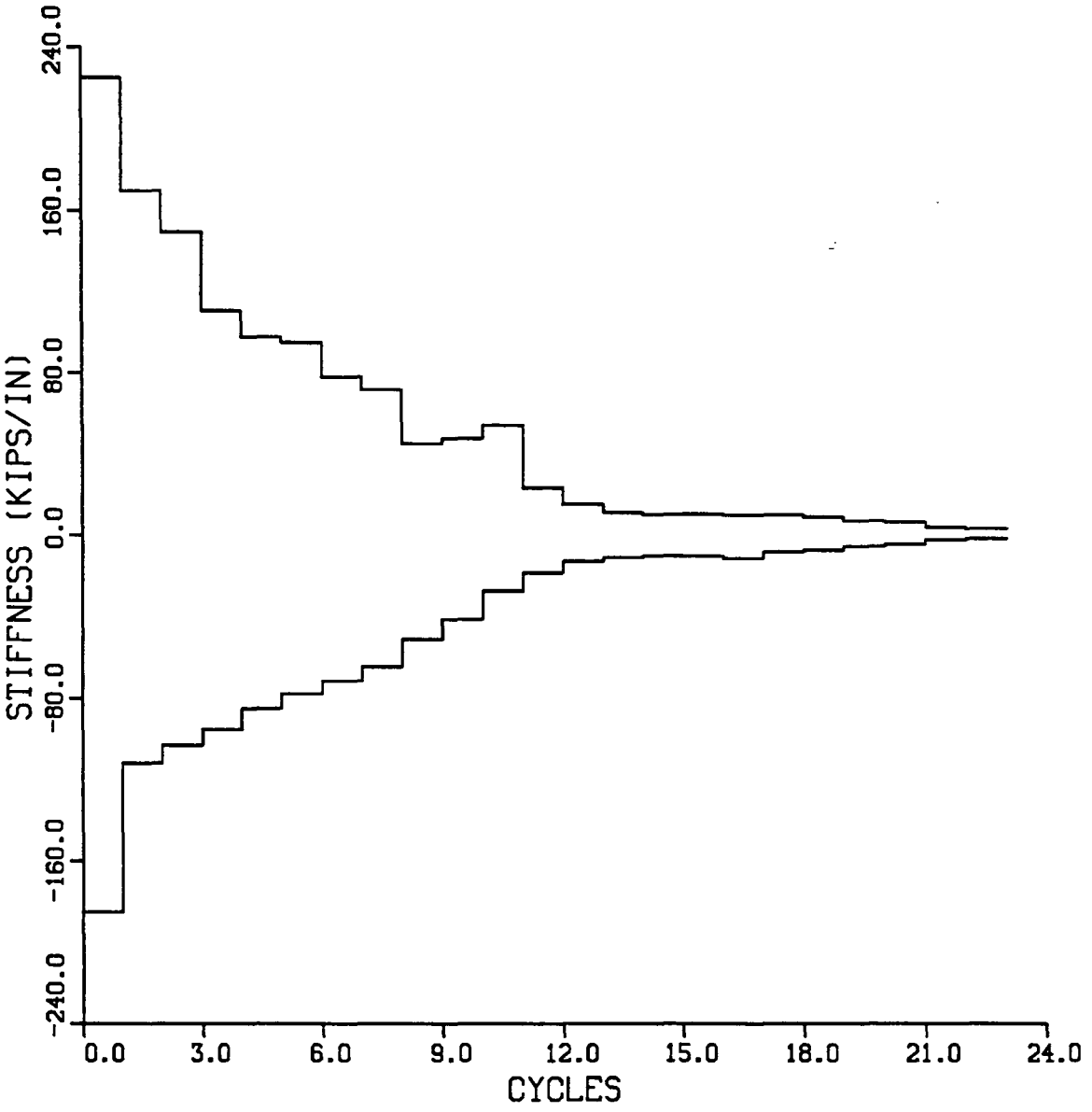

Figure 4-8: Stiffness Deterioration in Each Cycle of Shear Wall

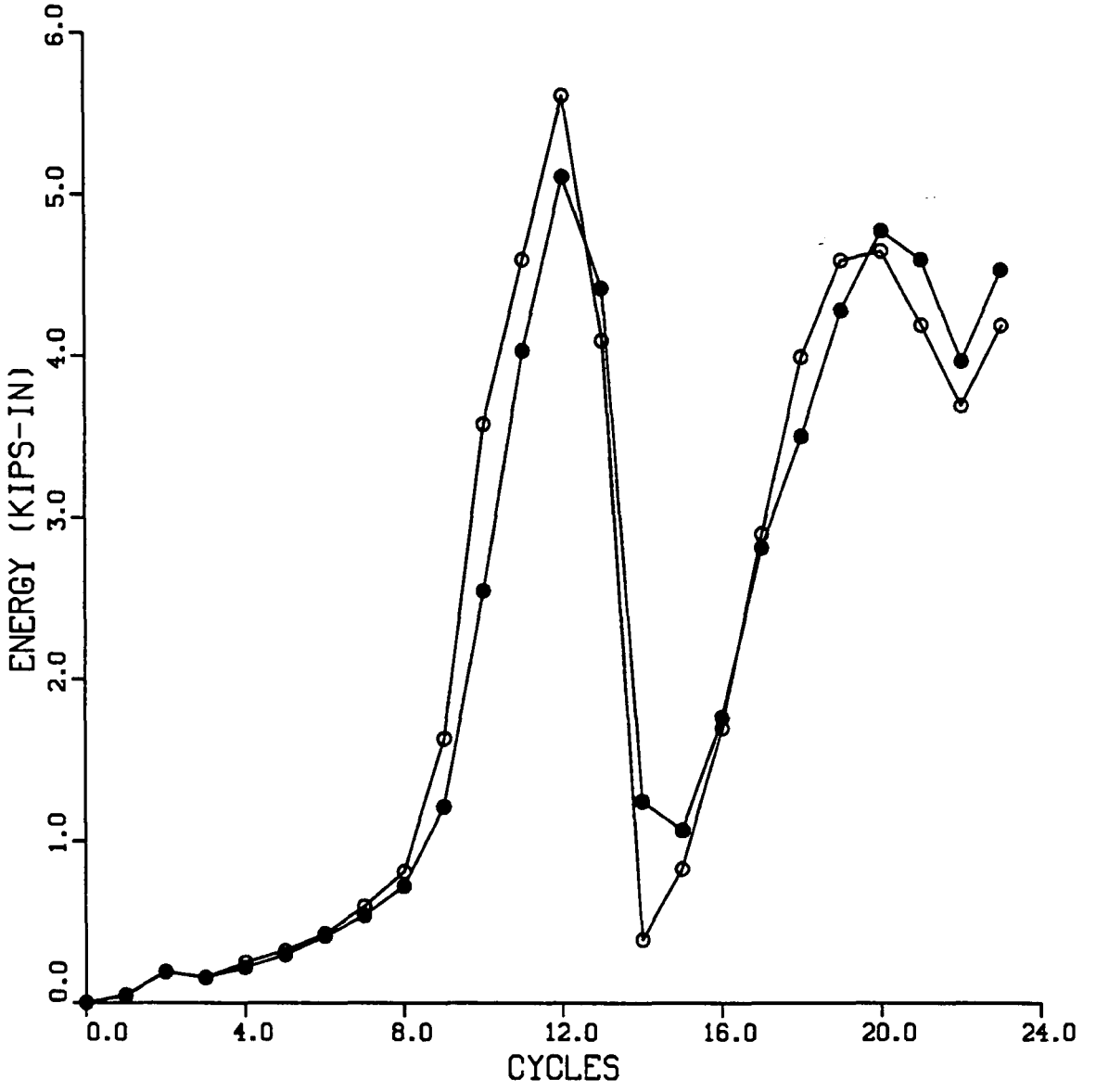

Figure 4-9: Energy Absorbed in Each Cycle of Shear Wall

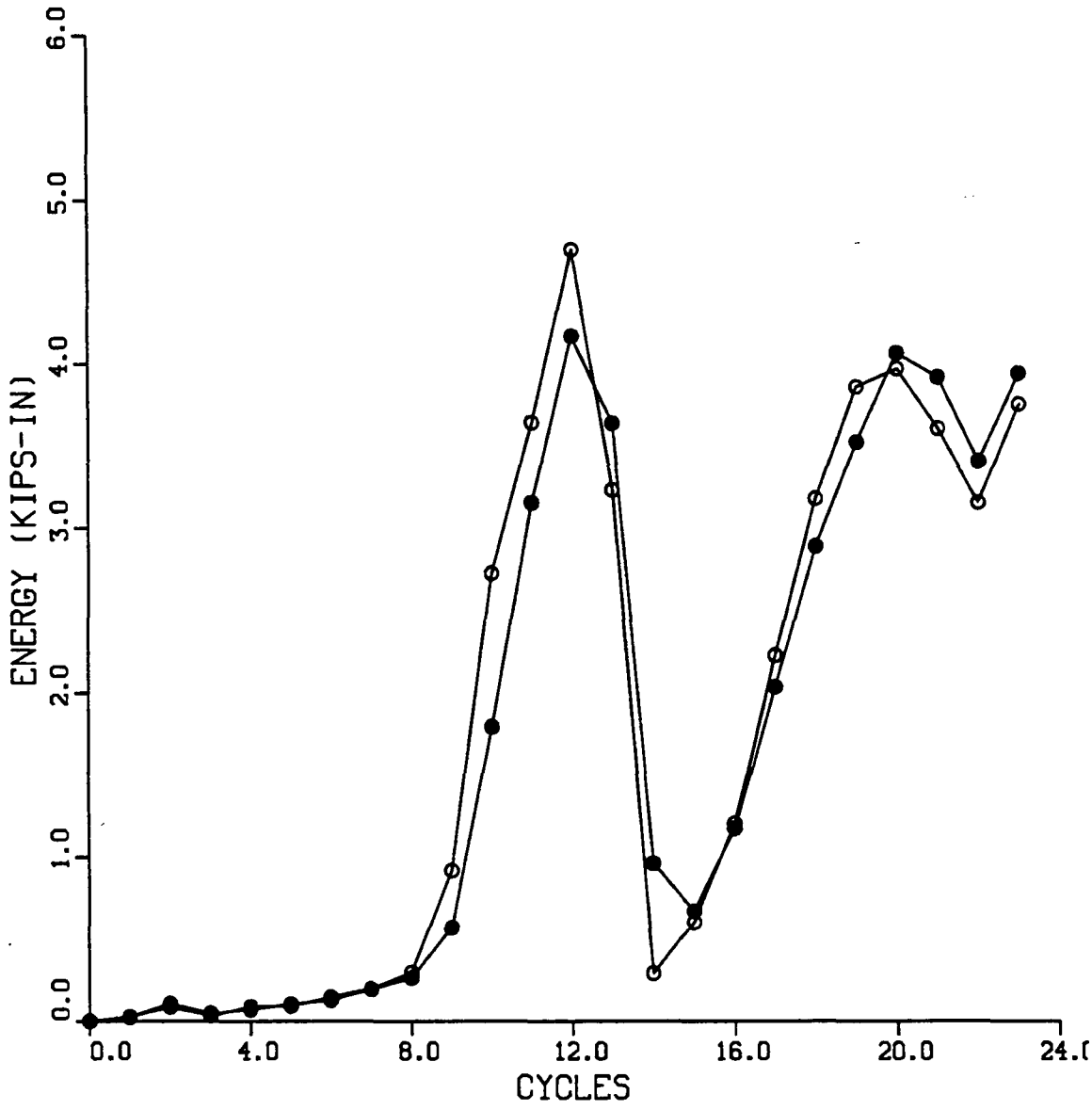

Figure 4-10: Energy Dissipated in Each Cycle of Shear Wall

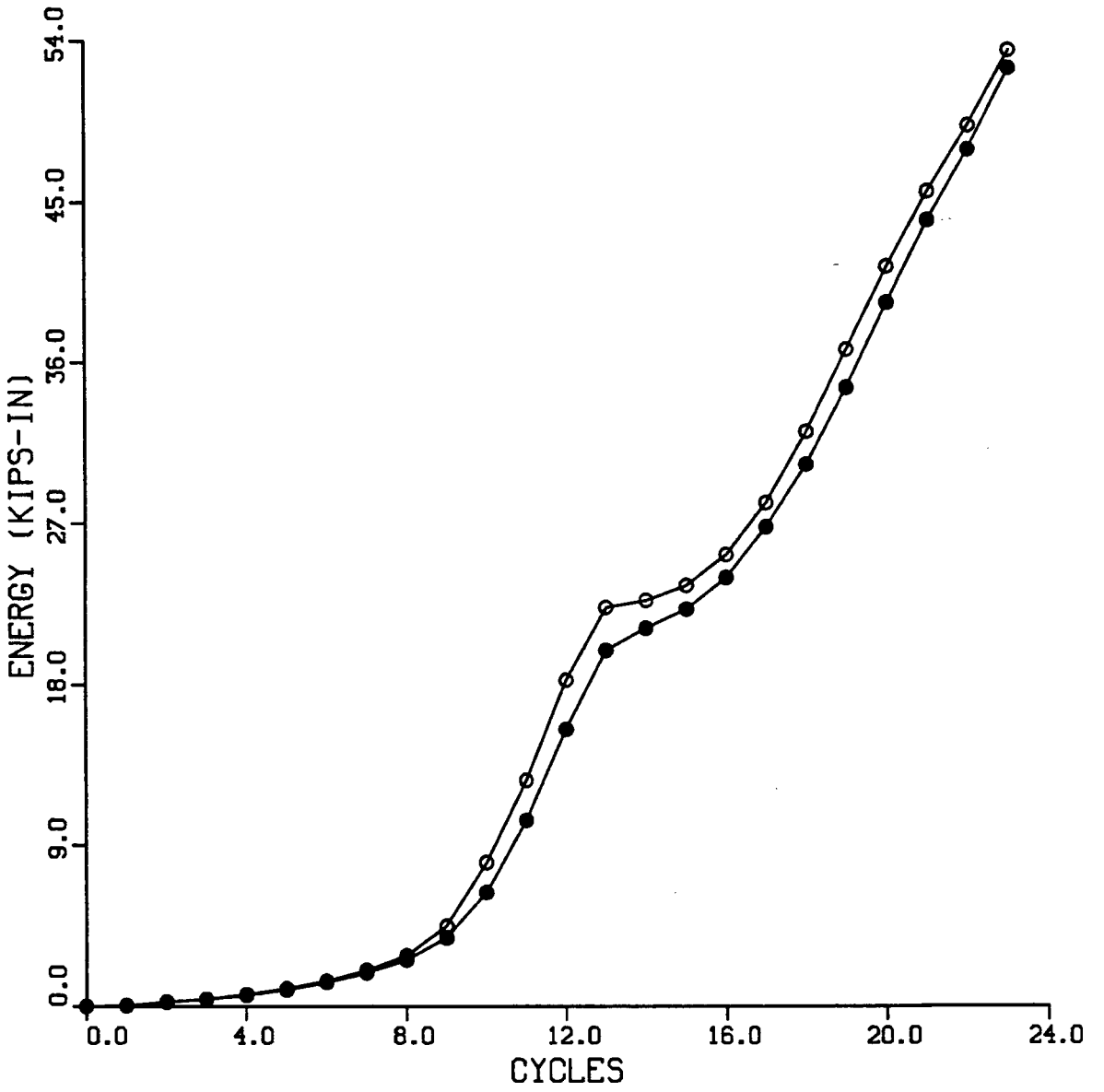

Figure 4-11: Accumulated Energy Absorbed in Shear Wall

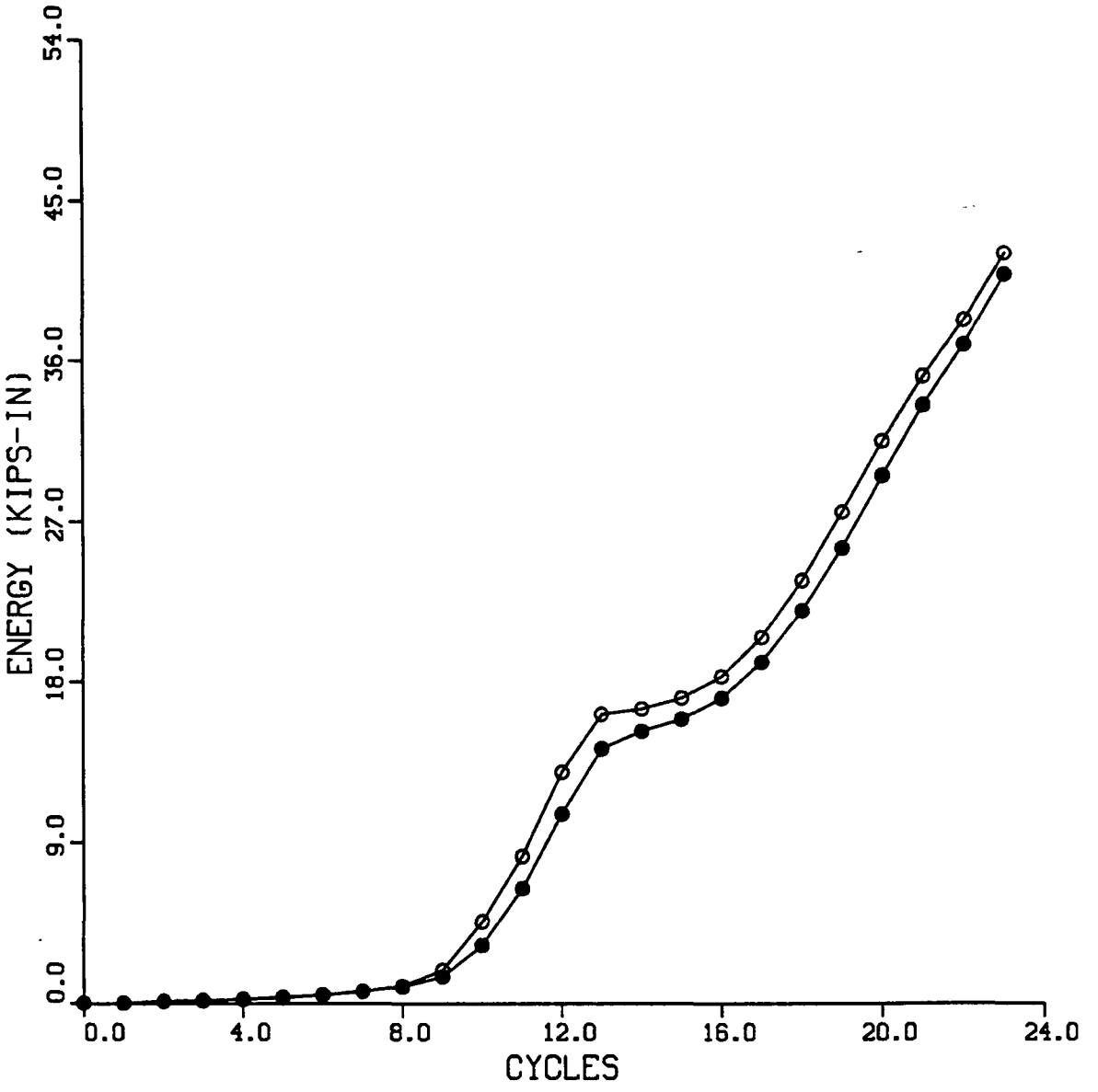

Figure 4-12: Accumulated Energy Dissipated in Shear Wall

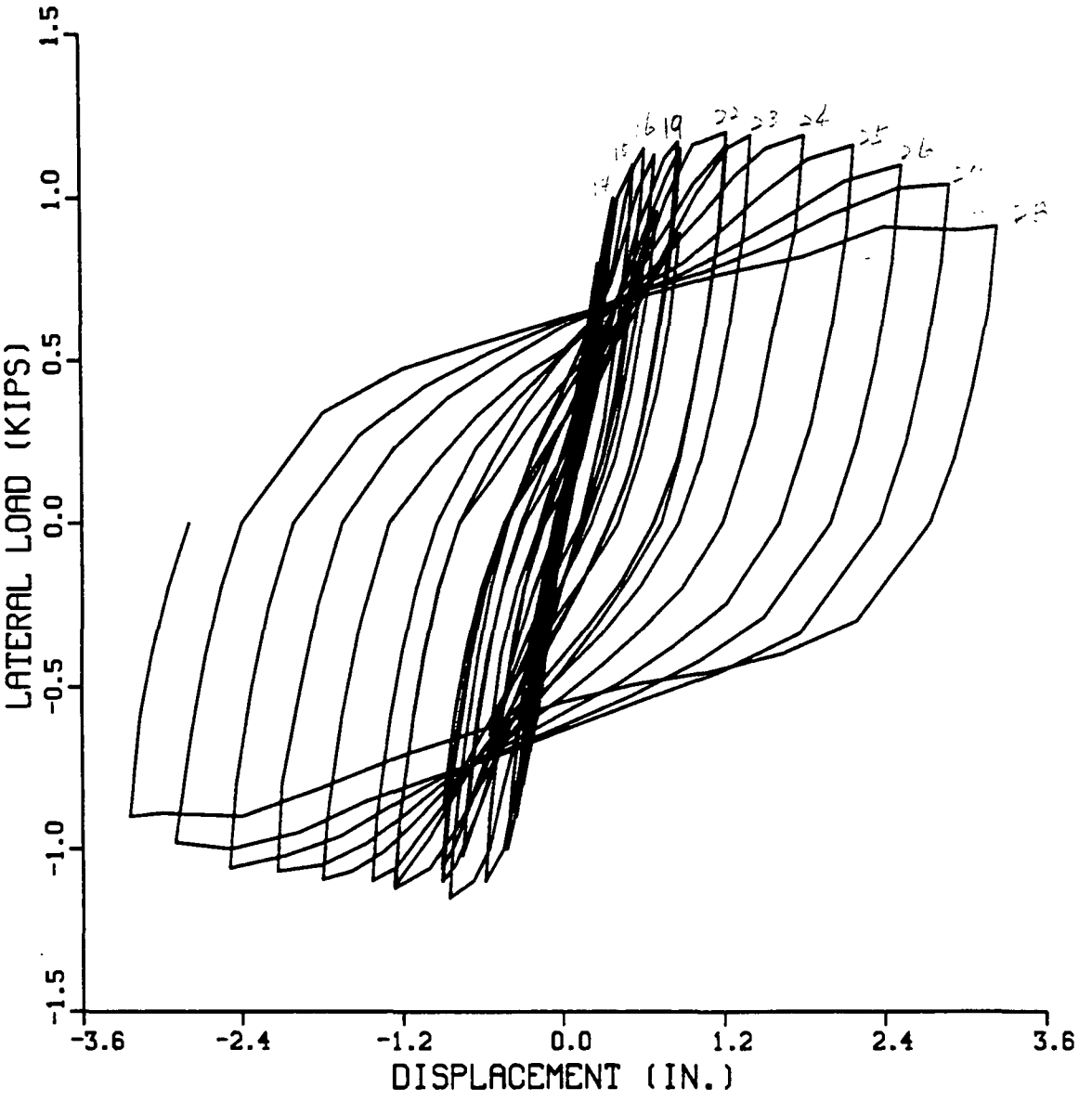

Figure 4-13: Load (P) vs. Displacement (Δ_t) of Frame

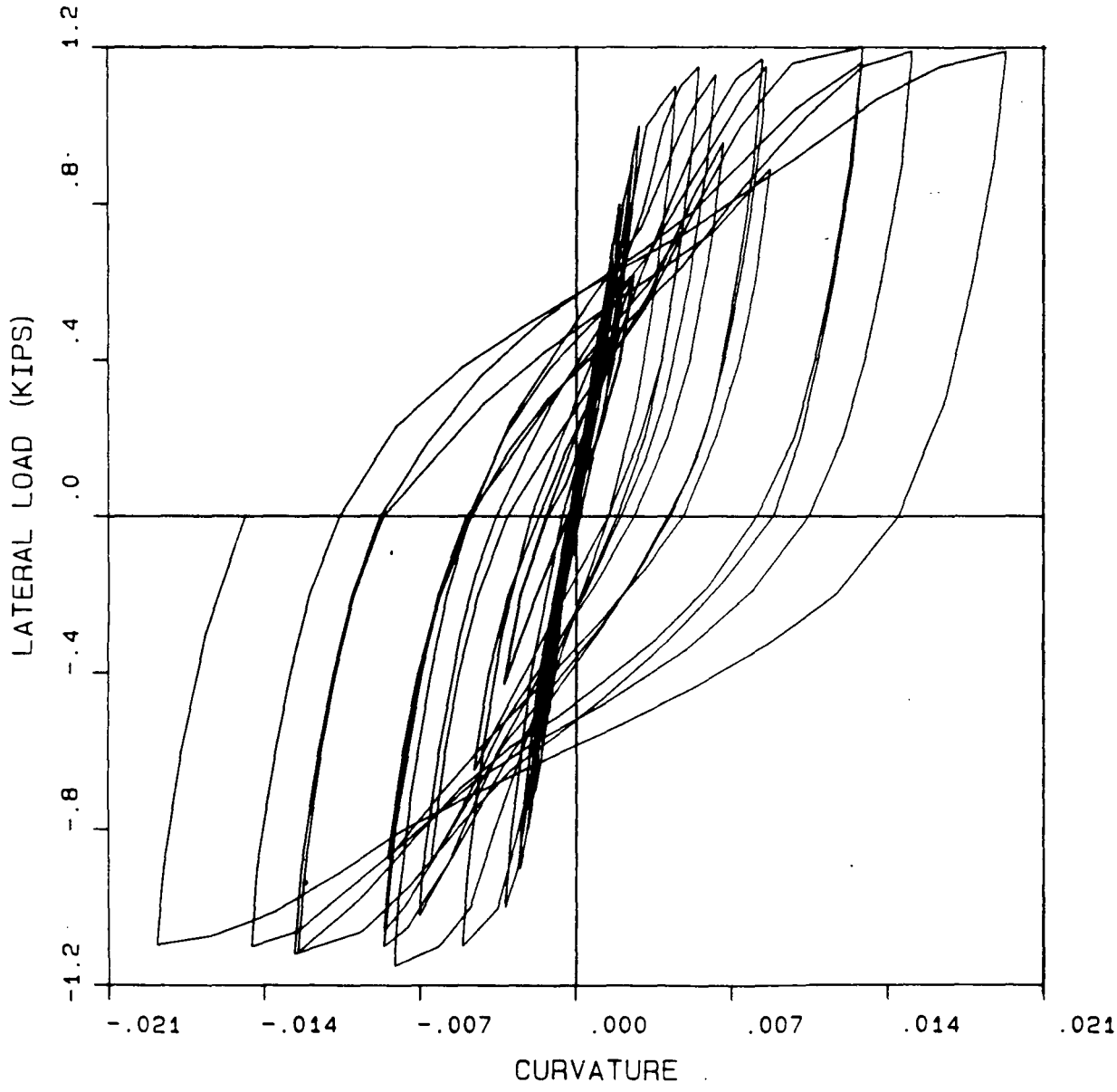

Figure 4-14: Load (P) vs. Column Curvature (θ_c) of Frame

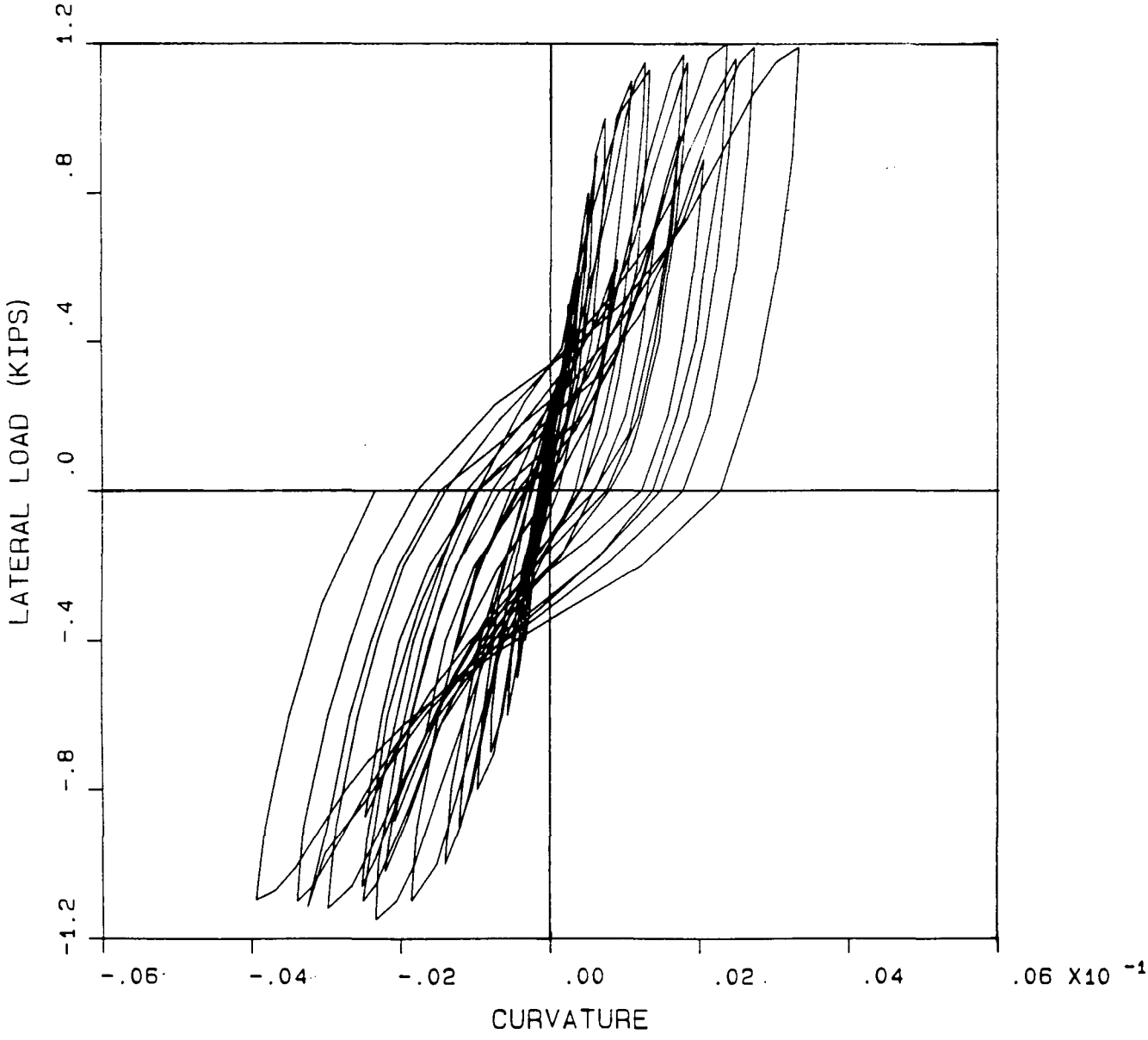

Figure 4-15: Load (P) vs. Beam Curvature (θ_b) of Frame

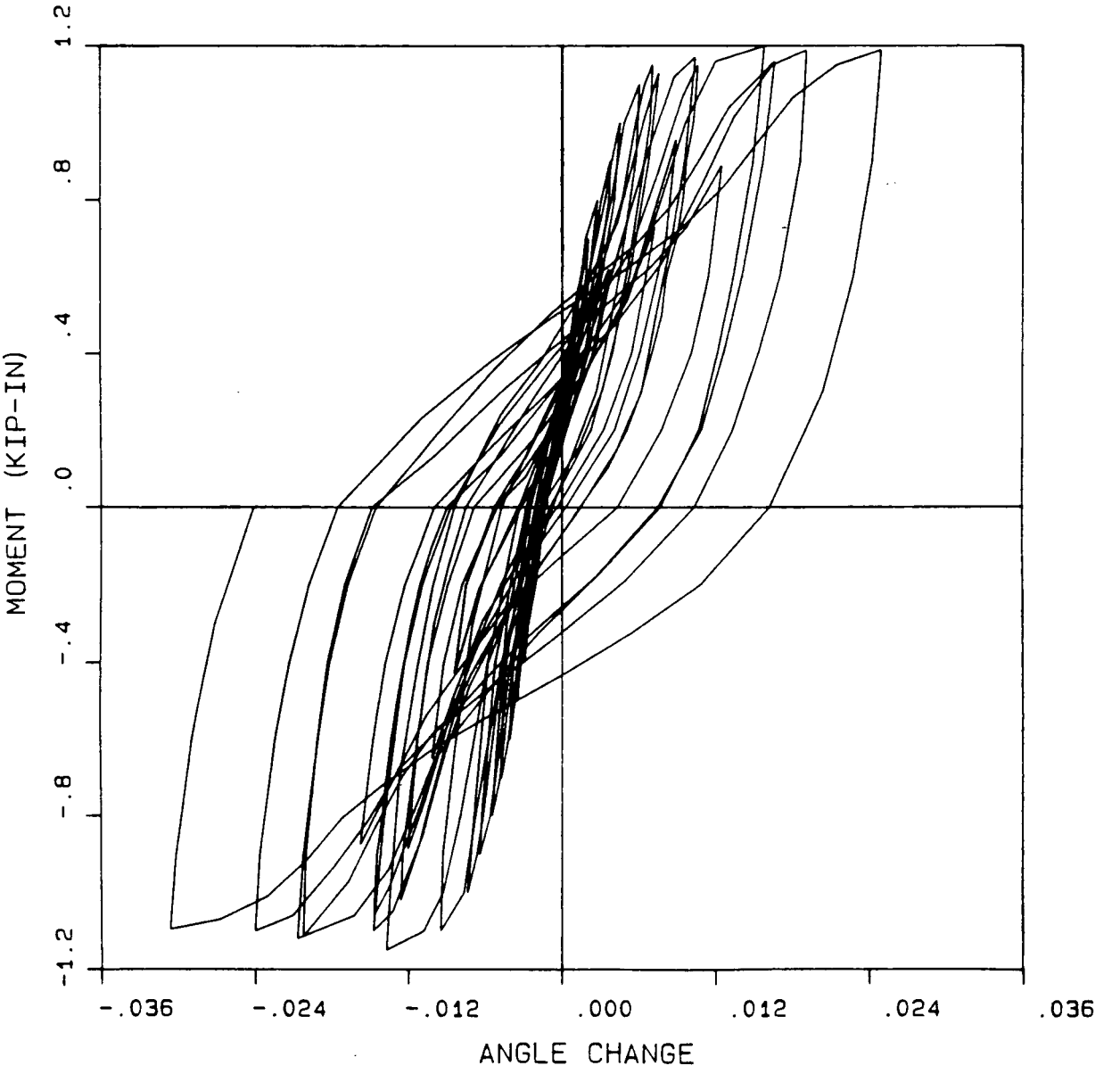

Figure 4-16: Load (P) vs. Angle Change (γ_{bc}) Between Beam and Column of Frame

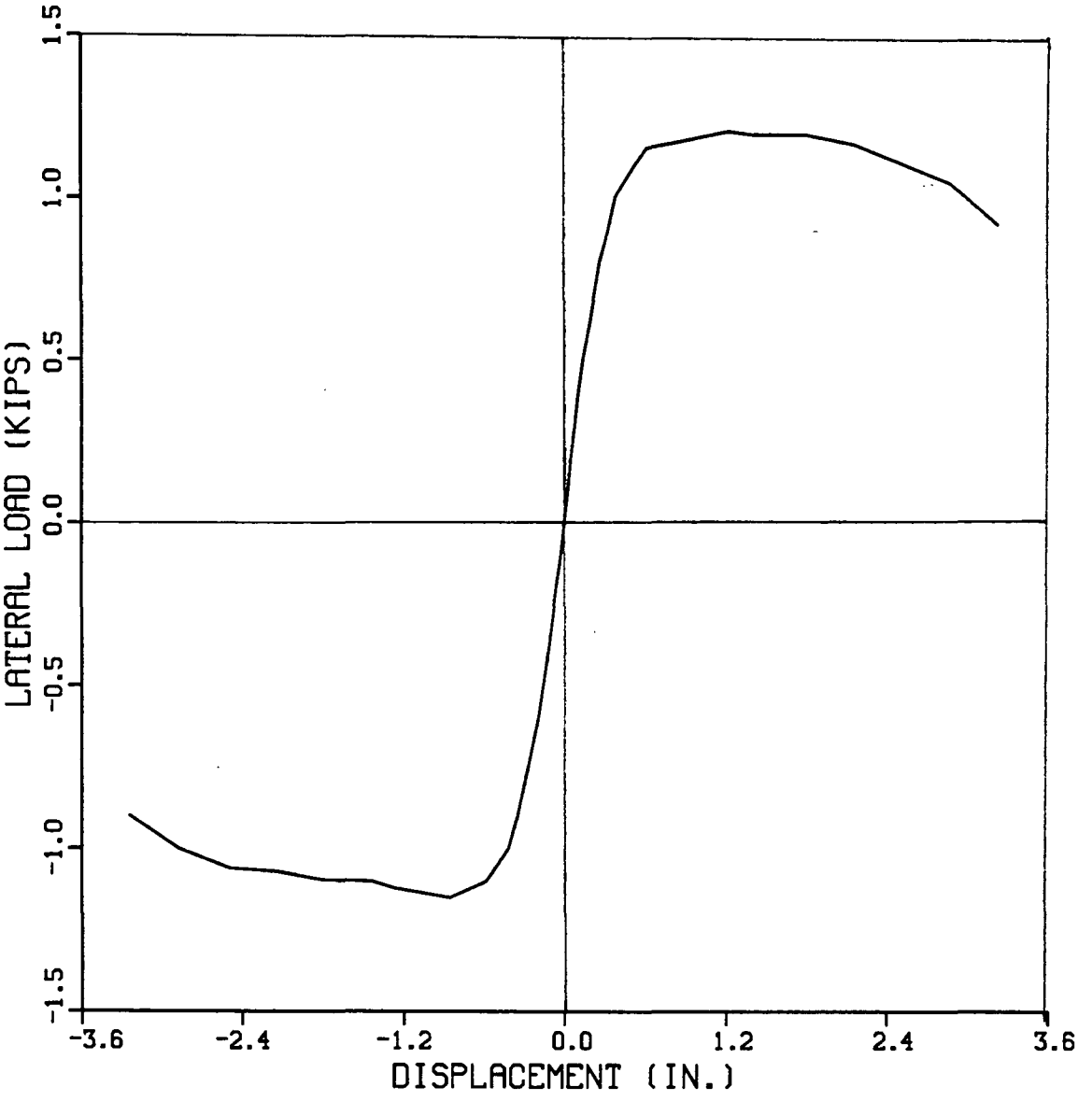

Figure 4-17: Skeleton Curve of Frame

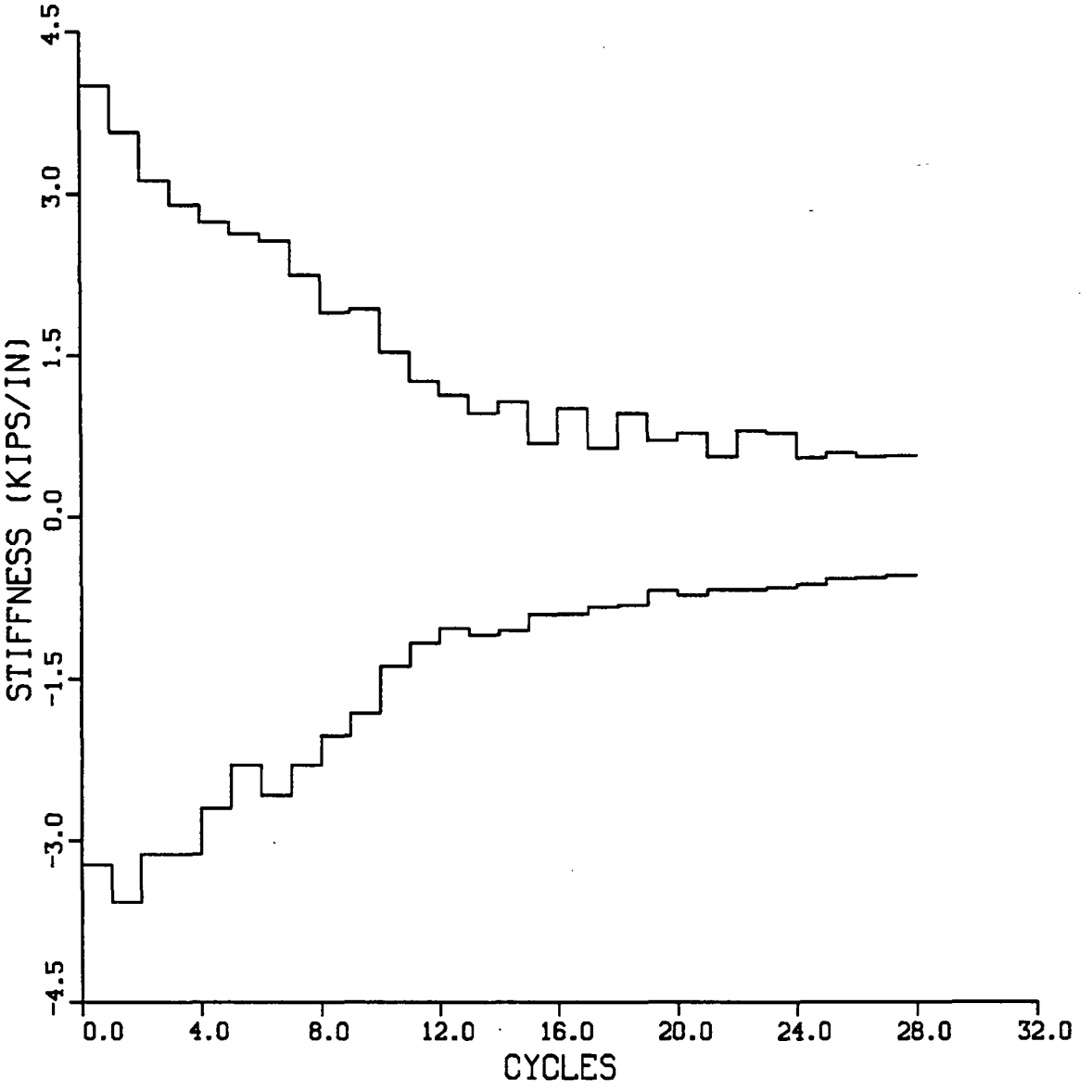

Figure 4-18: Stiffness Deterioration in Each Cycle of Frame

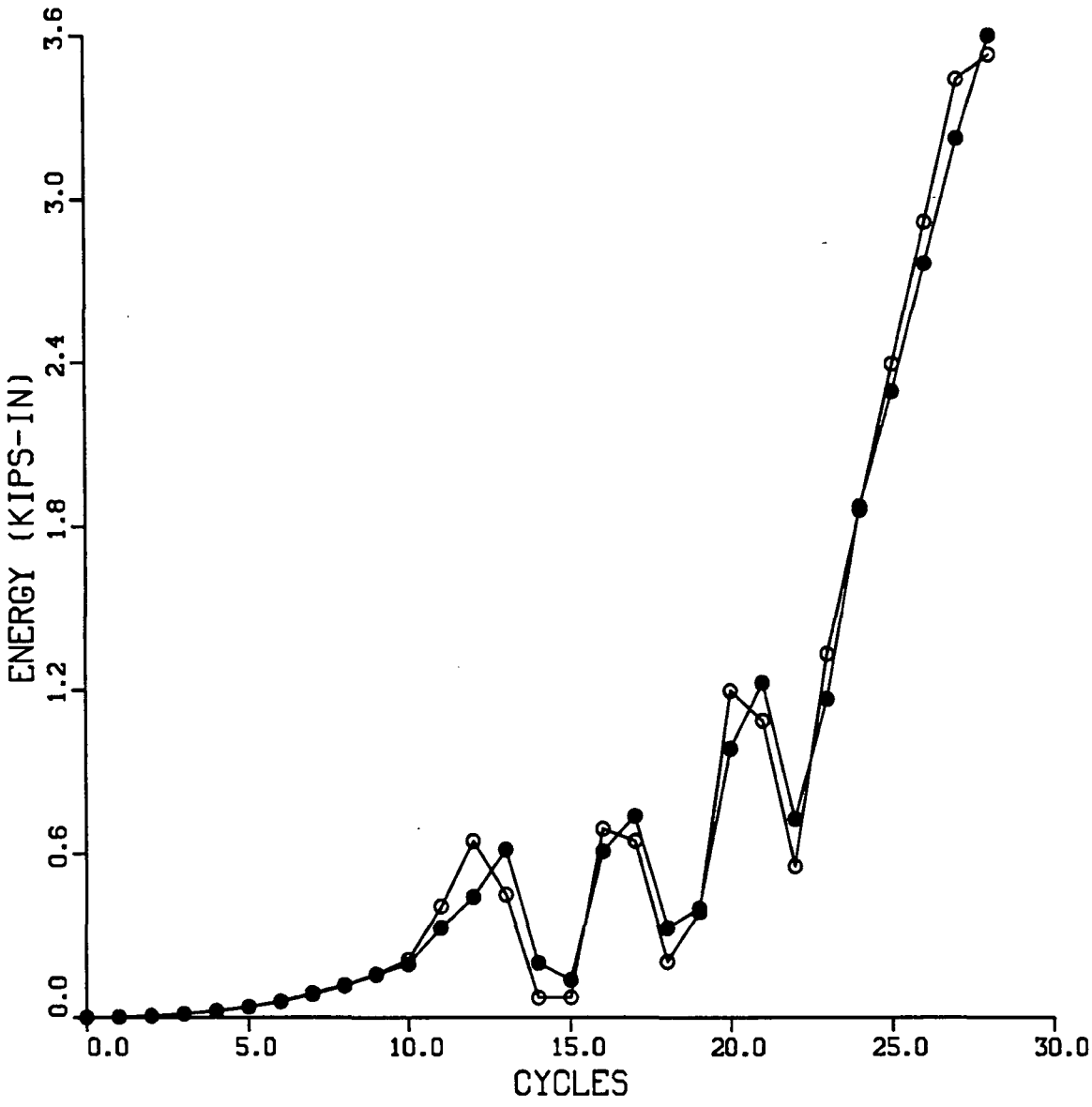

Figure 4-19: Energy Absorbed in Each Cycle of Frame

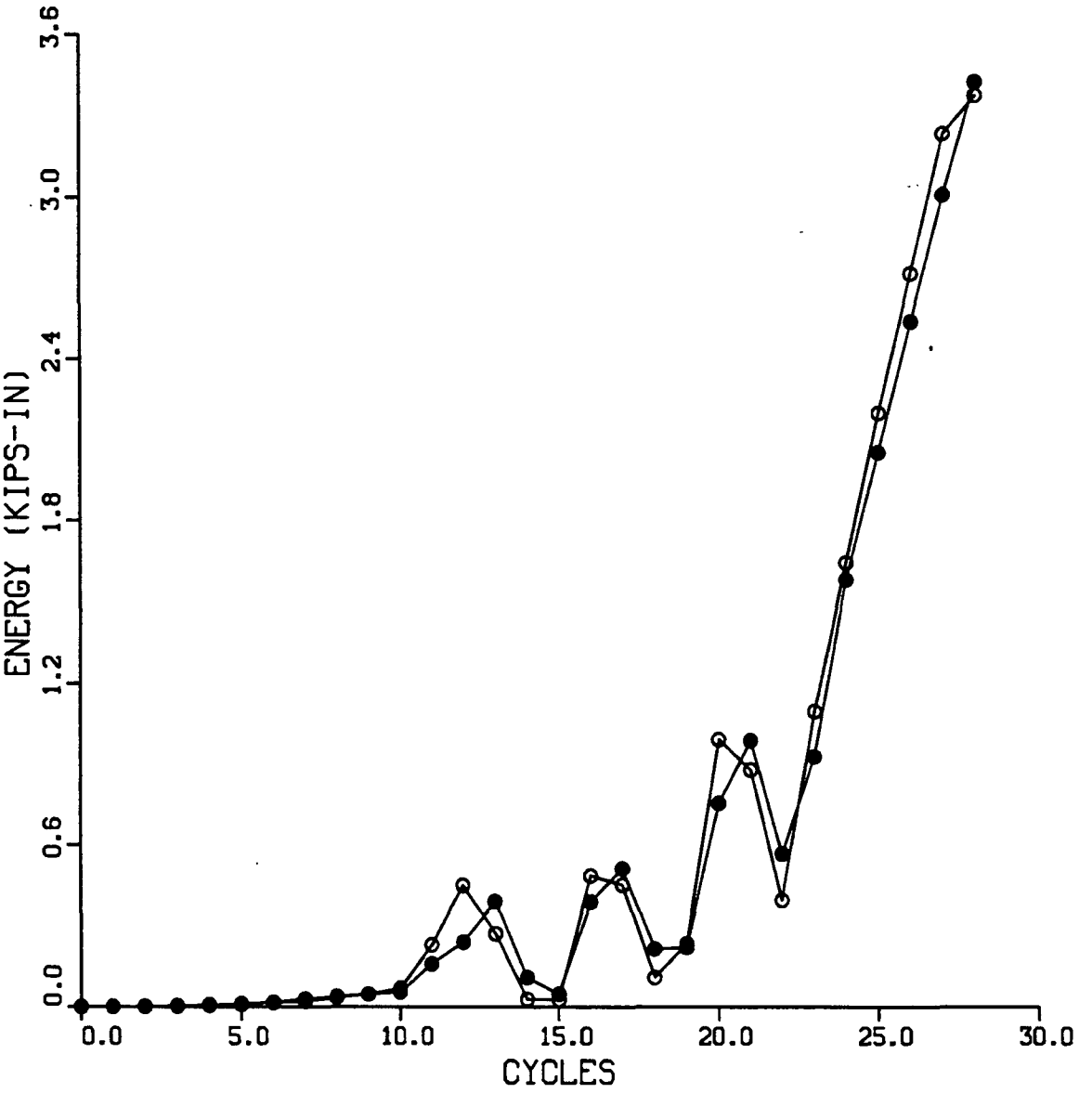

Figure 4-20: Energy Dissipated in Each Cycle of Frame

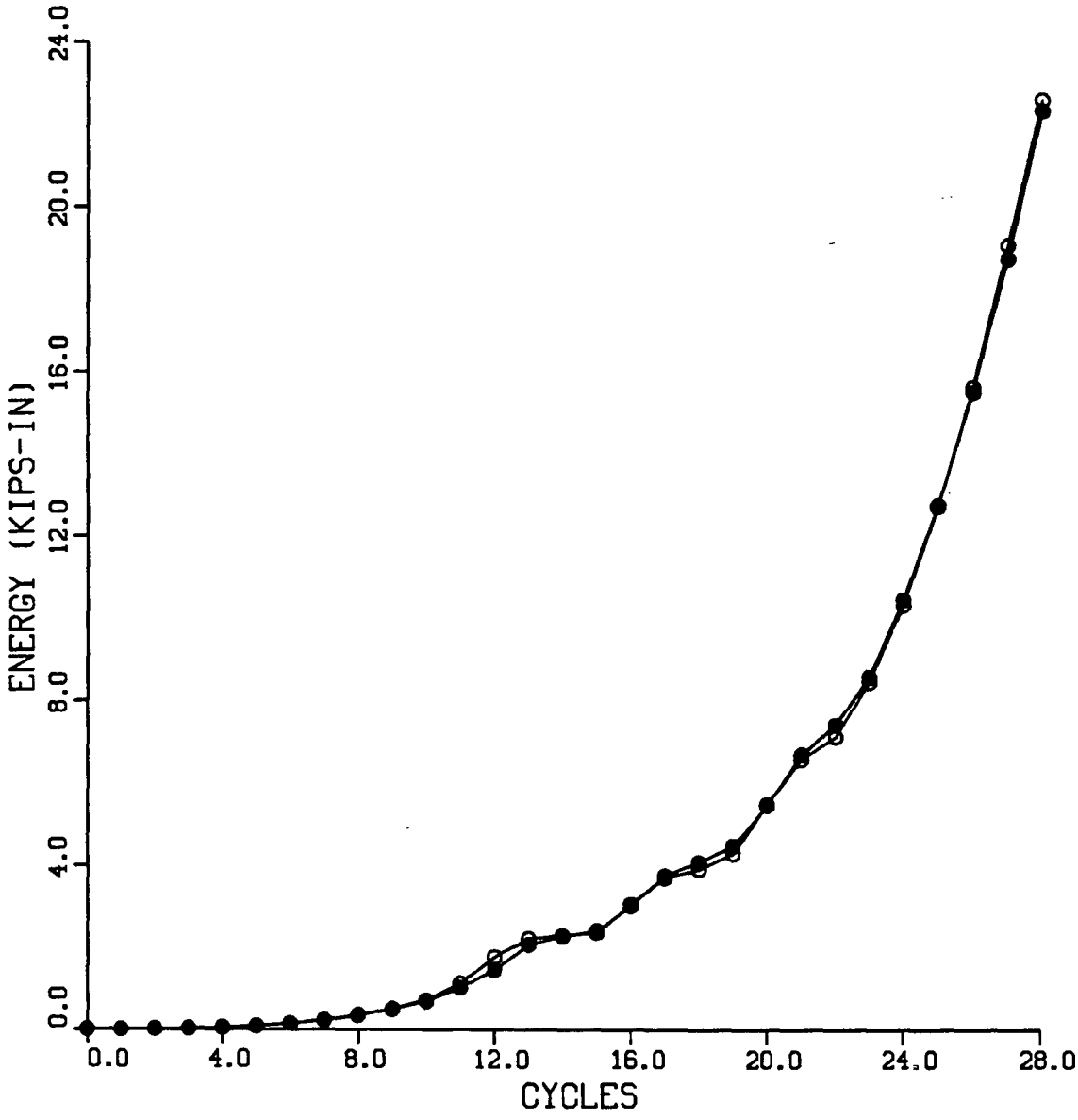

Figure 4-21: Accumulated Energy Absorbed in Frame

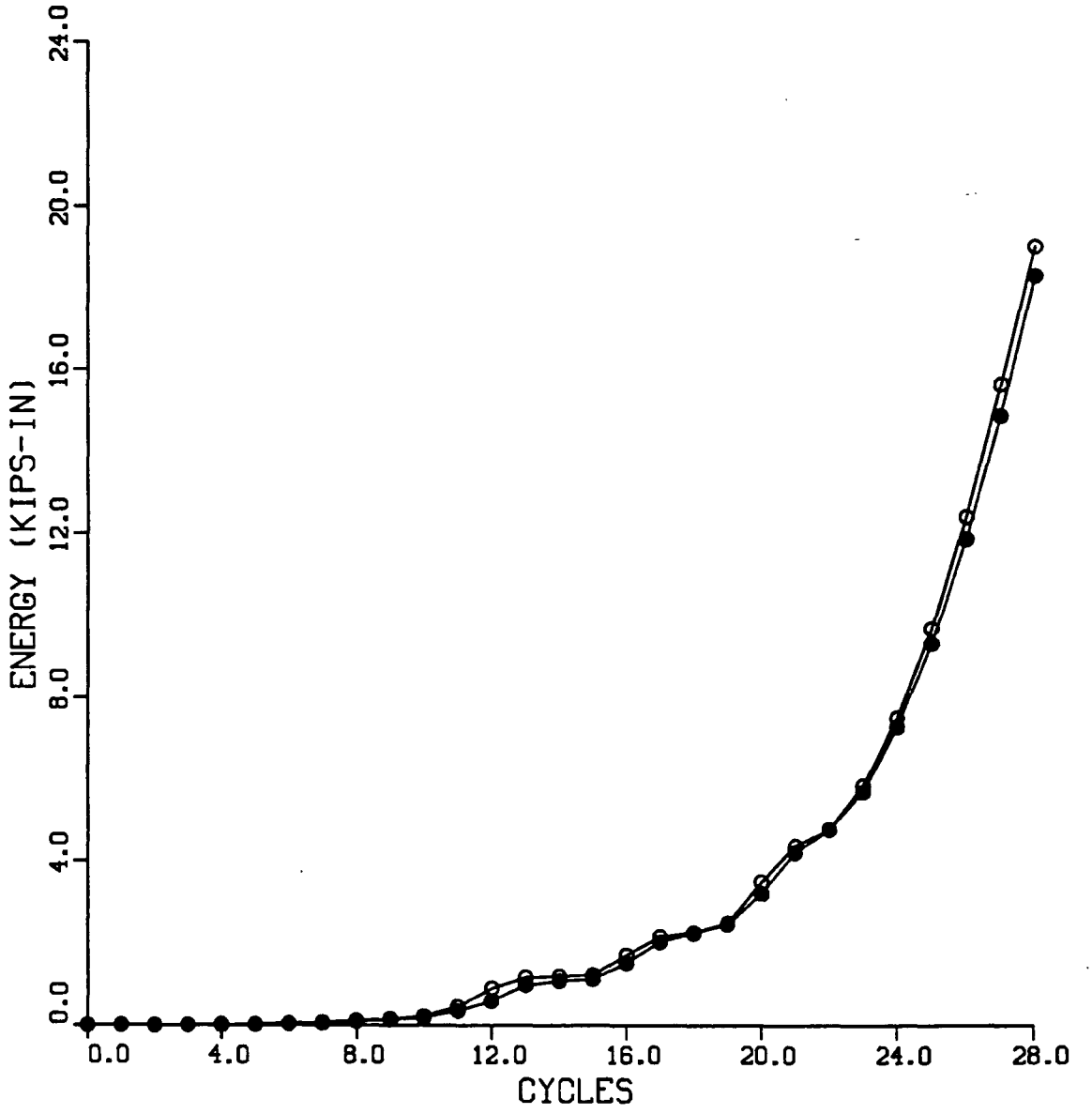

Figure 4-22: Accumulated Energy Dissipated in Frame

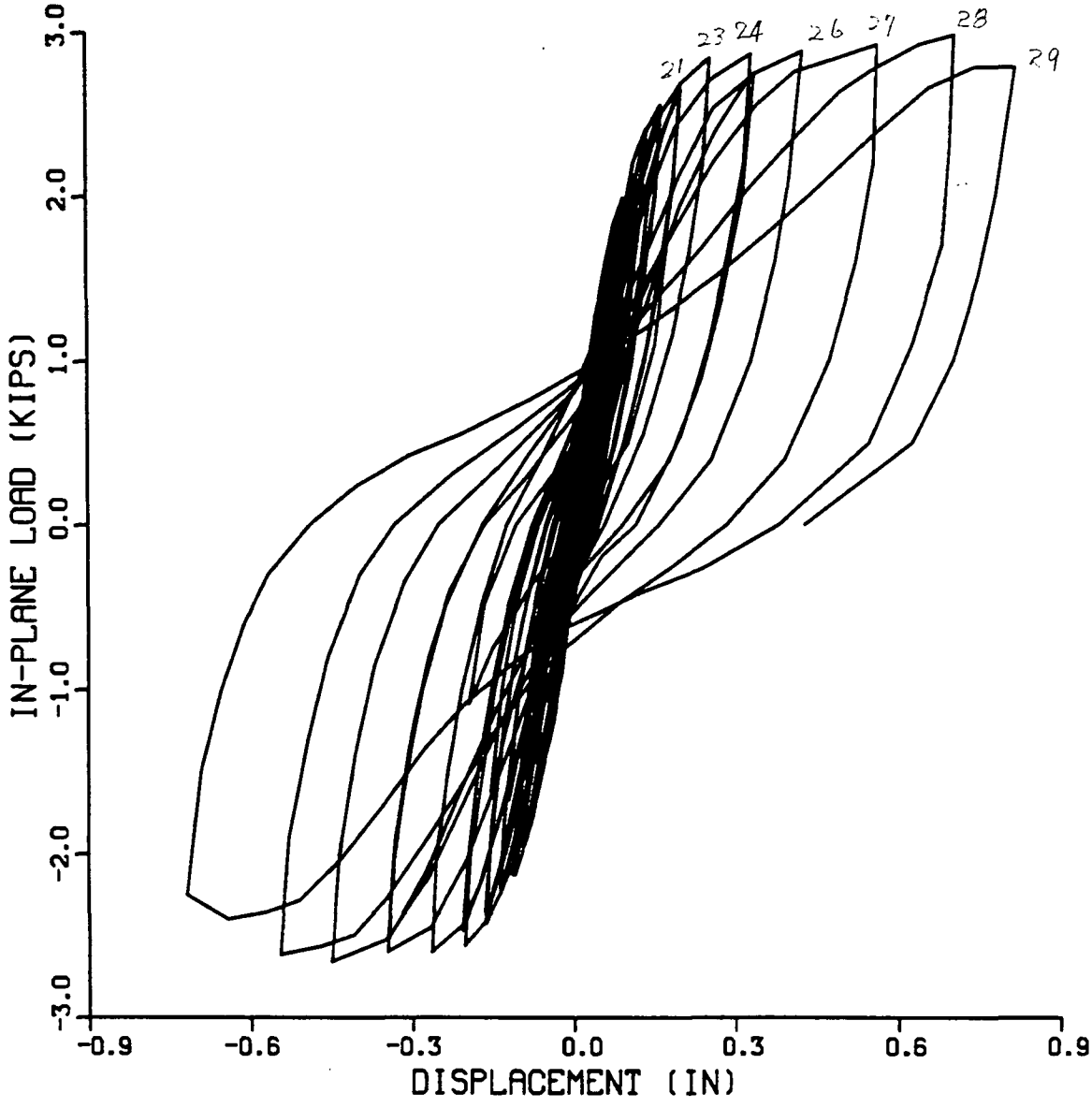

Figure 4-23: Load (P) vs. Displacement (Δ_t) of Slab

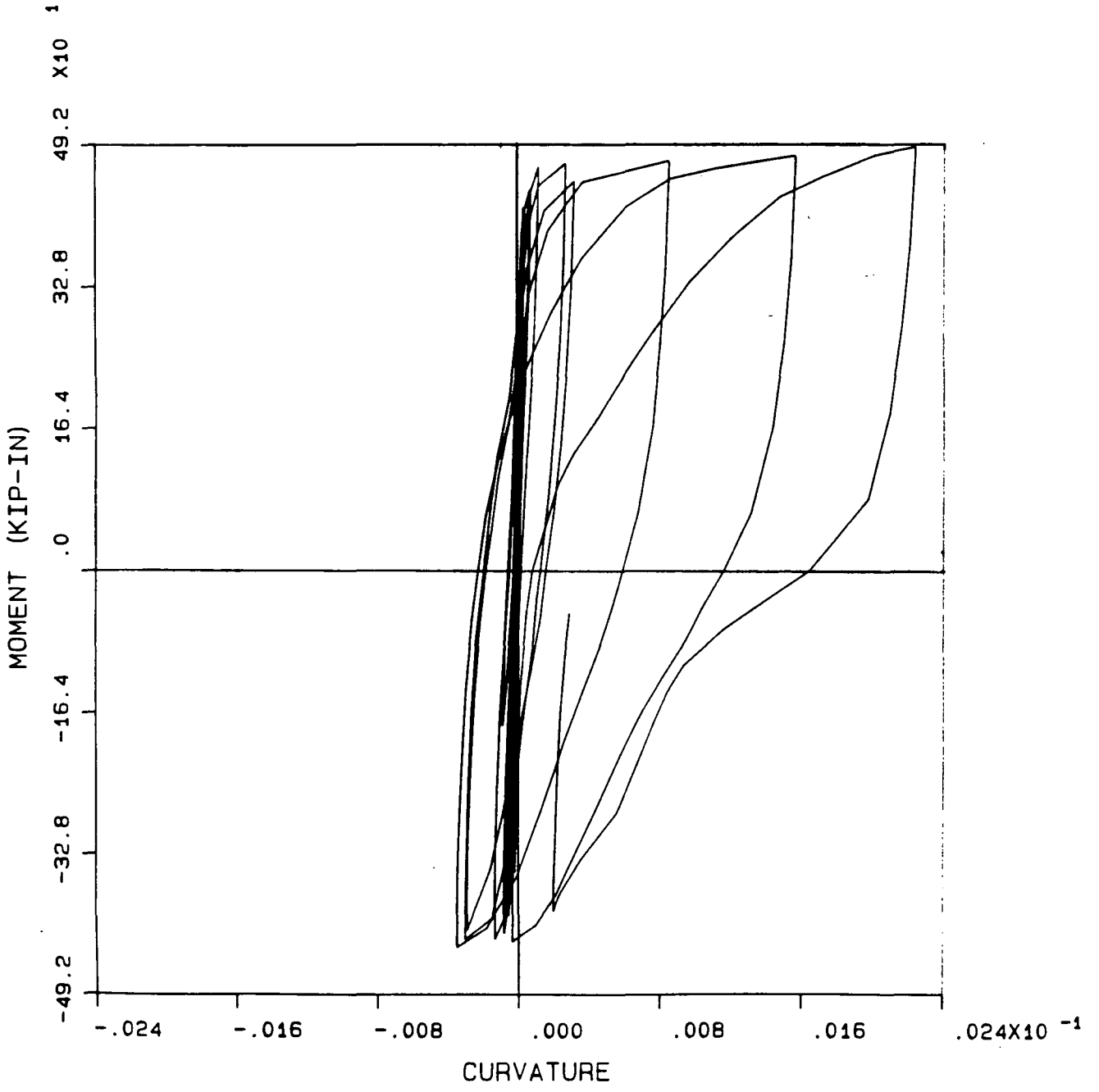

Figure 4-24: Moment (M) vs. Curvature (θ_s) of Slab

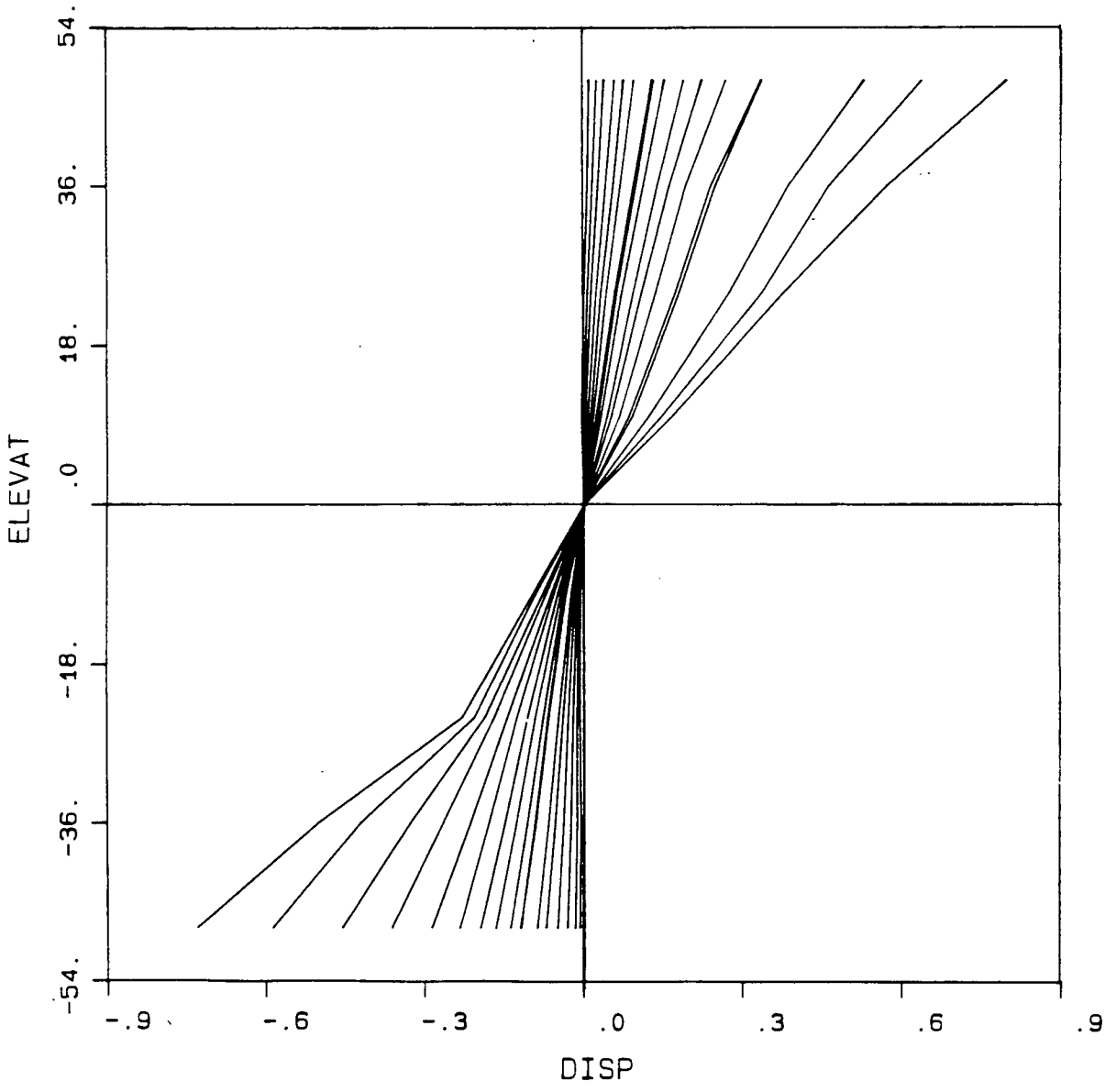

Figure 4-25: Sideway Displacement of Slab

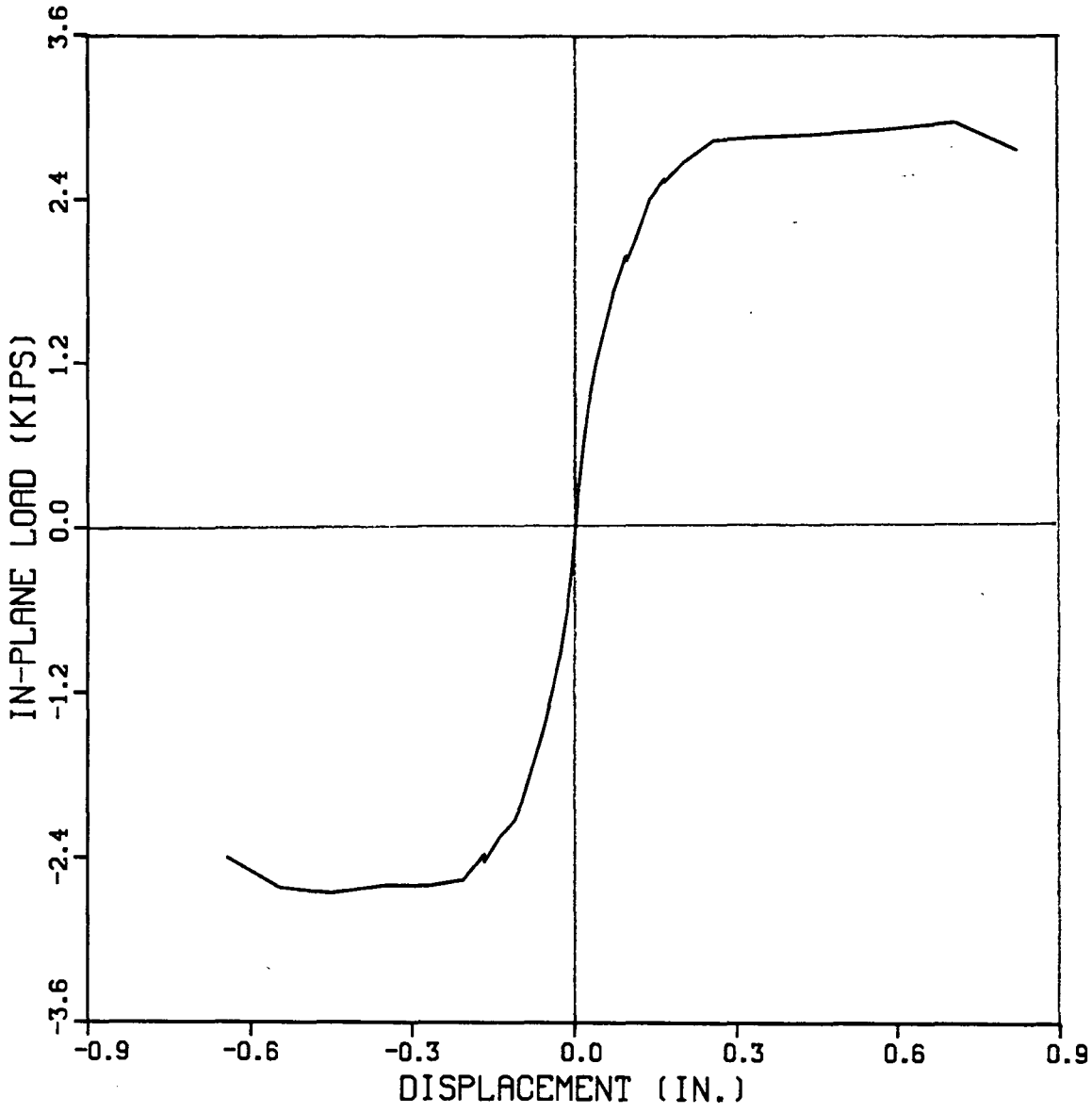

Figure 4-26: Skeleton Curve of Slab

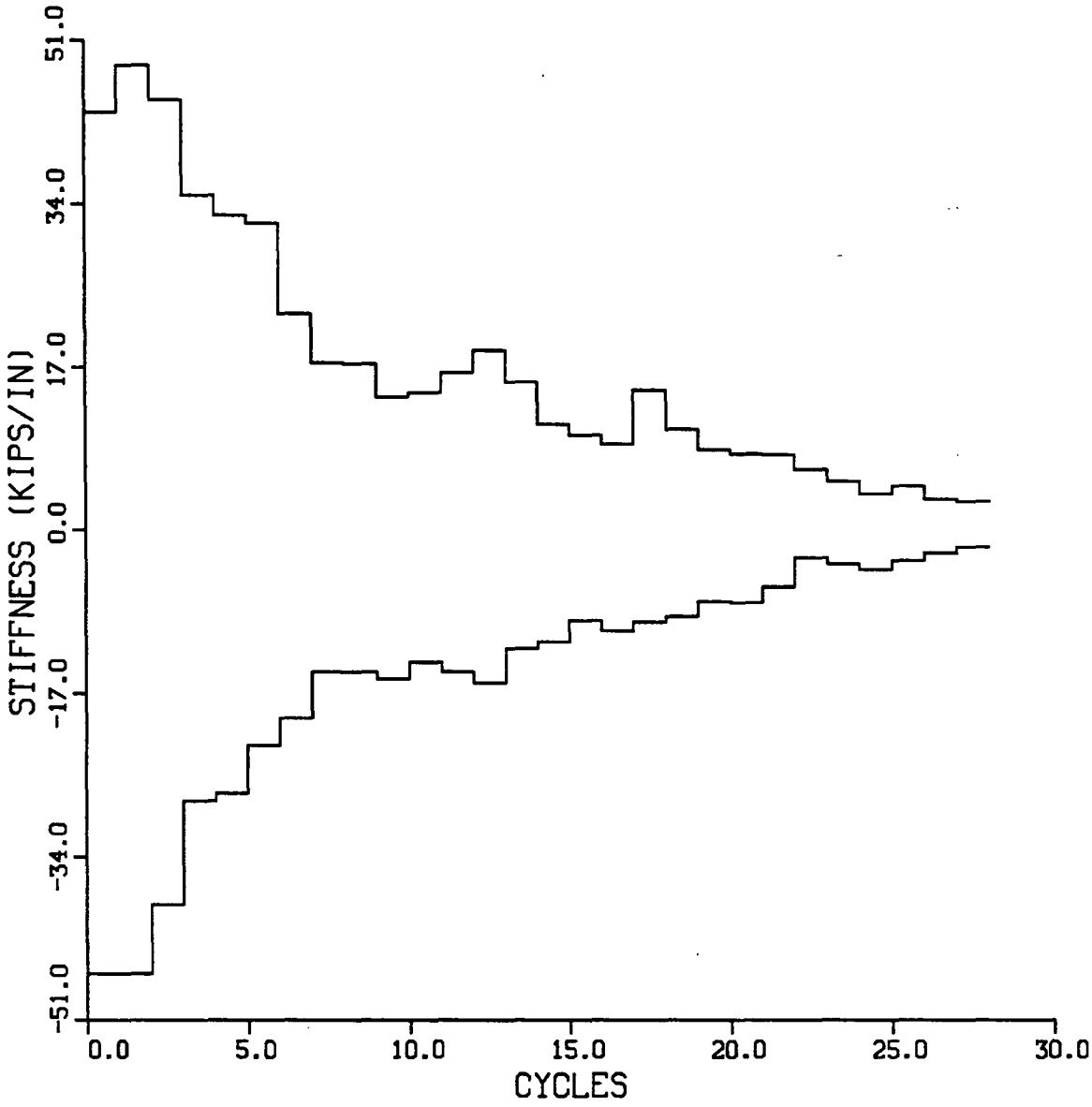

Figure 4-27: Stiffness Deterioration in Each Cycle of Slab

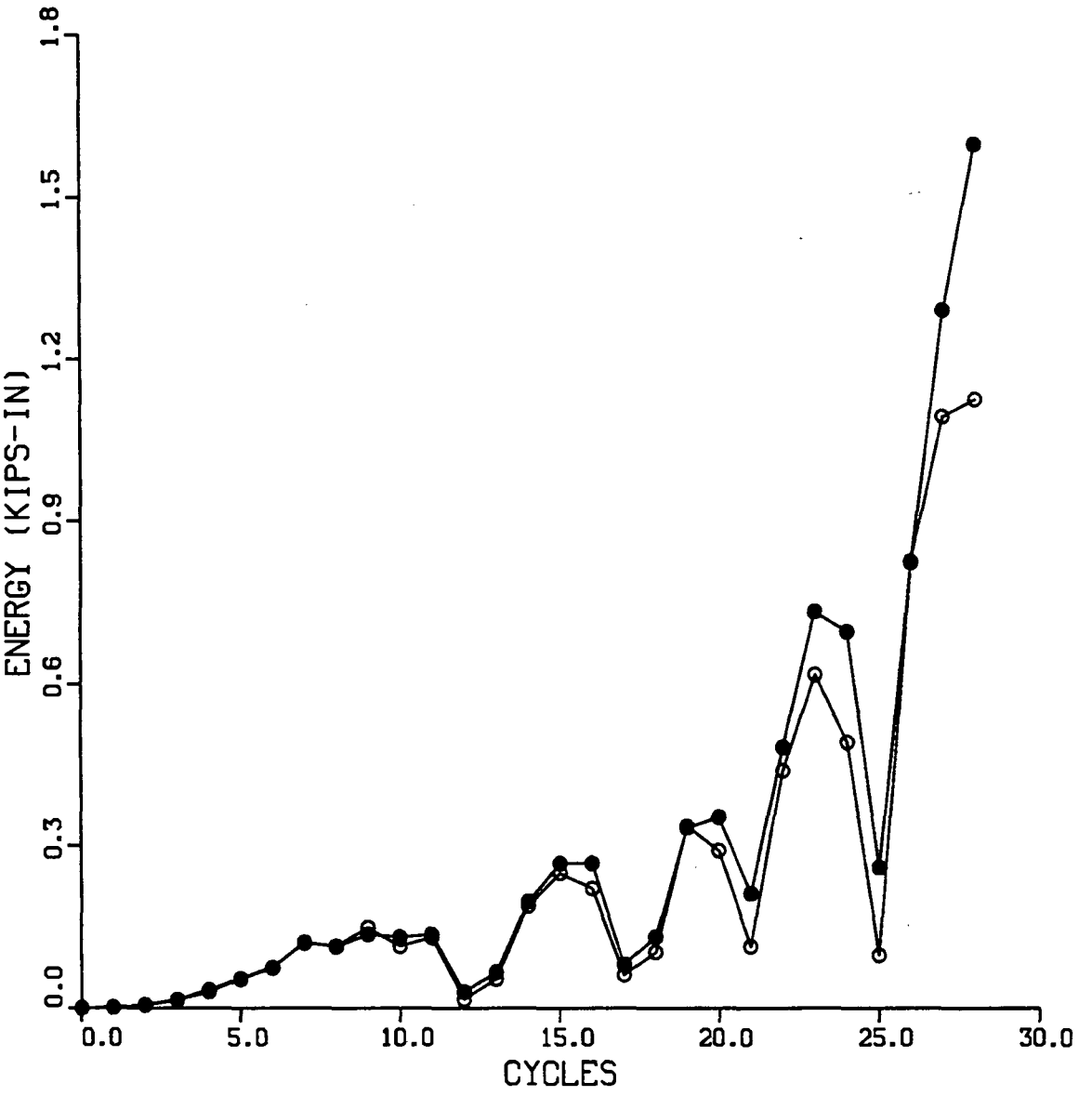

Figure 4-28: Energy Absorbed in Each Cycle of Slab

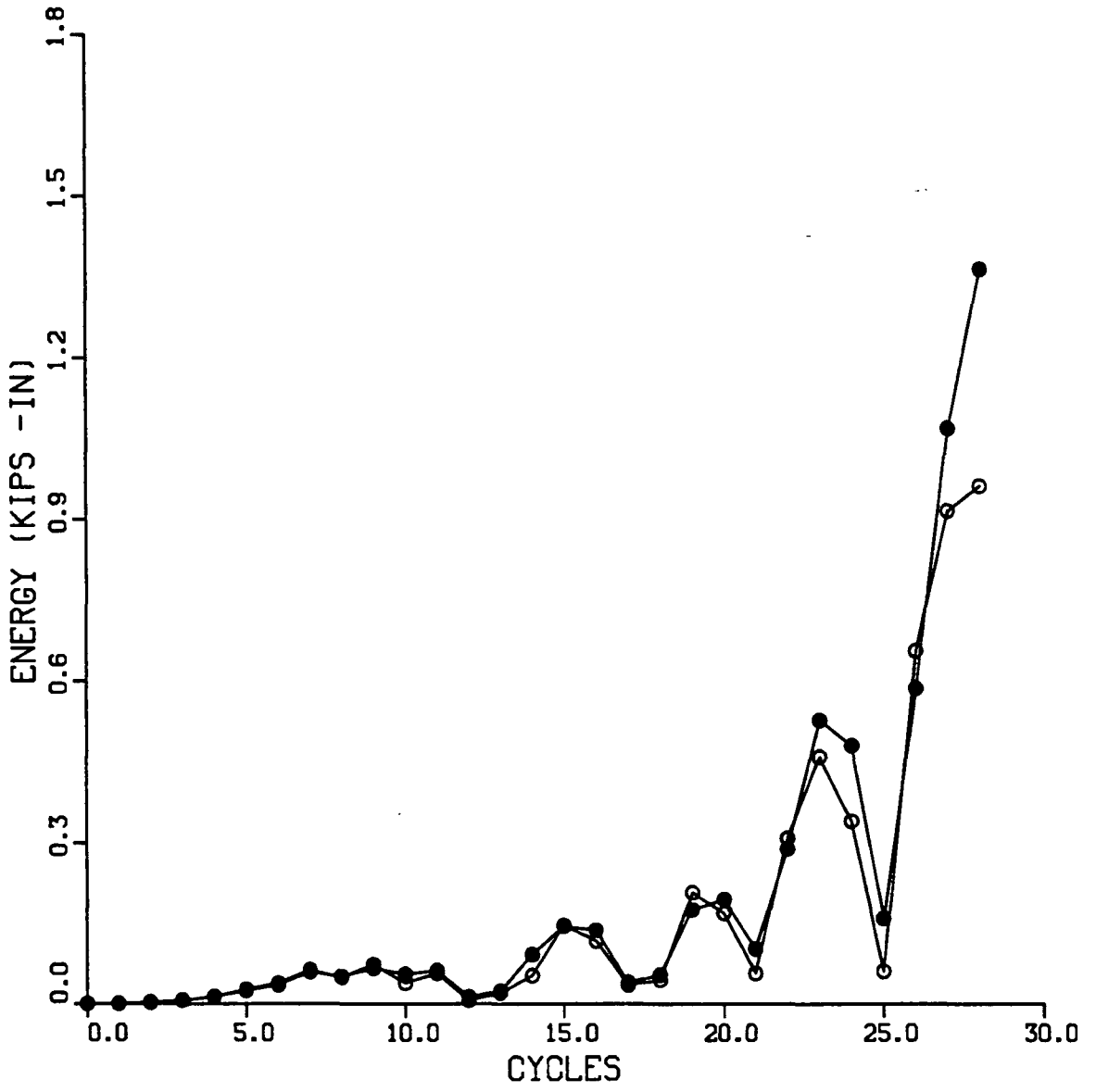

Figure 4-29: Energy Dissipated in Each Cycle of Slab

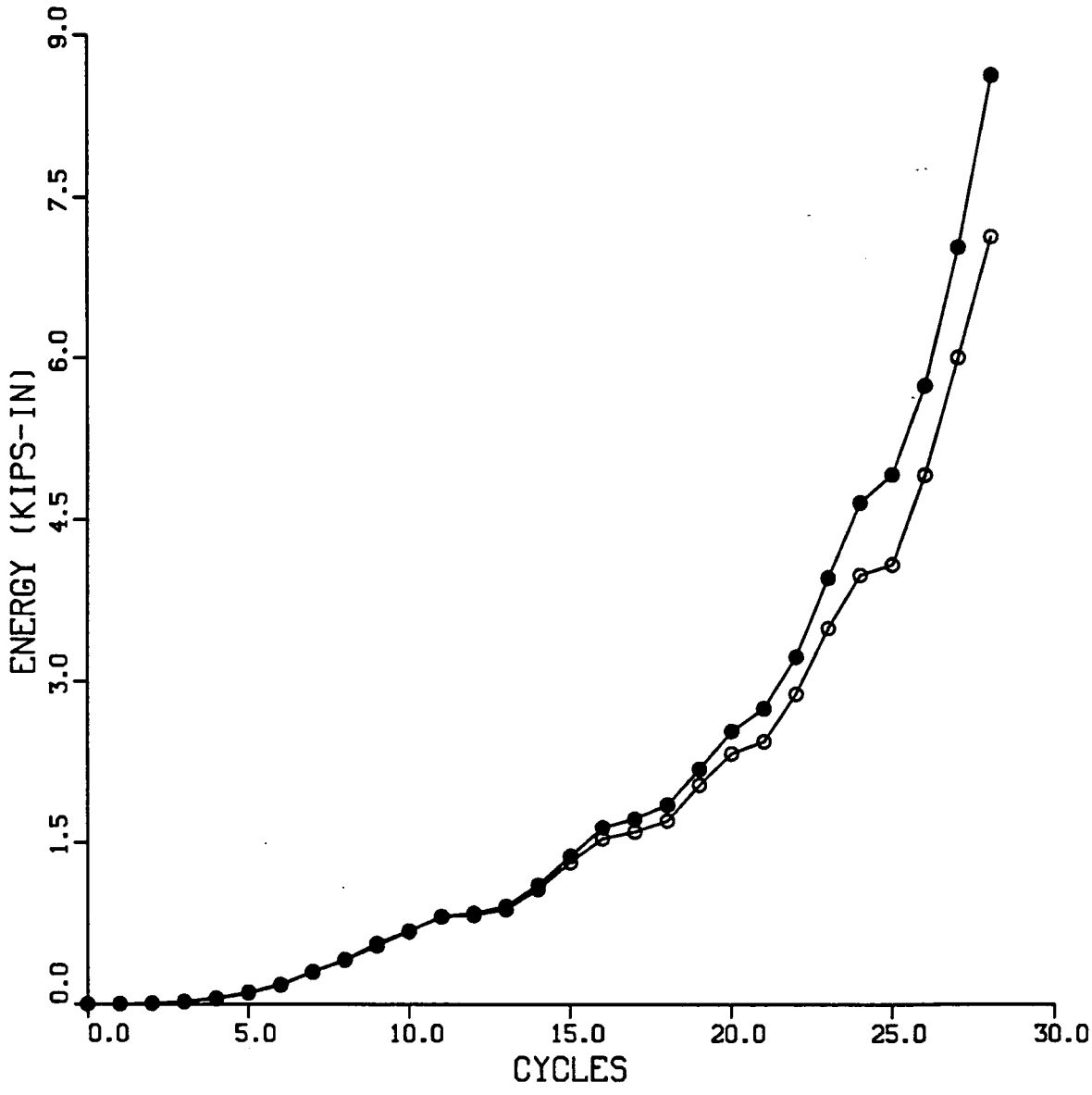

Figure 4-30: Accumulated Energy Absorbed in Slab

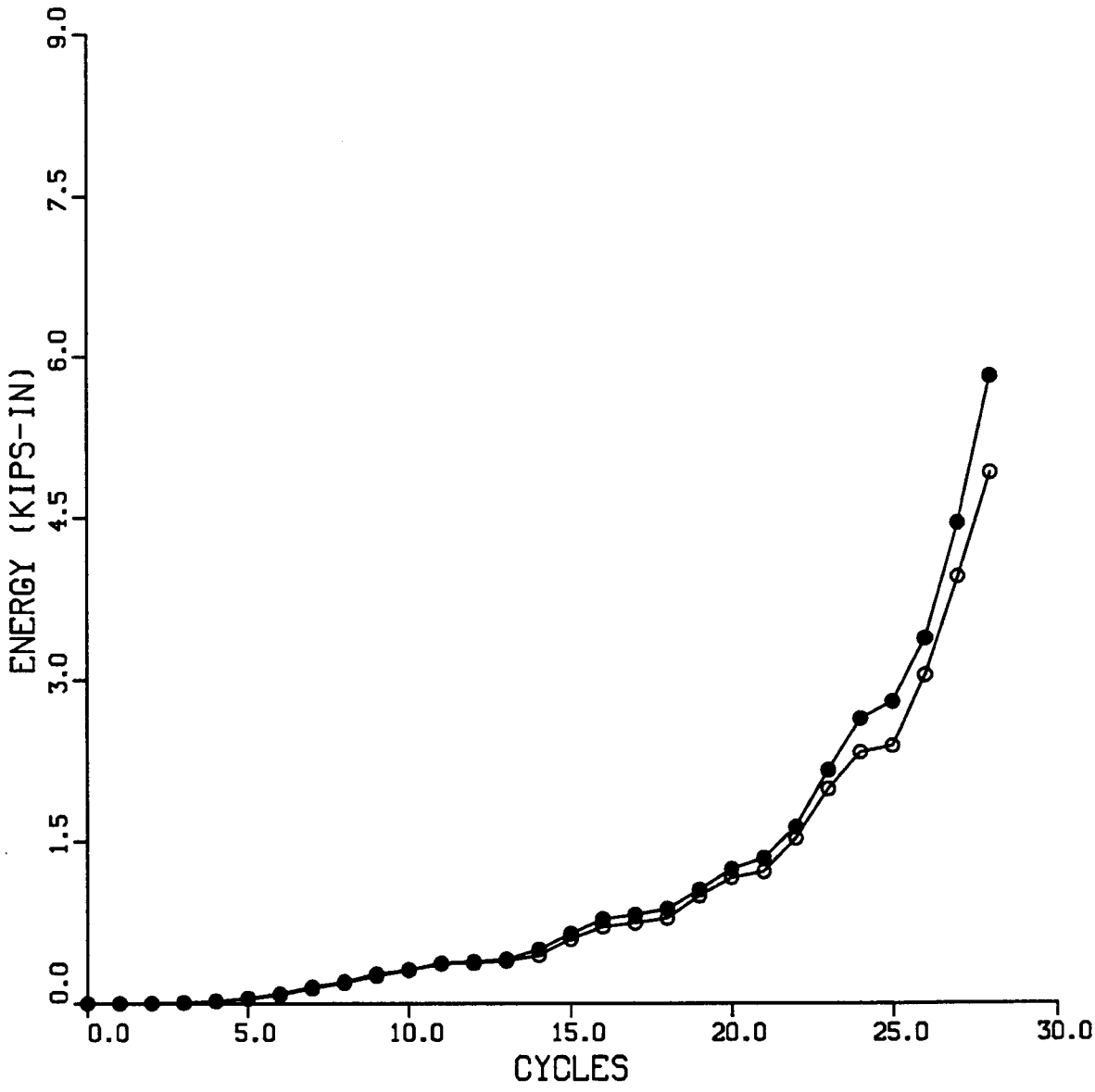

Figure 4-31: Accumulated Energy Dissipated in Slab

Chapter 5
Conclusions

The three reinforced concrete model structures were constructed and tested under quasi-static cyclic load to study the hysteresis behavior, ductility factor, and energy dissipation capacity of component structures under the seismic loading. The performance of each model structure during the procedure of test was closely observed and recorded completely. The test data was comprehensively examined and processed. Based on the results of these tests, the following conclusions can be drawn:

1. All three specimens displayed a stable inelastic behavior under a severe cyclic reversed severe seismic loading except that the shear wall specimen observed some pinched load-deflection behavior due to the high shear stress.

2. The strength and stiffness degradation of reinforced concrete shear wall during reversed repeated inelastic loading was closely related to the shear deformation. After it observed its maximum strength, the hyteresis behavior of the shear wall specimen was pinched severely and the nature of the overall deflection was changed from the flexural bending to the shear deformation due to the high level of the shear stress.

3. The overall behaviors of the three component structures designed by satisfying the requirements of ACI building code are symmetric regarding to the loading direction under cyclic reversed earthquake-type loading as long as the quality of the construction was controlled properly.

4. Although the additional weight used for the slab is four times (the full live load) as that required by the Uniform Building Code for seismic design, the slab specimen test came out with a very stable hysteresis behavior of

in-plane load vs. the in-plane deflection. This indicated that the gravity load would not alter the in-plane behavior of the slab primarily.

5. The small cyclic reversed loading will deteriorate the strength and stiffness of the reinforced concrete structure if the deflection of the structure is mainly contributed from shear deformation. This is because of that the extra repeated small shear deformation makes further bonding force loss between the reinforcement and concrete in the cracked region. Such behavior was observed in the shear wall test but not in the frame and slab tests.

6. All three model structures had a good energy dissipation capacity and a reasonable large ductility factor in inelastic seismic responses, which is an essential characteristics required for a structure to resistant a earthquake excitation.

References

(1) Jain, S.K.
Continuum Models for Dynamics of Buildings.
Journal of Engineering Mechanics, ASCE Vol. 110, No. 12:pp. 1713-1730, December, 1984.

(2) Jain, S.K. and Jennings, P.C.
Analytical Models for Low-Rise Buildings With Flexible Diaphragms.
Journal of Earthquake Engineering and Structural Dynamics Vol. 13, No. 2:pp. 225-241, March-April, 1985.

(3) Ji, X.R., Huang, T., Lu, L.W. and Chen, S.J.
An Experimental Study of The In-Plane Characteristics of Waffle Slab Panels.
Research Report No. 481.3, Fritz Engineering Laboratory, Lehigh University, Bethlehem, Pennsylvania, 1985.

(4) Karadogan, H.F. Huang, T., Lu, L.W. and Nakashima, M.
Behavior of Flat Plate Floor Systems Under In-Plane Seismic Loading.
In . 7th World Conference on Earthquake Engineering, Proceedings, Vol.5, pp. 9-16, Istanbul, Turkey, 1980.

(5) Nakashima, M., Huang, T. and Lu, L.W.
Experimental Study of Beam-Supported Slabs Under In-Plane Loading.
Journal of the American Concrete Institute Vol. 79, No. 1:pp. 59-65, January-February, 1982.

(6) Nakashima, M., Huang, T. and Lu, L.W.
Effect of Diaphragm Flexibility on Seismic Response of Building Structures.
In . 8th World Conference on Earthquake Engineering, Proceedings, Vol. IV, pp. 735-742, San Francisco, 1984.

(7) Panahshahi, N., Reinhorn, A.M., Kunnath, S.K. and Lu, L.W., Huang, T., Yu, K.
Seismic Response of a 1:6 R/C Scaled Model Structure With Flexible Floor Diaphragms.
In . ACI Fall Convention, San Diego, November 1,1989.

(8) Yu, K., Huang, T. and Lu, L.W.
Design, Analysis and Experiment Planning of One-Story Reinforced Concrete Frame-Wall-Diaphragm Assemblage.
Research Report No. 540.1, Fritz Engineering Laboratory, Lehigh University, Bethlehem, Pennsylvania, 1989.